International
Progress Report

IPR-05-07

Äspö Hard Rock Laboratory

Temperature Buffer Test

Scoping design calculations

Harlad Hökmark
Lennart Börgesson
Clay Technology AB

Jan Hernelind
FEMTech AB

January 2005

Svensk Kärnbränslehantering AB
Swedish Nuclear Fuel
and Waste Management Co
Box 5864
SE-102 40 Stockholm Sweden
Tel 08-459 84 00
+46 8 459 84 00
Fax 08-661 57 19
+46 8 661 57 19

Äspö Hard Rock
Laboratory

Report no.	No.
IPR-05-07	F12K
Author	Date
Harald Hökmark Lennart Börgesson Jan Hernelind	Jan. 2005
Checked by	Date
Bertrand Vignal Christer Svemar	2005-06-23
Approved	Date
Anders Sjöland	2005-07-05

Äspö Hard Rock Laboratory

Temperature Buffer Test

Scoping design calculations

Harlad Hökmark
Lennart Börgesson
Clay Technology AB

Jan Hernelind
FEMTech AB

January 2005

Keywords: Buffer, Bentonite, Hydration, Sand-shield, Thermal conductivity, permeability, Heater

Abstract

TBT (Temperature Buffer Test) is a joint project between SKB/ANDRA, ENRESA and DBE, that simulates a part of a repository for strongly exothermic waste, where the temperature on the canisters may exceed 100 ˚C. The test is carried out in Äspö HRL in a 8 meters deep and 1.75 m diameter deposition hole, with two canisters (3 m long, 0.6 m diameter), surrounded by a bentonite buffer and a confining plug on top anchored with 9 rods. The experiment, which has been running and delivering data since March 2003, has as its main objective to improve and increase the understanding of Thermo-Hydro-Mechanical processes in bentonite-based buffer materials, particularly under high-temperature conditions.

The present report describes a number of preliminary studies initiated prior to finalizing the test design. These studies were scoping calculations conducted in order to explore the general feasibility of the test, to find out what the power requirements would be to achieve the test objectives, and to get a first estimate of the time-scale of the water uptake process. The results of the studies were submitted to ANDRA and SKB as draft reports in early 2002.

The report includes a brief main text and a number of appendices which correspond to the draft reports of the different preliminary studies.

Sammanfattning

TBT (Temperature Buffer Test) är ett gemensamt projekt mellan SKB/ANDRA, ENRESA och DBE, som simulerar delar av ett slutförvar för starkt exotermiskt radioaktivt avfall där temperaturen på kapslarna kan överstiga 100 ˚C. Försöket görs på 420-metersnivån i Äspö HRL i ett 8 m djupt deponeringshål med diametern 1.75 m, och består av två kapslar, omgivande bentonitbuffert och en ovanliggande plugg, som förankrats med 9 stag. Experimentet, som har varit igång och levererat data sedan mars 2003, har som övergripande syfte att förbättra och öka förståelsen för Termo-Hydro-Mekaniska processer i bentonitbaserade buffertmaterial, speciellt vid högtemperaturförhållanden.

Denna rapport beskriver ett antal förberedande studier som igångsattes innan testet hade fått sin slutliga utformning. Dessa studier var inledande grova beräkningar som gjordes för att undersöka testets allmänna genomförbarhet, för att bestämma den effekt som skulle behövas för att uppnå försökets syfte, och för att få en första uppskattning av tidsskalan hos vattenupptagsprocessen. Resultat av studierna lämnades till ANDRA och SKB tidigt under år 2002.

Rapporten består av en kort huvudtext och ett antal appendix som vart och ett motsvarar rapportutkasten från de olika förberedande studierna.

Contents

1 Introduction and background

The Temperature Buffer Test is a large-scale field experiment carried out as a joint project between SKB/ANDRA ENRESA and DBE. The experiment is conducted at 500 m depth in granitic rock in the Äspö HRL, Southeast Sweden. An existing 8 m KBS3-type disposal pit has been selected to accommodate the experiment. The overall objective is to acquire information on the response of bentonite-based buffer materials to thermal loads with temperatures well over 100 °C and to improve the general understanding of the Thermo-Hydro-Mechanical processes in that temperature range.

Two barrier configurations are tried:

- Composite barrier in the upper part of the experiment with a 0.2 m thick sand shield between the heater and the surrounding bentonite buffer.
- Single material barrier with bentonite in all the space between heater and rock in the lower part of the experiment.

To achieve the objectives of the test, the temperature should exceed 100 °C in parts of the bentonite for both options, i.e. in an annular range of at least 0.2 m from the heater surface. The test should be run for sufficiently long that the majority of the bentonite will be close to full saturation at the time of dismantling.

The present report regards modeling work carried out in late 2001 and in early 2002 to explore the general feasibility of the Temperature Buffer Test. There are three separate sets of scoping calculations: Study 1, Study 2 and Study 3. At the time of preliminary planning the test definition and the objectives of the test were based on concerns relevant particularly to disposal of Vitrified Waste. Vitrified Waste will emit heat for a shorter period of time than un-processed spent fuel, which may mean that the barrier system could be subjected to temperatures well above 100 °C without being permanently affected. The question of high temperatures has, however, turned out to be of general interest for the understanding of the performance of bentonite-based buffer materials, and the explicit coupling of the field experiment to concepts for Vitrified Waste disposal has been dropped. Therefore the experiment was named the "Temperature Buffer Test" shortly after the completion of the three preliminary studies, i.e. Study 1, 2 and 3. The documentation of these studies makes out the main material of this report, while the text in the sections below gives just a brief account of the contents. The three studies are presented separately, and *in extenso*, as separate appendices. For Study 2, there are two appendices: Appendix IIa and Appendix IIb.

- Study 1 is simplistic thermal study performed to find the power required to achieve the objectives of the test. The study is based on analytical solutions of the temperature field around a line heat source and on steady-state expressions for the temperature distribution between two cylindrical surfaces, i.e. the heater surface and the wall of the disposal pit. The heater package is represented by a line heat source. The analytical line source solution is used to calculate the temperature at the wall of the disposal pit as a function of time, and the steady-state expression to find the temperatures in the annular space between heater and rock. There are calculations for both barrier configurations.

- Study 2 is a numerical quasi 3-D thermal calculation of the temperature field around the TBT heater package. The calculations are performed using the finite element code Abaqus. There is one main set of calculations and one supplementary set with different (or modified) assumptions regarding the geometry and the distribution of the heat power. The two sets of calculations are presented in Appendices IIa and IIb, respectively.

- Study 3 regards numerical 1-D radial symmetry Hydro-Thermal calculations of the water uptake process. The calculations are performed with Finite Element Program Code_Bright. There are two model geometries: one for the composite sand-bentonite barrier and one for the single material barrier. The thermal input to the finite element models is based on the results of Study 1.

2 Test layout

Figure 1-1, left, shows the geometry of the experiment as it was laid out originally. There is a rod-shaped heater that extends 3 m below the bottom of the existing disposal pit. Study 1 (Appendix I) and Study 3 (Appendix III), as well as the first part of Study 2 (Appendix IIa) are based on this geometry. The supplementing Study 2 calculations (Appendix IIb) are based on the modified design shown in the right part of the figure.

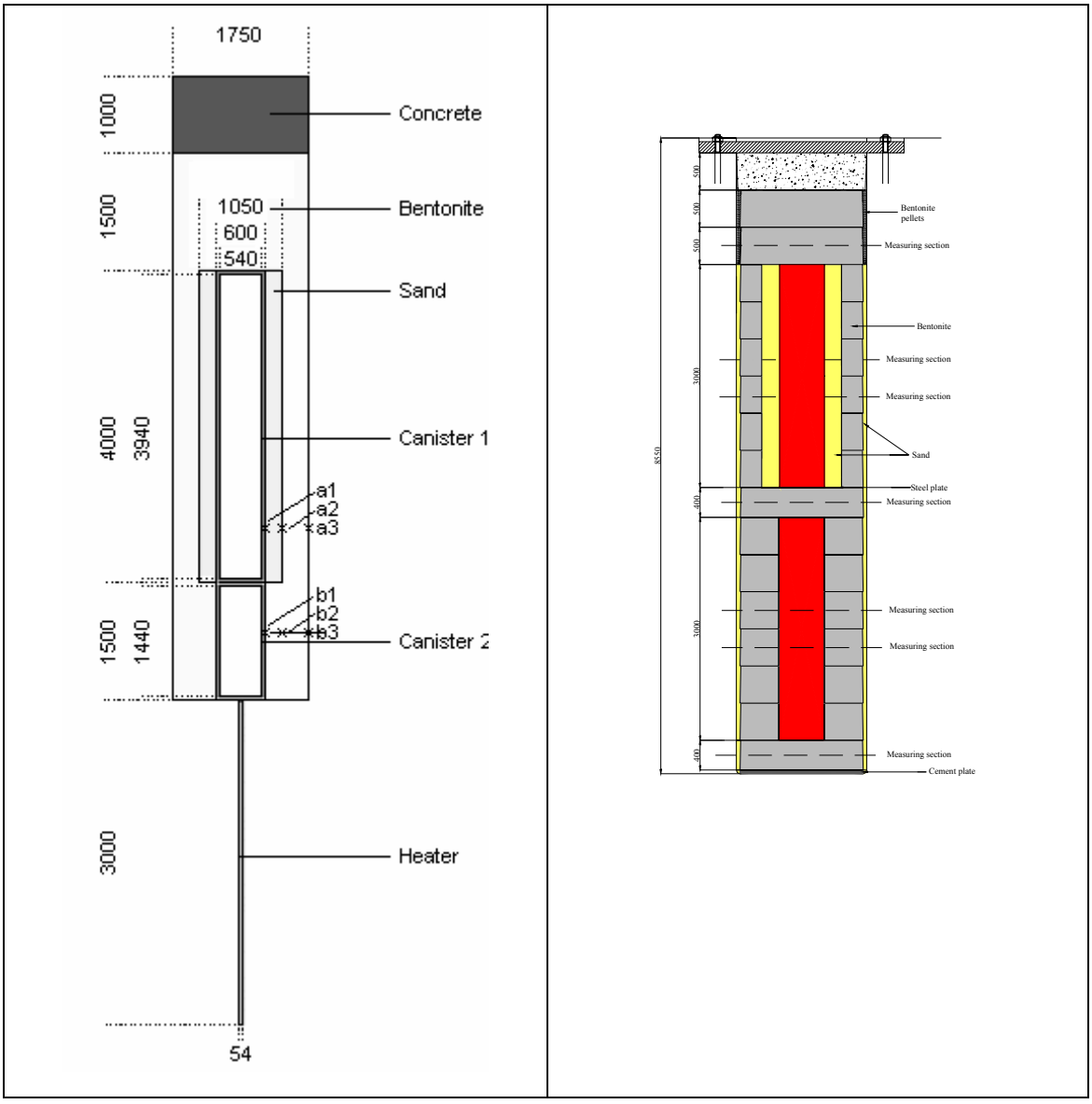

Figure 1-1. *Schematics of test geometry*

Based on the findings of Study 2, the decision has been taken to design the experiment as outlined in the right part, i.e. to omit the heater extension, and to separate the two heaters and to power them individually.

3 Results summary

Results and conclusions from the individual sub-studies are found in the different appendices. Here only a very brief summary is provided.

The main conclusion of Study 1 is that the power should be about 500 W per meter of heater length, given that the temperature at 0.2 m radial distance from the heater surface should not be less than 100°C. The temperature at the surface of the heater depends on whether the heater is surrounded by a sand shield, as in the upper part, or bentonite only as in the lower part. In Study 1, it is assumed that the experiment is run either with the composite sand/bentonite barrier or with a single material bentonite barrier. This means that interactions between the lower and the upper parts are not accounted for.

Study 2 confirms, in a general sense, the Study 1 findings regarding the temperature levels and the power needed to reach sufficiently high temperatures. However, the quasi 3-D representation captures also the heat transfer in the axial direction, and this is found to be considerable for the design considered initially (Fig. 1-1 left). The poorly cooled sand shield part of the heater package looses heat to the better-cooled lower part. This means that the radial heat output will vary along the height of the heater package. The second part of Study 2 (Appendix IIb) is performed using the geometry shown in the right part of Fig. 1-1. A bentonite block is inserted between two identical, 3 m long heaters, and the rod-shaped heater extension has been omitted.

Study 3 is, again, a 1-D radial symmetry analysis that does not take into account that the actual experiment will be run with both options (with and without sand shield) being tried simultaneously. The thermal input is obtained from the Study 1 results (500 W/m and 400 W/m power options). The results of Study 3 indicate that there will be a considerable drying of the bentonite close to the heater surface for the single material option and much less drying of the bentonite outside the sand shield for the composite barrier option. For the geometry assumed in the study (8.7 m total heater length), the 500 W/m option gives temperatures well over the required 100°C at 0.2 m radial distance from the heater surface. The high power model (500 W/m) indicates the possibility that a saturation front may form, such that the water uptake process is significantly impeded.

APPENDIX I

TEST OF VITRIFIED WASTES

STUDY 1 - THERMAL

One-dimensional radial heat flow in cavity interior

Harald Hökmark

Clay Technology AB

December 2001

Contents

1 Introduction and background

ANDRA plans to conduct a full scale Vitrified Waste Test at Äspö HRL.

The present text shows the results of the first study of a series of studies, aimed at assessing the feasibility, costs and general prospects of the test. This particular study regards the basics of radial heat transfer across the annular gap between waste package and rock wall. Most specifications of the study have been provided by ANDRA in a document entitled “Test of vitrified wastes.”

The results here are intended to be of guidance, or to be used as a point of departure, when planning two following studies which will regard the more detailed two-dimensional thermal development around the waste package (study 2), and the hydration of the buffer material (study 3).

2 Problem statement and problem geometry

A long cylindrical heater of radius R1 = 0.3 m is depositioned vertically in a cylindrical cavity of radius R3 = 0.88m. The medium surrounding the cavity is granite. The annular space between heater and granite is filled with bentonite (case 1) or bentonite and sand (case 2). In case 2, the sand/bentonite interface is at radius R2 = 0.5m. The problem is to find relevant relations between the power per unit heater length and the temperatures at R1, R2 and R3. For radius R2, a 100°C target temperature is prescribed.

Figure 1 shows a horizontal slice at package mid-height. The problem domain is between R1 and R3. The heater is long enough that, within the problem domain, the heat flow can be approximated to be purely radial.

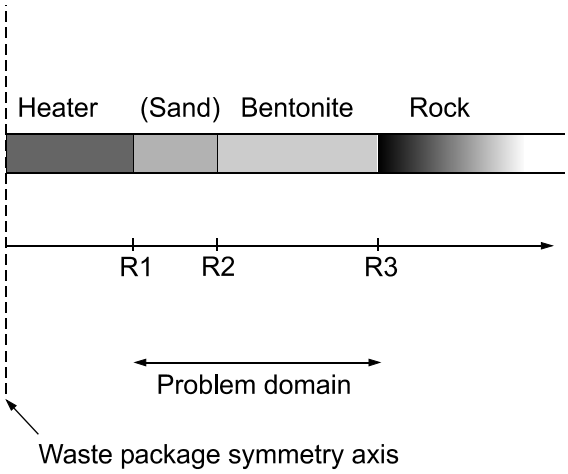

Figure 1. *Problem geometry.*

In the following, four cases of cavity material thermal properties are considered (Table 1).

Table 1. Cavity material properties

	Bentonite only (case 1)		**Bentonite and sand (case 2)**	
Initial state of saturation	80 %, W/(m·K)	1.2	80 % (bentonite) W/(m·K),	1.2
			0% (sand) W/(m·K)	0.3
Full saturation	100 % W/(m·K)	1.3	100% (bentonite) W/(m·K)	1.3
			100% (sand) W/(m·K)	2.0

The conductivity values for sand are from Börgesson (1982), while bentonite values are from Börgesson et al. (1994).

The rock thermal conductivity value provided by ANDRA, 2.6 W/ (m·K), is used as base case value. In the Final Results section, a higher value, 3.0 W/(m·K), is tried for comparison.

3 Problem conceptualization

A few days after the heating test has started, the front of the thermal pulse will reach and pass the buffer/rock interface. After that, the heat flow through the annular space between heater and rock is quasi-stationary, i.e. the heat flow per unit of heater length across the cylindrical surface of radius R1 is equal to those across surfaces of radii R2 and R3 (c.f. Fig. 1). This means that the temperature gap between R2 and R1 is given by:

$$\Delta T_{2,1} = T_1 - T_2 = \frac{Q}{2 \cdot \pi \cdot \lambda_s} \cdot \ln\left(\frac{R_2}{R_1}\right) \quad (1)$$

where Q is the power per unit heater length and λ_s is the thermal conductivity of the material (sand or bentonite) between R1 and R2. Correspondingly, the gap between R3 and R2 is:

$$\Delta T_{3,2} = T_2 - T_3 = \frac{Q}{2 \cdot \pi \cdot \lambda_b} \cdot \ln\left(\frac{R_3}{R_2}\right) \quad (2)$$

where λ_b is the bentonite thermal conductivity.

The above formulas are sufficient to calculate the temperature gaps $\Delta T_{2,1}$ and $\Delta T_{3,2}$ and the thermal gradients within the different parts of the problem domain, but not the absolute temperature values. The temperature T3 is a slowly varying temperature boundary condition that needs to be determined in order to find values of T1 and T2. The boundary temperature T3 depends on:

1. the initial undisturbed rock temperature and
2. the increase in rock temperature that takes place over time as a result of the heat supplied to the rock from the cylindrical heater.

Here, the undisturbed rock temperature is set at 15 °C.

The rock temperature increase depends on the length of the heater, the power per unit heater length and on the rock thermal properties. As soon as quasi steady-state heat flow has been established within the cavity, the thermal properties of the cavity materials become unimportant. The line source solution given in Eqn. (3) below can then be used to determine the temperature $T_{rock}\,(r,z,t)$ in any arbitrary rock mass point outside the cavity. The solution reads:

$$T_{rock}(r,z,t) = \frac{Q}{4\pi\lambda_r} \cdot \int_{-H_c}^{H_c} \left\{ \frac{1}{\sqrt{r^2+(z'-z)^2}} \cdot erfc\left[\frac{\sqrt{r^2+(z'-z)^2}}{\sqrt{4at}} \right] \right\} dz' \qquad (3)$$

where r is the radial distance from the line source, z the height above line source mid-height, t is time, λ_r is the rock heat conductivity and Q is the power per unit line source length. H_c is the half-length of the line source and a is the rock thermal diffusivity ($a = \lambda_r/(\rho \cdot c)$, where ρ is rock density and c is rock specific heat). This equation is readily obtained by integration of a continuous line of point sources along the length of heater, see for instance Claesson, (1994) and Hökmark and Claesson, (2001).

Temperatures T3, T2 and T1 are determined as follows:

1. Use Eqn. (3) to calculate T3(t) = $T_{rock}(0.88, 0, t)$ +15.
2. Use Eqn. (2) to find T2
3. Use Eqn. (1) to find T1

Eqn (3) is not a steady state solution, which means that values for heat storage must be provided. For this study, the values 2600 kg/m^3 and 800 J/(kg·K) were used for density and specific heat, respectively.

For each case of T3, there will be two cases of T2 and four cases of T1, as shown in Table 2.

Table 2

T3	T2	T1
Independent of cavity interior conditions	Initial state of saturation	Sand/bentonite
		Bentonite only
	Full saturation	Sand/bentonite
		Bentonite only

4 Using line source solution for calculation of T3

Below some examples are given that demonstrate the use of Eqn. (3)

Heater length

Figure 2 shows temperature T3 (without inclusion of initial rock temperature) calculated for four assumptions regarding the heater length.

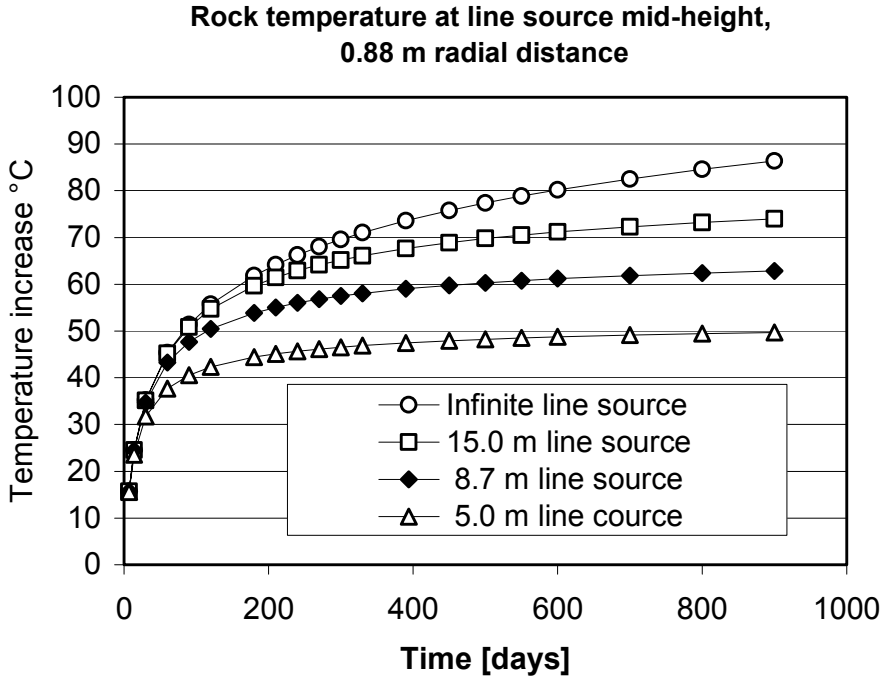

Figure 2*. Temperature T3 as function of time for different assumptions regarding heater length. The power per unit heater length is Q= 500 W/m.*

The figure shows that the finite length of the heater is unimportant for the first 50 days. After 900 days the assumption of an infinitely long heater will overestimate the boundary temperature T3 by between 20 and 25 °C. For the Vitrified Waste Test in Äspö HRL, the heater length will be about 8.7 m. In all calculation examples presented in the following text, this value will be used.

Thermal plateau.

Figure 3 shows temperature T3 (without inclusion of initial rock temperature) at three different levels: heater mid-height, 1.25 m above (or below) heater mid-height, and 2.5 m above (or below) heater mid-height. The results show that within a 2.5 m central length section (1.25 m distance) the rock wall temperature differences are less than 1.2 °C. A corresponding 5 m section (distance 2.5 m) gives temperature differences of about 5.5 °C. This verifies that the central 2.5 m length section is indeed a thermal plateau.

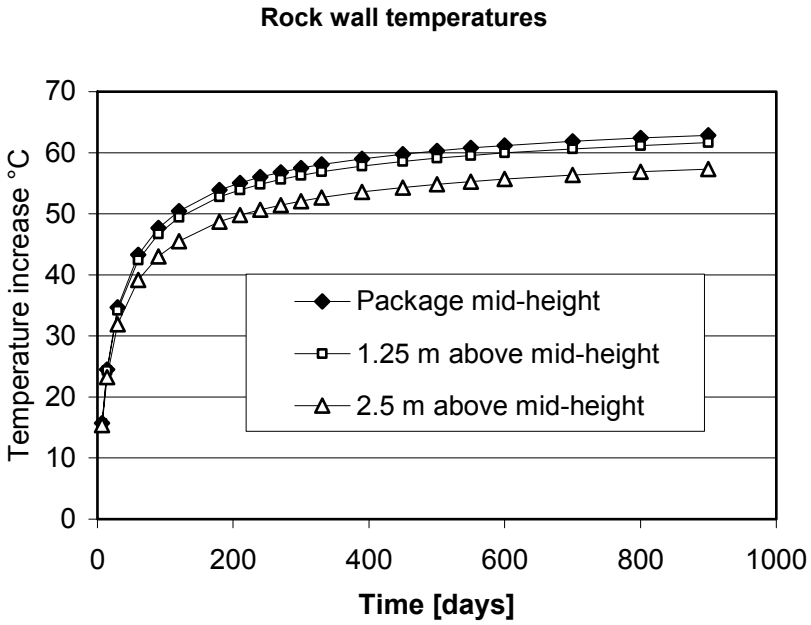

Figure 4. *Verification of existence of 2.5 m thermal plateau.*

Cooling effects of the tunnel.

The line source solution regards linear heat conduction in an infinite, homogeneous and isotropic medium. All these conditions are seldom fully satisfied in reality. For the Vitrified Waste Test, for instance, the drift floor 2.5 m above the upper heater end will cause some disturbance. A conservative upper bound estimate of this cooling effect can be obtained by superimposing the temperature field generated by an additional line source of power $-Q$ per unit length as shown in Figure 5.

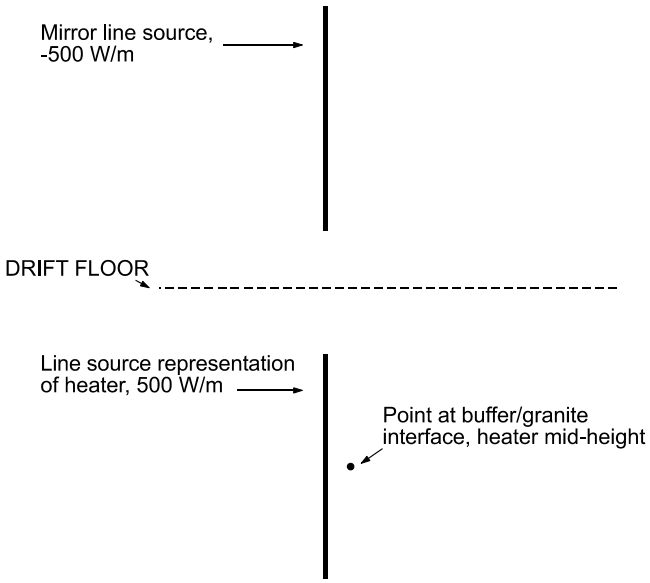

Figure 5. *Upper bound estimate of cooling caused by the open tunnel above the heater.*

Figure 6 shows the temperature at the buffer/granite interface with and without inclusion of the mirror source. The initial rock temperature is not included. The mirror source imposes an anti-symmetry plane on the temperature field and locks the temperature to the pre-test values in the entire infinite plane of the floor, which is a much more efficient cooling than that provided by the real three-dimensional tunnel. The results show that ignoring the tunnel effect can cause an error of perhaps two degrees in T3 at late times and much less at early stages of the experiment. Therefore, in this set of preliminary calculations, the effects of cooling will not be included.

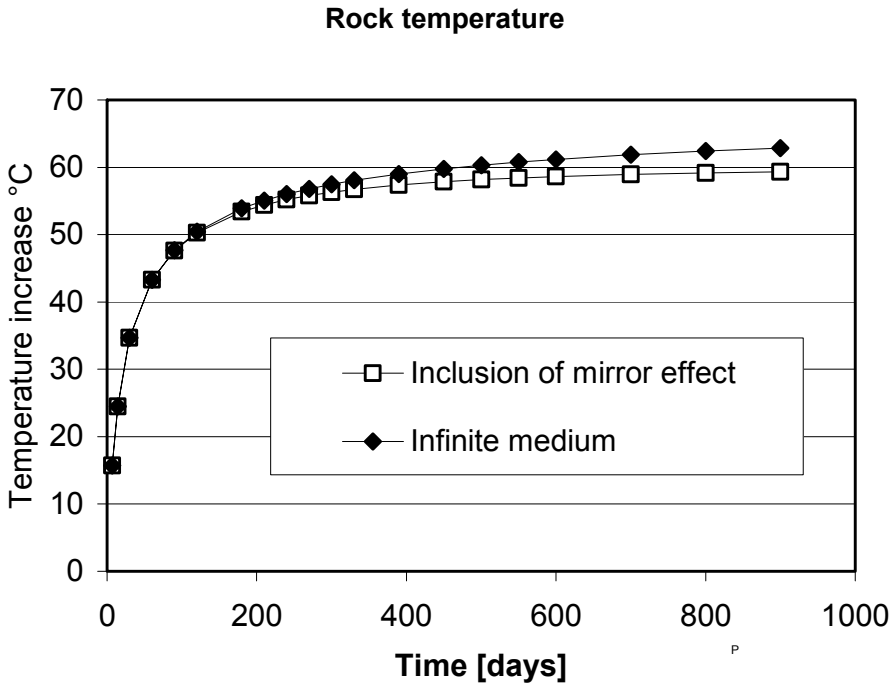

Figure 6. *Upper bound estimate of effects of cooling caused by the open tunnel.*

5 Temperature Calculations – Constant Power

5.1 Boundary temperature T3

Figure 7 shows the influence of line source power on the rock wall temperature at heater mid-height. Temperatures include an initial 15 °C undisturbed rock temperature. Since T3 does not depend on the thermal properties in the interior of the cavity, there is only one set of curves.

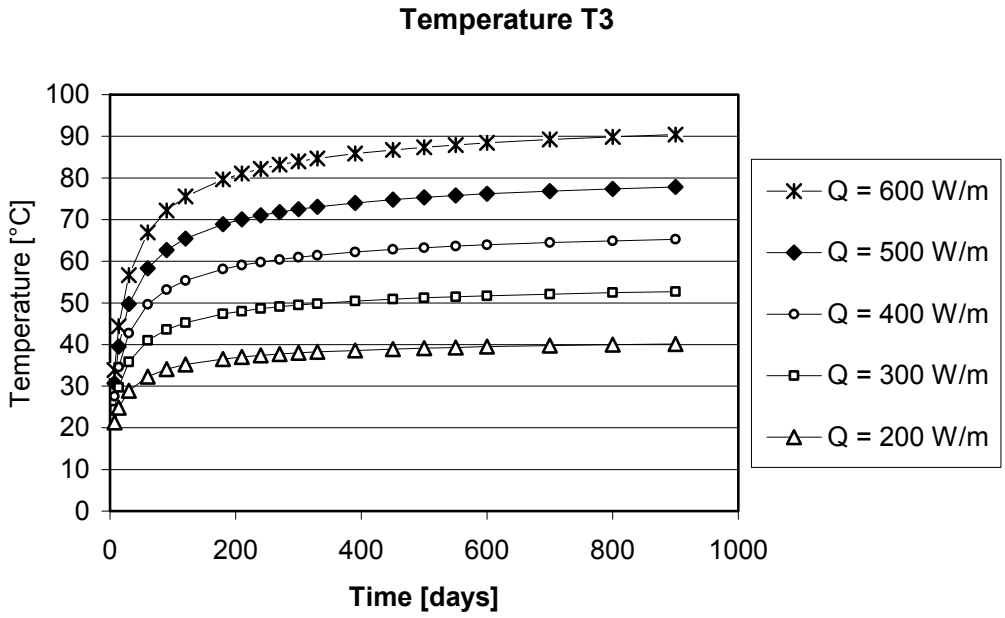

***Figure** 7. Temperature T3 for different assumptions regarding line source power. All cases regard a line source of length 8.7m.*

5.2 Temperature T2 at 0.5 m radial distance

Figure 8 shows temperature T2, calculated by use of Eqn. (2) and by use of the boundary T3 temperatures shown in Fig. 7. These results do not depend on the conditions inside R2, only on the thermal power of the heater and on the heat transfer conditions outside R2. Therefore, for the T2 temperature, it is not important if the inner part of the annular space is filled with bentonite or sand. Consequently, there are only two sets of curves, corresponding to the two possible saturation/conductivity states between R2 and R3, (Table 2).

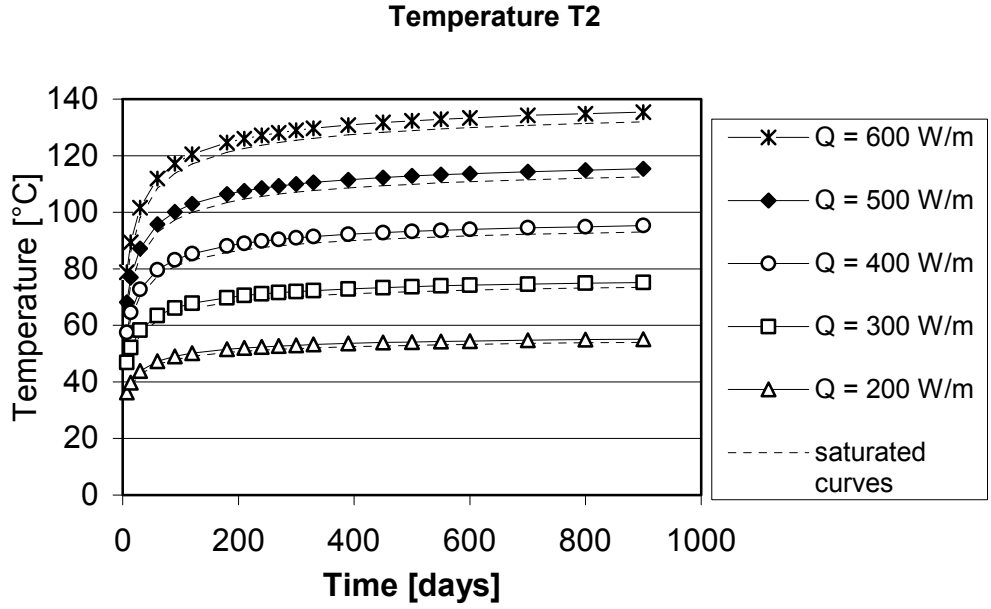

***Figure 8**. Temperature T2 for five different power assumptions. Lines with markers represent the case of 80% saturation (λ_b=1.2 W/(m·K)). Corresponding dotted lines without markers represent case of full saturation (λ_b =1.3 W/(m·K)).*

Obviously, a power of 300 W/m or less does not bring the temperature T2 even close to the target temperature 100°C. Therefore, in the following sections, power cases 200 W/m and 300 W/m will not be further considered.

It can be noted here that the curves corresponding to 500 W/m and 400 W/m bracket the target temperature prescribed for T2, i.e. 100 °C. The power needed to arrive at 100 °C after about 900 days time can be estimated to about 425 W/m. To arrive at the target temperature faster and then lock T2 at that value, some initial power over-shooting and subsequent power reduction will be necessary.

In section 6 an easy and straightforward method of representing and analyzing heater power reductions is suggested and exemplified.

5.3 Temperature T1 at heater/buffer interface

Figures 9 and 10 show the temperature T1 for case 1 (bentonite only) and case 2 (sand and bentonite), respectively.

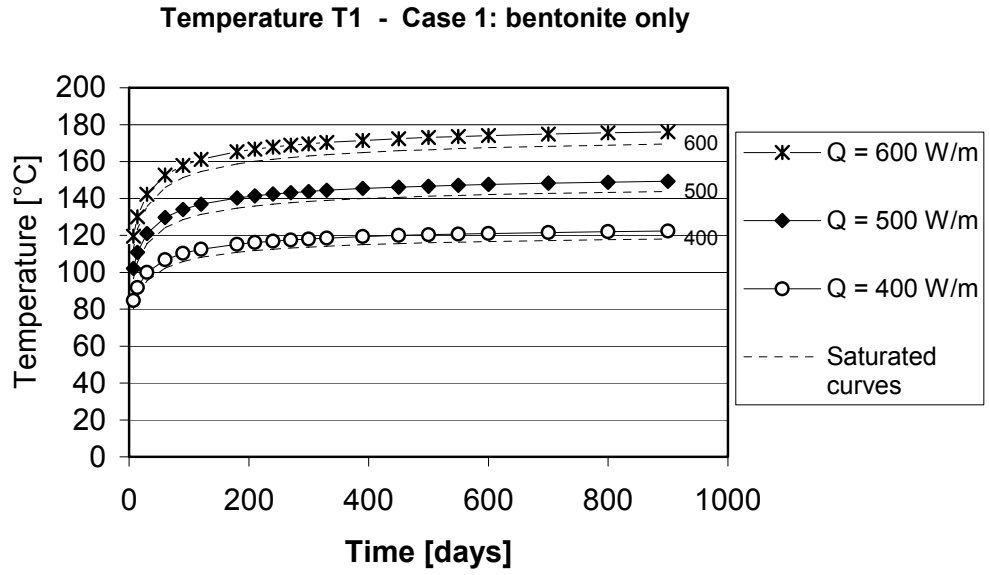

***Figure 9**. Temperature T1. Lines with markers: 80% saturation. Dotted lines without markers: full saturation.*

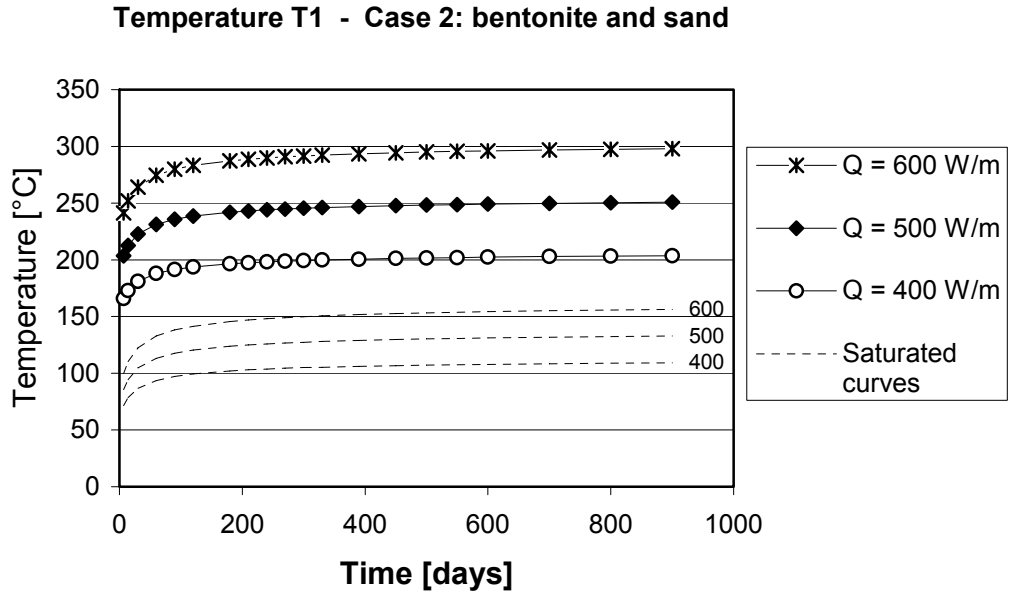

***Figure 10.** Temperature T1. Lines with markers: 80% saturation in bentonite part and 0% in sand part. Dotted lines without markers: full saturation.*

6 Power changes

To account for power changes, the law of superposition can be used to determine the boundary temperature T3(t). The effect of a 100 W/m reduction is obtained by adding the field generated by a fictive -100 W/m line source to the solution corresponding to the initial power. Temperature T2(t) and T1(t) are then calculated as described in previous sections. Figures 11, 12 and 13 show the effects for two reduction schemes: Reduction from 500 W/m to 400 W/m after 50 days and after 200 days.

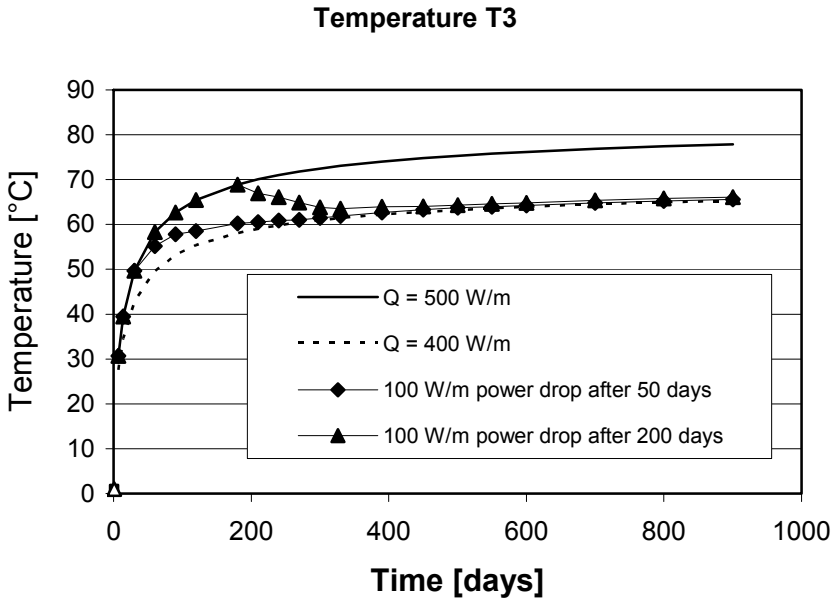

***Figure 11**. Power drop effect on T3. Lines without markers: constant power.*

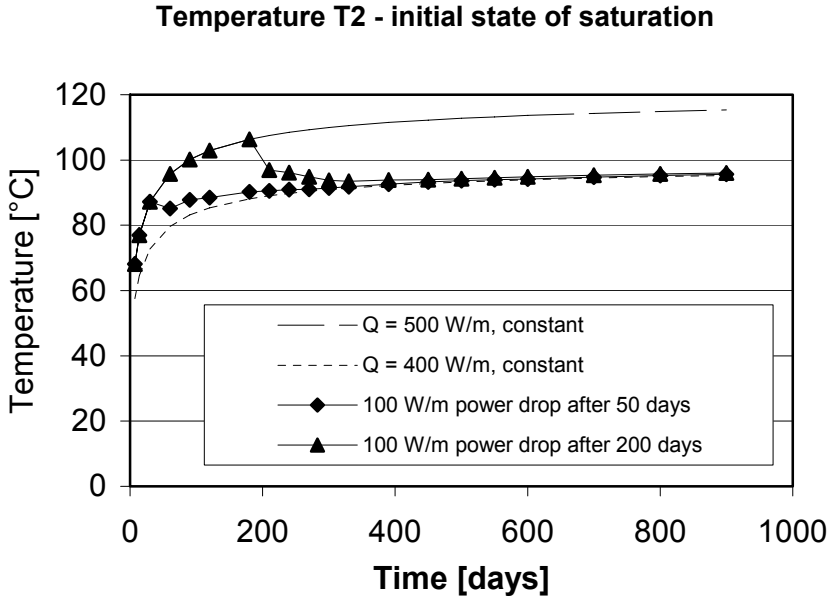

***Figure 12**.Power drop effect on T2, initial saturation.*

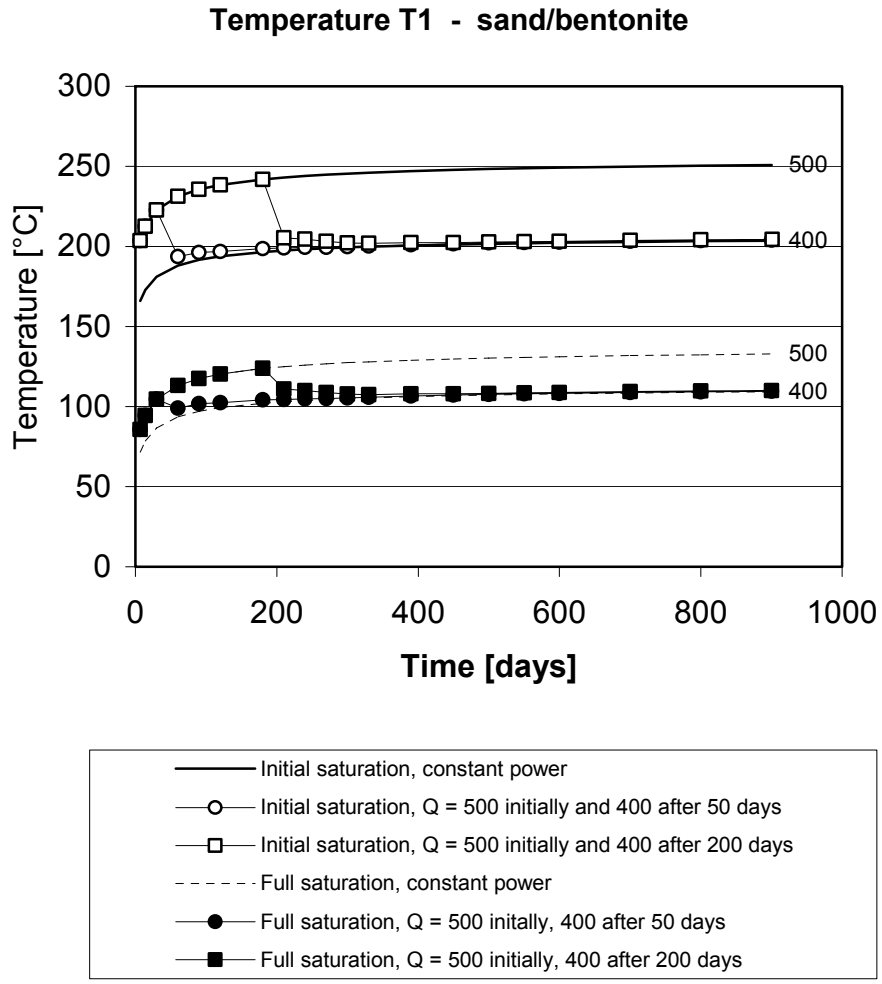

Figure 13. *Power drop effect on T1 for case 2 (bentoníte and sand). Both saturation states are included. Lines without markers: constant power.*

Figures 11, 12 and 13 show that the power reduction results are logical and consistent with the input assumptions. It is also clear from Figure 12 that a step by-step-reduction scheme is required to keep T2 at the target temperature 100°C for the duration of the experiment.

7 Imposing target temperature T2 – Final results

Figure 14 shows the result of performing power reduction in three 25 W/m steps from an initial value of 500 W/m. After about 110 days the temperature T2 at 0.5 m radial distance is fairly well locked at the target value of 100°C. Here the rock conductivity specified by ANDRA, 2.6 W/(m·K) has been assumed (as in all previous cases).

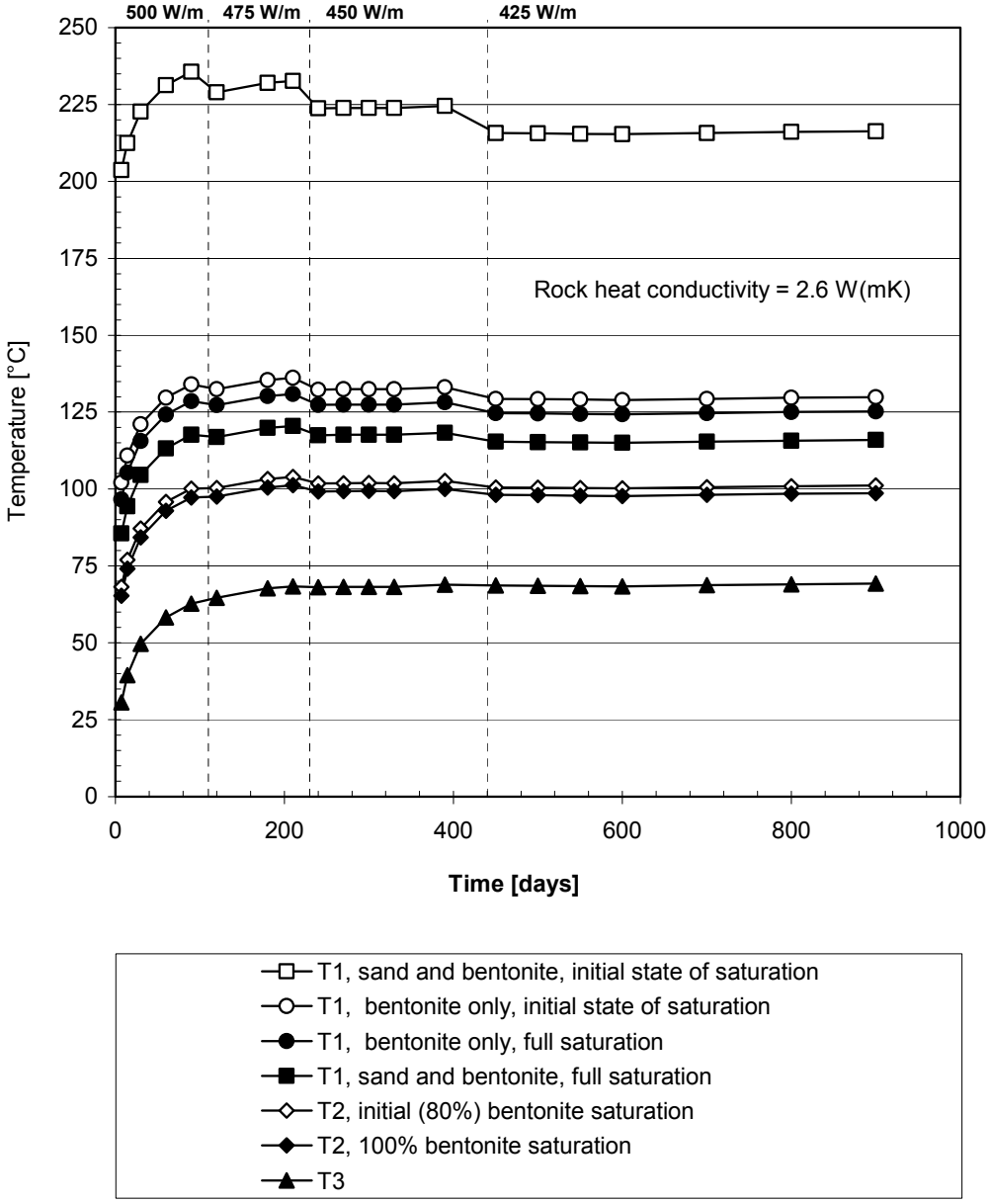

***Figure 14**. Temperature T1, T2 and T3, for all cases in Table 2. The power is shown on top of the diagram.*

Figure 15 shows the effects of increasing the rock conductivity to 3.0 W/(m·K). Heat will dissipate faster from the buffer/granite interface. In order to keep T2 at the target temperature, the initial power needs to be increased to 550 W/m. The same scheme for power reduction has been used as in the case shown in Figure 14.

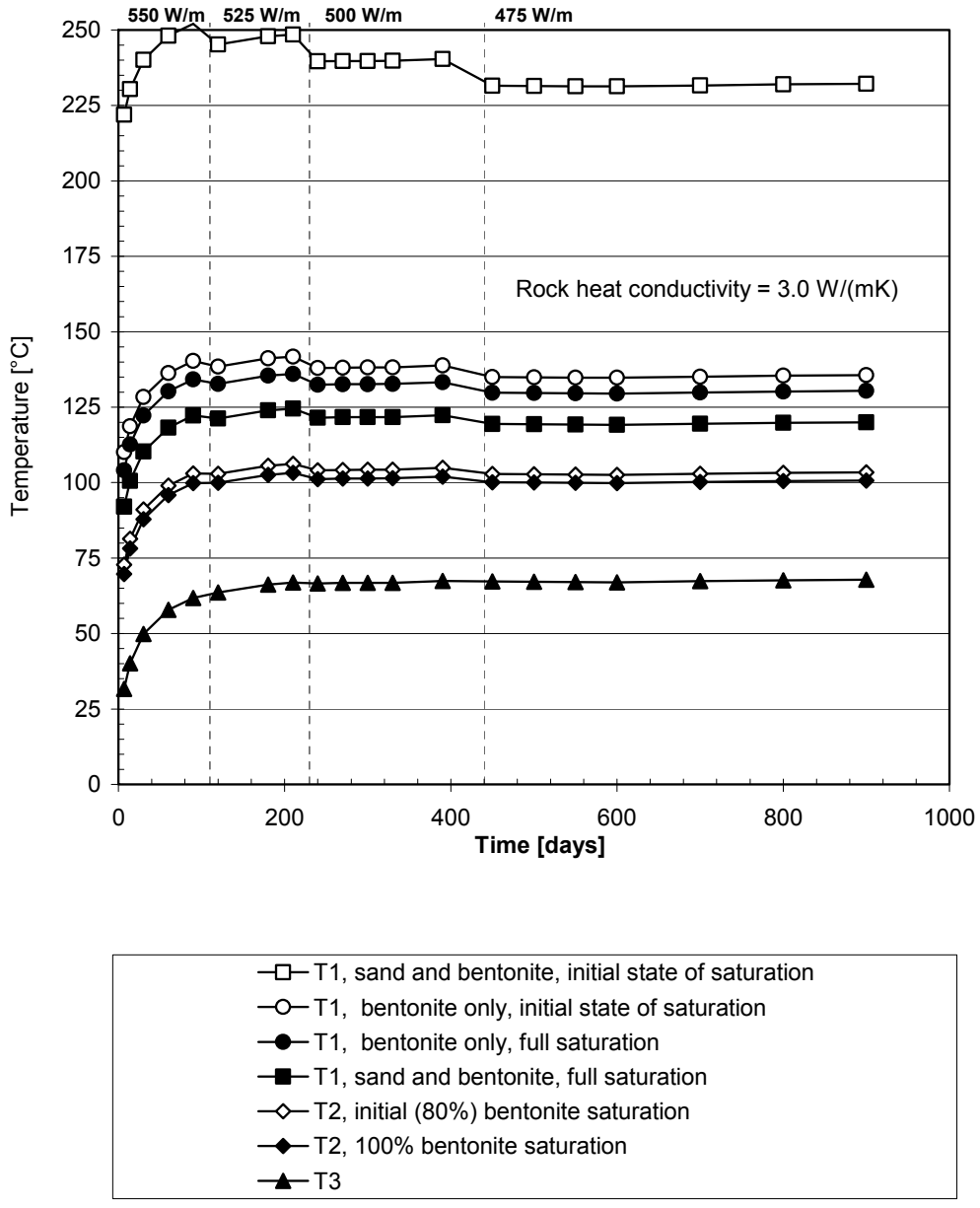

Figure 15*. Same as figure 14, but the rock conductivity is 3.0 W/(m·K) and the power is higher.*

8 Conclusions and discussion

8.1 Conclusions

Two cases of rock thermal property values have been considered: 2.6 W/(m·K) and 3.0 W/(m·K). The predominant rock type in Äspö HRL, Äspö Diorite, has been reported to have a conductivity of 2.8 W/(m·K), (Sundberg and Gabrielsson, 1998) . Therefore, the final results of the two cases should provide reasonable bounds to the real case. This means that the initial power should be between 500 W/m and 550 W/m.

The target temperature is reached after about 100 days. The results here indicate that after that the power needs to be reduced by about 100 W/m. To lock T2 to the target temperature, this should be done in steps not larger than 25 W/m. The reduction steps should be distributed over time, (between 100 and 500 days) after heating has started.

If it is necessary to achieve the target temperature sooner, then more power over-shooting will be needed. Also more and faster power reduction will be needed.

8.2 Discussion

The use of Eqn. (3) implies that rock heat conduction is linear. However, for granitic rocks there is a small non-linearity: Heating from 20 °C to 100 °C typically gives conductivity reductions of 10-15% , (Kukkonnen and Lindberg, 1995). For the results here this is of small importance. Therefore, the errors in T3 are probably small.

Eqns. (1) and (2) imply that steady state heat transfer conditions prevail in the annular space between the heater and the rock wall. No storage parameters (specific heat and density) are needed. Figure 16 shows the transient temperature response *p(x,t)* of a semi-infinite slab to a sudden temperature step change at x=0. The response (Eqn. (4) is given by (Carslaw and Jaeger, 1959):

$$p(x,t) = 1 - erf\left(\frac{x}{\sqrt{4at}}\right) \qquad (4)$$

where *a* is the thermal diffusivity.

In Figure 16, density and specific heat values (i.e. thermal diffusivity) that are typical of buffer materials have been used. The curves show that the front of the pulse has moved well beyond 60 cm (distance between heater and rock wall) after 6 days. Between 0 cm and 60 cm the curve is approximately a straight line, which means that quasi steady state conditions prevail. This indicates that the assumption in section 3 regarding quasi steady-state heat transfer after a few days is reasonably justified.

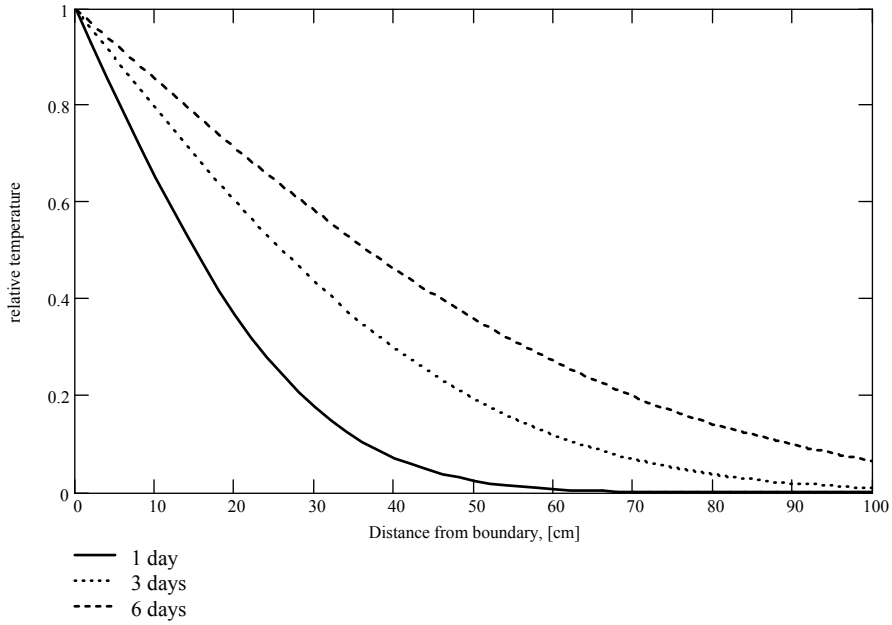

***Figure 16**. Propagation of temperature front in a semi-infinite slab.*

The largest uncertainties are probably in the conductivity values of the cavity materials:

- The sand data will depend on compaction and on the quartz content. Here, generic values have been used. However, errors in sand data will have an impact on T1 only, not on T2 or T3.

- The values of all cavity material have been assumed constant, while in reality there will be both spatial and temporal variations. Because of evaporation and vapor transport the conductivity of the bentonite may decrease below the initial saturation values. Errors in bentonite conductivity will influence both T1 and T2.

Another source of error is the possibility of gaps. Here it is assumed that the different materials are in direct thermal contact. Gaps may cause temperature offsets and increase T1 and T2.

References

Börgesson L., 1982. BUFFER MASS TEST - Predictions of the behavior of the bentonite-based buffer materials. Stripa Project international report 82-08. SKB, Stockholm.

Börgesson L., Fredriksson A., Johannesson L-E., 1994. Heat conductivity of buffer materials. SKB Technical Report TR-94-29. SKB, Stockholm.

Claesson, 1996. Partial differential equations - Technical applications. Depts. of Mathematical and Building Physics. Lund University of Technology, Lund.

Carslaw H. S., Jaeger J.C., 1959. Conduction of Heat in Solids. 2nd edition. Oxford University Press, Oxford.

Hökmark H., Claesson J., 2001. Use of analytical solution for calculating repository host rock temperatures. Proceedings of the 6th KIWIR workshop in Paries. In preparation.

Kukkonen I., Lindberg A., 1995. Thermal conductivity of rocks at the TVO investigation sites Olkiluoto, Romuvaara and Kievetty. Report YJT-95-08, Nuclear Waste Commission of Finnish Power Companies, Helsinki Finland.

Sundberg J., Gabrielsson A., 1998. Field measurementas of thermal properties of the rocks in the prototype repository at Äspä HRL. SKB Progress Report HRL-98-28. SKB, Stockholm.

APPENDIX IIa

TEST OF VITRIFIED WASTE

STUDY 2, TEMPERATURE FIELD

Lennart Börgesson

Clay Technology AB

Jan Hernelind

FEMTech AB

January 2002

Contents

1 Introduction

The present study (study 2) deals with thermal modelling of a full-scale test in Äspö Hard Rock Laboratory, planned by ANDRA for simulating processes involved in parts of a repository for vitrified waste. The aim of the study is to simulate the thermal processes in the test and calculate the expected temperature development both for a base case and several variations of the base case. The results will be the basis of final design of the test. The calculations are only thermal, i.e. there is no hydraulic or mechanical coupling and thus no account taken to the influence of drying or wetting.

The study is part of the first preliminary modelling of the processes and is run in parallel with two basic 1D studies of the temperature and moisture development in the test (studies 1 and 3).

The test and the background are described in specifications provided by ANDRA in a document entitled “Test of vitrified wastes”.

The calculation of study 2 has been made with the finite element program ABAQUS.

2 Model geometry

The test will be performed in a hole drilled in ÄHRL with the diameter 1.76 and depth about 8m. The basic idea of the test configuration is to simulate two kinds of long deposition holes.

1. A heater with the diameter 60 cm and a buffer of bentonite to fill the rest of the hole

2. The same heater but sand between the heater and the buffer of bentonite in order to keep the temperature in the bentonite below 100 degrees C

Figure 2-1 shows the test layout proposed by ANDRA. Since the disposal concept aims at using deep deposition holes (about 50 m) a large part of the heat flow through the buffer will be solely radial. In order to minimize the end effects in the test a heater is proposed to be installed in the bottom of the hole to about 3 meters depth below the bottom. This geometry is used as base case for the calculations.

In order to study the heat flux in the entire test the base case with specified geometry and properties is chosen. The influence of the geometry and the properties of the materials is then studied by changing one item at a time. The aim of the sensitivity study is to find a test design that fulfils the desires noted in the specifications with the following main points:

1. A temperature of 100 degrees at the radial interface between the sand and the bentonite.

2. A “thermal plateau” in the bentonite with only radial heat flow and vertical isotherms for about a meter length of both parts

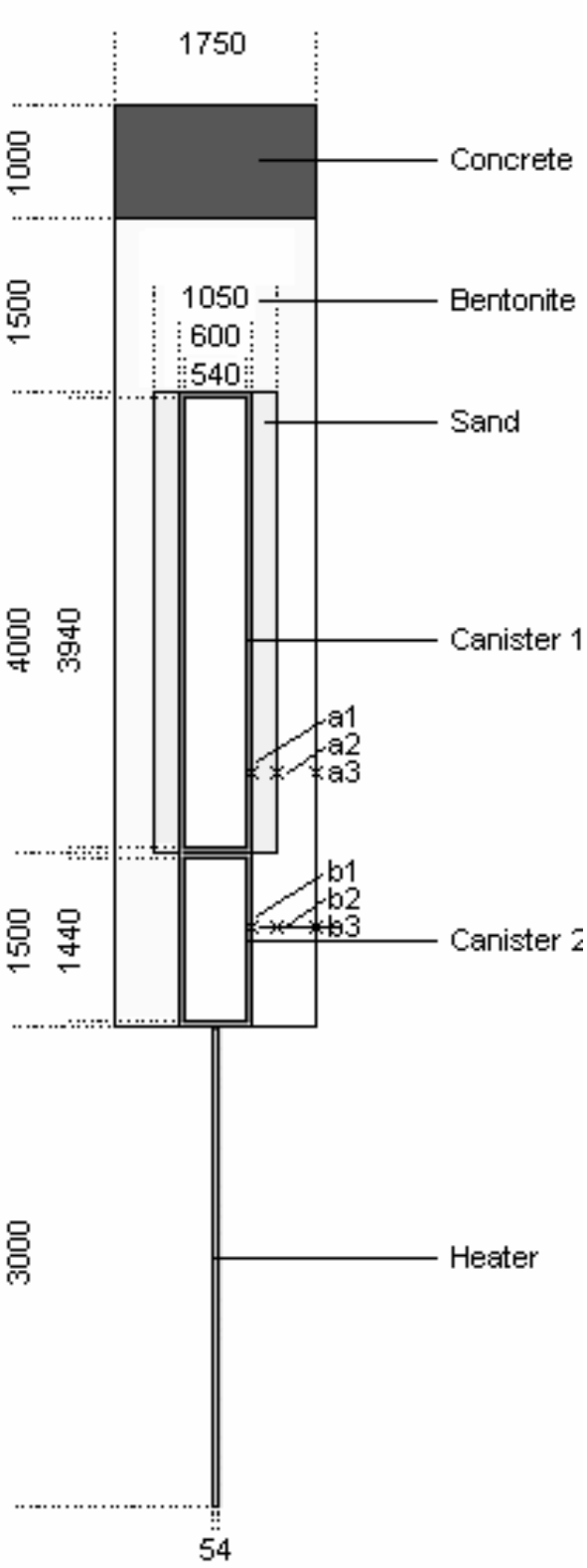

Figure 2-1. *Layout of the test and figuring (mm) of different parts of the base case. The sections between a1 and b1, a2 and b2, and a3 and b3 are studied in detail. a1-a3 are located 0.98 m above the bottom of canister 1 and b1-b3 are located 0.89 m below.*

3 Base case

3.1 Element mesh

The finite element mesh used for the base case is shown in Fig 3-1. The mesh is axial symmetric with the dimensions 30 m x 40 m, that is the radius of the outer rock boundary is 30 m and the lower rock boundary is placed 40 m below the floor. The upper part of the model ends with the floor, which means that the rock at the walls of the tunnel is not included (since the influence is negligible).

Fig 3-2 shows a detail of the mesh and the different materials in the model of all parts except the rock. The dimensions were shown in Fig 2-1.

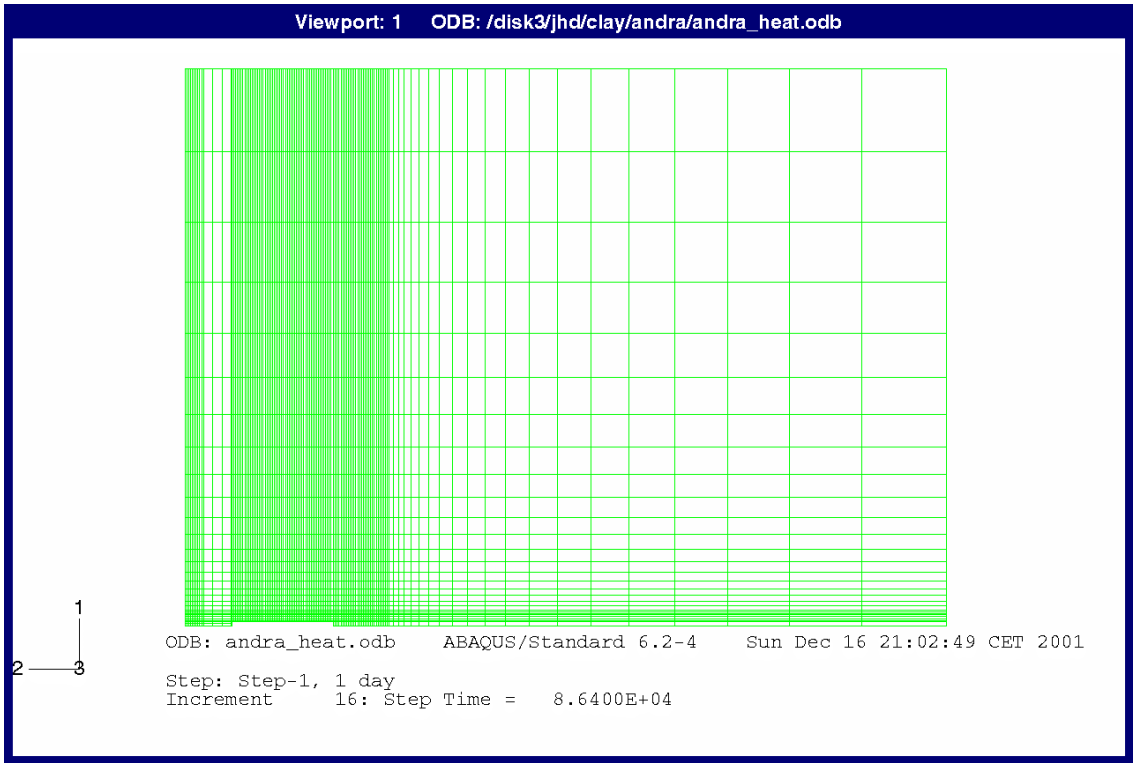

Figure 3-1. *Entire element mesh of the model (lower boundary=symmetry axis). The model is rotated 90 degrees, which means that axis 2 is directed upwards*

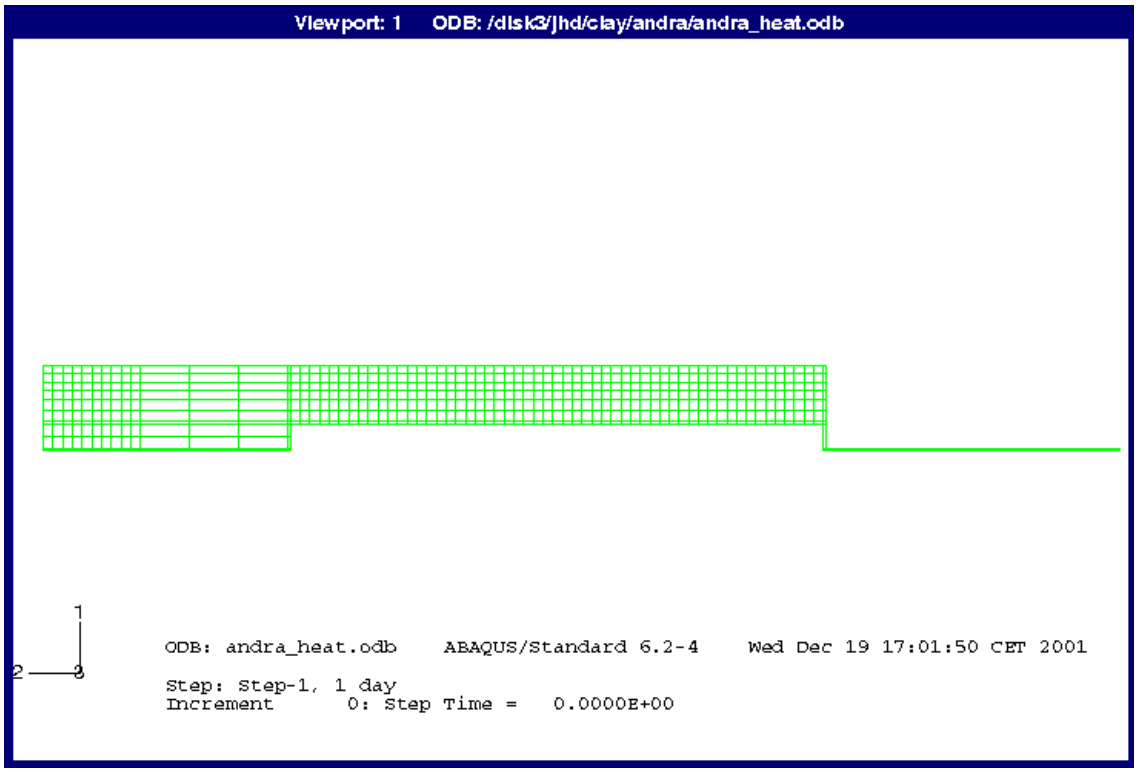

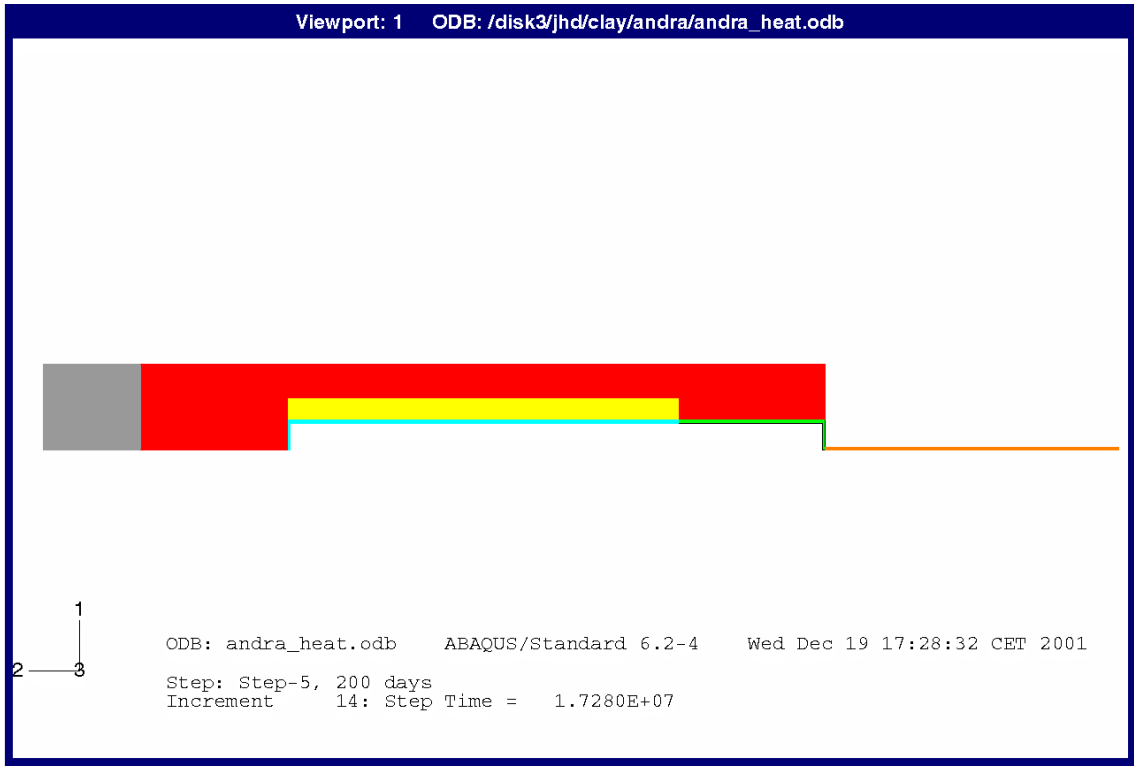

Figure 3-2. *Element mesh of the details (no rock)(upper) and the different materials (lower) (rotated 90 degrees). Grey=Concrete; Red=Bentonite; Yellow=Sand; Blue=Canister 1; Green=Canister 2; Orange=Heater.*

3.2 Boundary and initial conditions

The boundary condition at the floor, at the outer radial rock boundary and at the lower rock boundary is a constant temperature of

T_b = 16 °C.

At the floor there is also a heat transfer film coefficient of

α = 10 W/m^2

The initial temperature of all elements is

T_0 = 16 °C.

3.3 Thermal properties

The thermal properties applied for the materials in the base case are shown in Table 3-1.

Table 3-1. Thermal properties used in the base case (see Fig 1-1)

Material	λ **(W/m,K)**	***c*** **(Ws/kg,K)**	ρ **(kg/m^3)**	**Remark**
Concrete	1.7	900	2400	
Canister 1	50	460	7850	3 cm wall
Canister 2	50	460	7850	3 cm wall
Heater	50	460	7850	solid
Rock	2.6	800	2600	
Sand	0.3	800	1800	dry
Bentonite	1.2	1300	2000	*w*=17%

3.4 Calculation sequence

Heating of the canisters and the heater has been simulated for 1200 days. A constant power of 500 W per meter length of canisters and heater has been applied and the calculation made in 7 steps according to Table 3-2. The power was applied during the first day by increasing it from 0 W to 500 W in 24 hours. The power is modeled by applying volumetric power intensity in the steel, which yields

P = 9307 W/m^3 for canisters 1 and 2

P = 218320 W/m^3 for the heater

Table 3-2. Calculation steps

Step No	Step duration (days)	Total time after each step (days)	Remark
1	1	1	500 W applied
2	9	10	
3	90	100	
4	100	200	
5	200	400	
6	400	800	
7	400	1200	

3.5 Results of the base case calculation

The results are shown as contour plots of temperature after step 3 (100 days) and after step 7 (1200 days) in Figs 3-3 and 3-4. The upper pictures in the figures show the temperature distribution in a large part of the model including the rock while the lower pictures show only the engineering parts (no rock).

Fig 3-5 shows the temperature distribution along lines a1-b1, a2-b2 and a3-b3 (see Fig 1-1) at different times.

The results show that

1. the maximum temperature is as high as 225 °C
2. the temperature distribution in the intended plateau region is rather uneven
3. the temperature along line a2-b2 (sand/bentonite interface) is a few degrees below 100 °C in the sand section but 20 degrees higher in the section with only bentonite
4. the maximum temperature in the bentonite is as high as 180 °C

It is interesting to study the heat flux in order to try to understand the reasons for the uneven temperature distribution. Fig 3-6 shows the radial flux of the power through the surface at the radius 0.525 m, i.e. along line a2-b2 all the way from the top of canister 1 to 1.5 m below the bottom of the hole. The heat flux is expressed as W per meter canister length, i.e. it can be compared with the generated power 500 W/m.

Fig 3-6 also shows the corresponding axial heat flux with positive sign for flux directed upwards.

Fig 3-6 shows that the radial heat flux from the heater in the rock is higher than 500 W/m due to axial heat flux in the steel coming from canister 2. It also shows that canister 2 yields a higher heat flux than 500 W/m in spite of that it gives away heat to the heater since the axial heat flux from canister 1 is even higher. The reason for the strong heat flux from canister 1 is of course the low thermal conductivity of the surrounding sand, which yields a high temperature in canister 1, and thus a strong axial temperature gradient and a high heat flux.

4 Influence of changes in properties and design

4.1 General

The base case calculation shows that the difference in thermal conductivity of the dry sand and the bentonite causes strong temperature differences between the bentonite located outside canister 1 and 2 beyond the radius 0.525 m. In order to study how different materials, degree of saturation, and design may influence the temperature distribution a number of additional calculations have been performed. The following variations of the base case have been studied:

1. Thermal conductivity of the sand
2. Thermal conductivity of the bentonite
3. Outer diameter of the sand filling
4. Thickness of the canister walls
5. Length of the heater in the rock
6. Diameter of the heater in the rock
7. Horizontal isolation between the bentonite part and the rock
8. Horizontal isolation between the bentonite/sand part and the bentonite part
9. Different power in canister 1 and canister 2
10. Horizontal isolation between both the bentonite/sand part and the bentonite part and between the bentonite part and the rock

The thermal properties of the materials in the base case and the different variations are shown in Table 4-1. The changes in thickness of the canister wall (case 4) and diameter of the heater (case 6) have been done by changing the thermal properties and *not the geometry.*

Table 4-1. Thermal properties for the analyses of variance

Material (base case and variation)	λ (W/m,K)	c (Ws/kg,K)	ρ (kg/m^3)	Remark (b=base case v=variation)
Concrete	1.7	900	2400	b
Canister 1	50	460	7850	b: 3 cm wall
" (case 4a)	17	153	7850	v: (1 cm wall)
" (case 4b)	83	767	7850	v: (5 cm wall)
Canister 2	50	460	7850	b: 3 cm wall
" (case 4a)	17	153	7850	v: (1 cm wall)
" (case 4b)	83	767	7850	v: (5 cm wall)
Heater	50	460	7850	b: D=5.4 cm
" (case 6a)	100	920	7850	v: (D=10.8 cm)
" (case 6b)	25	230	7850	v: (D=2.7 cm)
Rock	2.6	800	2600	b
Sand	0.3	800	1800	b: dry
" (case 1a)	2.0	1600	2100	v: mixture
Isolation bentonite/rock	1.2	1300	2000	b: no isolation (bentonite)
" (case 7a)	0.05	1000	300	v: 10 cm isolation)
Isolation sand /bentonite	0.3	800	1800	b: no isolation (sand)
" (case 8a)	0.05	1000	300	v: 10 cm isolation)
Bentonite	1.2	1300	2000	b: w=17%
" (case 2a)	1.3	1550	2050	v: w=28%
" (case 2b)	0.8	1100	1850	v: w=10%

4.2 Higher thermal conductivity of the sand (case 1a)

In the base case the sand is assumed to be dry. If the thermal conductivity can be increased with some admixture the temperatures will be quite different. In this case the thermal conductivity of the sand is assumed to be 2.0 W/m, K.

Figure 4-1 shows the results as contour plots of temperature after step 7 (1200 days). Fig 4-2 shows the temperature distribution along lines a1-b1, a2-b2 and a3-b3 (see Fig 1-1) after different times. Fig 4-3 shows the radial flux of the power through the surface at the radius 0.525 m, i.e. along line a2-b2 all the way from the top of canister 1 to 1.5 m below the bottom of the hole expressed as W per meter canister length and the corresponding axial heat flux.

The results show that the variation in temperature at the same distances from the heater is only a few degrees between the radius 0.525 and the rock surface (between lines a2-b2 and a3-b3). In this case the loss of power takes place in canister 2, but the loss is not so strong that the temperature is affected very much.

The conclusion is thus that mixing the sand with some stuff that increases the thermal conductivity to 1.0-2.0 W/m, K would create the requested thermal plateau.

4.3 Wet and dry bentonite (cases 2a and 2b)

In the base case the bentonite is assumed to have the initial water content 17%. If the thermal conductivity is changed to 1.3 W/m, K it corresponds to completely water-saturated bentonite (case 2a) and if the thermal conductivity is changed to 0.8 W/m, K it corresponds to initial water content 10% (case 2b).

Completely water saturated bentonite (case 2a)

Figure 4-4 shows the results as temperature distribution along lines a1-b1, a2-b2 and a3-b3 (see Fig 1-1) after different times. The results do not differ very much from the base case since the change in properties is small

Dry bentonite (case 2b)

Figure 4-5 shows the results as contour plots of temperature after step 7 (1200 days). Fig 4-6 shows the temperature distribution along lines a1-b1, a2-b2 and a3-b3 (see Fig 1-1) after different times. Fig 4-7 shows the radial flux of the power through the surface at the radius 0.525 m, i.e. along line a2-b2 all the way from the top of canister 1 to 1.5 m below the bottom of the hole expressed as W per meter canister length and the axial heat flux in the canisters and heater.

The results show that the temperature in the bentonite along line a2-b2 increases rather much (almost 20 °C) due to the lower thermal conductivity. Otherwise the trends are similar as in the base case

4.4 Changed thickness of the sand filling (cases 3a and 3b)

In these calculations the thickness of the sand filling has been changed from 0.225 m to 0.125 m and 0.325.

Sand thickness 0.125 m (case 3a)

Figure 4-8 shows the results as contour plots of temperature after step 7 (1200 days). Fig 4-9 shows the temperature distribution along lines a1-b1, a2-b2 and a3-b3 (see Fig 1-1) after different times. Line a2-b2 is located at the sand bentonite interface that is at the radius 0.425. Fig 4-10 shows the radial flux of the power through the surface at the radius 0.425 m, i.e. along line a2-b2 all the way from the top of canister 1 to 1.5 m below the bottom of the hole expressed as W per meter canister length and the corresponding axial heat flux.

The results show that the temperature at the sand/bentonite interface is high and have the same uneven distribution in the zone between lines a2-b2 and a3-b3.

Sand thickness 0.325 m (case 3b)

Figure 4-11 shows the results as contour plots of temperature after step 7 (1200 days). Fig 4-12 shows the temperature distribution along lines a1-b1, a2-b2 and a3-b3 (see Fig 1-1) after different times. Line a2-b2 is located at the sand bentonite interface that is at the radius 0.625. Fig 4-13 shows the radial flux of the power through the surface at the radius 0.625 m, i.e. along line a2-b2 all the way from the top of canister 1 to 1.5 m below the bottom of the hole expressed as W per meter canister length and the corresponding axial heat flux.

The results show that the temperatures at the sand bentonite interface is lower due to the larger radius but have the same uneven distribution in the zone between lines a2-b2 and a3-b3.

4.5 Changed canister wall thickness (cases 4a and 4b)

In these calculations the thickness of the canister walls has been changed from 3 cm to 1 cm and 5 cm. The change in thickness has been modeled by changing the thermal properties instead of the geometry.

Canister wall thickness 1 cm (case 4a)

Figure 4-14 shows the results as contour plots of temperature after step 7 (1200 days). Fig 4-15 shows the temperature distribution along lines a1-b1, a2-b2 and a3-b3 (see Fig 1-1) after different times. Fig 4-16 shows the radial flux of the power through the surface at the radius 0.525 m, i.e. along line a2-b2 all the way from the top of canister 1 to 1.5 m below the bottom of the hole expressed as W per meter canister length and the corresponding axial heat flux.

The results show that there is still a temperature difference at the a2-b2 line although it is a little smaller due to the lower loss of heat from canister 1 to canister 2.

Canister wall thickness 5 cm (case 4b)

In this case the temperature difference is higher than in the base case. No diagrams are shown.

4.6 Changed heater length and heater diameter (Cases 5a, 5b, and 6a)

The influence of the heater geometry has been investigated by changing the length from 3.0 m to 1.5 m and 6.0 m and by changing the diameter from 5.4 cm to 2.7 cm and 10.8 cm.

Heater length 1.5 m (case 5a)

Figure 4-17 shows the results as contour plots of temperature after step 7 (1200 days). Fig 4-18 shows the temperature distribution along lines a1-b1, a2-b2 and a3-b3 (see Fig 1-1) after different times. Fig 4-19 shows the radial flux of the power through the surface at the radius 0.525 m, i.e. along line a2-b2 all the way from the top of canister 1 to 1.5 m below the bottom of the hole expressed as W per meter canister length and the corresponding axial heat flux.

The results show that the temperature in the bentonite is reduced with about 5 degrees, not because of a reduced radial heat flux but mainly because of a reduced rock temperature.

Heater length 6.0 m (case 5b)

Figure 4-20 shows the results as contour plots of temperature after step 7 (1200 days). Fig 4-21 shows the temperature distribution along lines a1-b1, a2-b2 and a3-b3 (see Fig 1-1) after different times. Fig 4-22 shows the radial flux of the power through the

surface at the radius 0.525 m, i.e. along line a2-b2 all the way from the top of canister 1 to 1.5 m below the bottom of the hole expressed as W per meter canister length and the corresponding axial heat flux.

The results show that the temperature in the bentonite is increased with about 5 degrees, not because of an increased radial heat flux but mainly because of an increased rock temperature.

Heater diameters 2.7 cm and 10.8 cm (cases 6a and 6b)

The influence of the heater diameter, which was modeled by changing the thermal properties, was negligible. No results are shown.

4.7 Horizontal isolation between different parts (cases 7a and 8a)

In order to avoid the influence of axial heat flux some calculations with horizontal isolations between the different parts of canisters and buffers have been made. The isolations are covering the entire hole and the canisters as well. The thickness is 10 cm and the thermal conductivity is assumed to be 0.05 W/m, K.

Horizontal isolation between the bentonite part and the rock (case 7a)

Figure 4-23 shows the results as contour plots of temperature after step 7 (1200 days). Fig 4-24 shows the temperature distribution along lines a1-b1, a2-b2 and a3-b3 (see Fig 1-1) after different times. Fig 4-25 shows the radial flux of the power through the surface at the radius 0.525 m, i.e. along line a2-b2 all the way from the top of canister 1 to 1.5 m below the bottom of the hole expressed as W per meter canister length and the corresponding axial heat flux.

The results show that the influence of isolation in the bottom of the deposition hole is rather small.

Horizontal isolation between the bentonite/sand part and the bentonite part (case 8a)

Figure 4-26 shows the results as contour plots of temperature after step 7 (1200 days). Fig 4-27 shows the temperature distribution along lines a1-b1, a2-b2 and a3-b3 (see Fig 1-1) after different times. Fig 4-28 shows the radial flux of the power through the surface at the radius 0.525 m, i.e. along line a2-b2 all the way from the top of canister 1 to 1.5 m below the bottom of the hole expressed as W per meter canister length and the corresponding axial heat flux.

The results show that the influence of isolation in the centre between the bentonite/sand part and the bentonite part is dramatic. The difference in temperature along lines a2-b2 and a3-b3 is only a few degrees and the radial heat flux through the lower half of the sand/bentonite interface is rather constant and close to 500 W/m.

The conclusion is thus that isolation between these parts would create the desired temperature plateau.

4.8 Different power in the canisters (cases 9a and 9b)

In order to study if different power in the canisters can compensate the axial loss in power, two cases have been considered.

Reduced power of canister 2 (case 9a)

The power of canister 2 is reduced to 400 W/m.

Figure 4-29 shows the results as contour plots of temperature after step 7 (1200 days). Fig 4-30 shows the temperature distribution along lines a1-b1, a2-b2 and a3-b3 (see Fig 1-1) after different times. Fig 4-31 shows the radial flux of the power through the surface at the radius 0.525 m, i.e. along line a2-b2 all the way from the top of canister 1 to 1.5 m below the bottom of the hole expressed as W per meter canister length and the corresponding axial heat flux.

The results show that the overall temperature in the bentonite is decreased and that the temperature difference along lines a2-b2 and a3-b3 is reduced a little but far from enough.

Further reduced power of canister 2 and increased power of canister 1 (case 9b)

The power of canister 2 is reduced to 250 W/m and the power in canister 1 is increased to 600 W/m.

Figure 4-32 shows the results as contour plots of temperature after step 7 (1200 days). Fig 4-33 shows the temperature distribution along lines a1-b1, a2-b2 and a3-b3 (see Fig 1-1) after different times. Fig 4-34 shows the radial flux of the power through the surface at the radius 0.525 m, i.e. along line a2-b2 all the way from the top of canister 1 to 1.5 m below the bottom of the hole expressed as W per meter canister length and the corresponding axial heat flux.

The results show that the level of temperature in the two parts along line a2-b2 is the same but also that there is a rather strong temperature difference in each part especially the bentonite part. The situation is improved but not good.

4.9 Double isolation and no heater (case 10a)

The effect of having both isolations (both case 7a and 8a) and no heater has been studied in case 10a).

Figure 4-35 shows the results as contour plots of temperature after step 7 (1200 days). Fig 4-36 shows the temperature distribution along lines a1-b1, a2-b2 and a3-b3 (see Fig 1-1) after different times. Fig 4-37shows the radial flux of the power through the surface at the radius 0.525 m, i.e. along line a2-b2 all the way from the top of canister 1 to 1.5 m below the bottom of the hole expressed as W per meter canister length and the corresponding axial heat flux.

The results show that there is still a temperature difference along line a2-b2 but it is not very large (6 degrees) and that the radial heat flux is close to 500 W/m for large parts of the canisters. However the temperature difference at the rock surface (line a3-b3) is rather large due to cooling from the rock below the deposition hole.

5 Conclusions

This study yields the following conclusions:

1. The influence of axial heat flow in the canisters and surrounding material is strong due to the difference in thermal conductivity of the dry sand and the bentonite and leads to that there will be no thermal plateau in the desired zone of the bentonite
2. It is difficult to compensate the temperature gradients by having different power in the canisters
3. The length and thickness of the heater in the rock is not important
4. The thickness of the canisters plays a role but is not crucial
5. The heater in the rock below the deposition hole cannot be excluded by isolation due to the cooling of the rock
6. The only two ways to reach the desired thermal plateau seems to be to either apply horizontal isolation between the different parts or to adjust the thermal conductivity of the sand

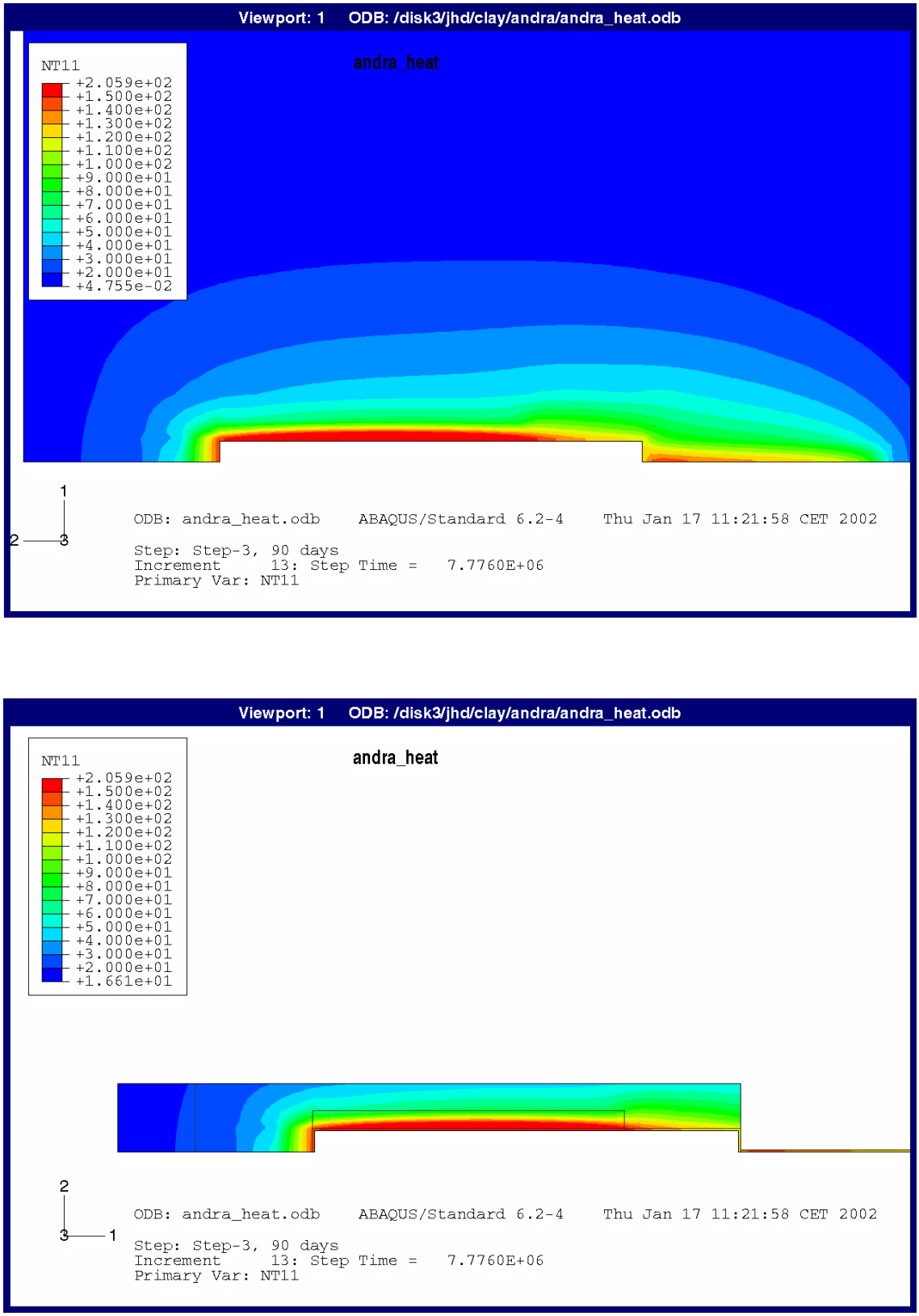

Figure 3-3. *Base case. Contour plots of the temperature (°C) distribution after 100 days in the rock and the excavated parts (upper) and solely in the excavated parts (rotated 90 degrees)*

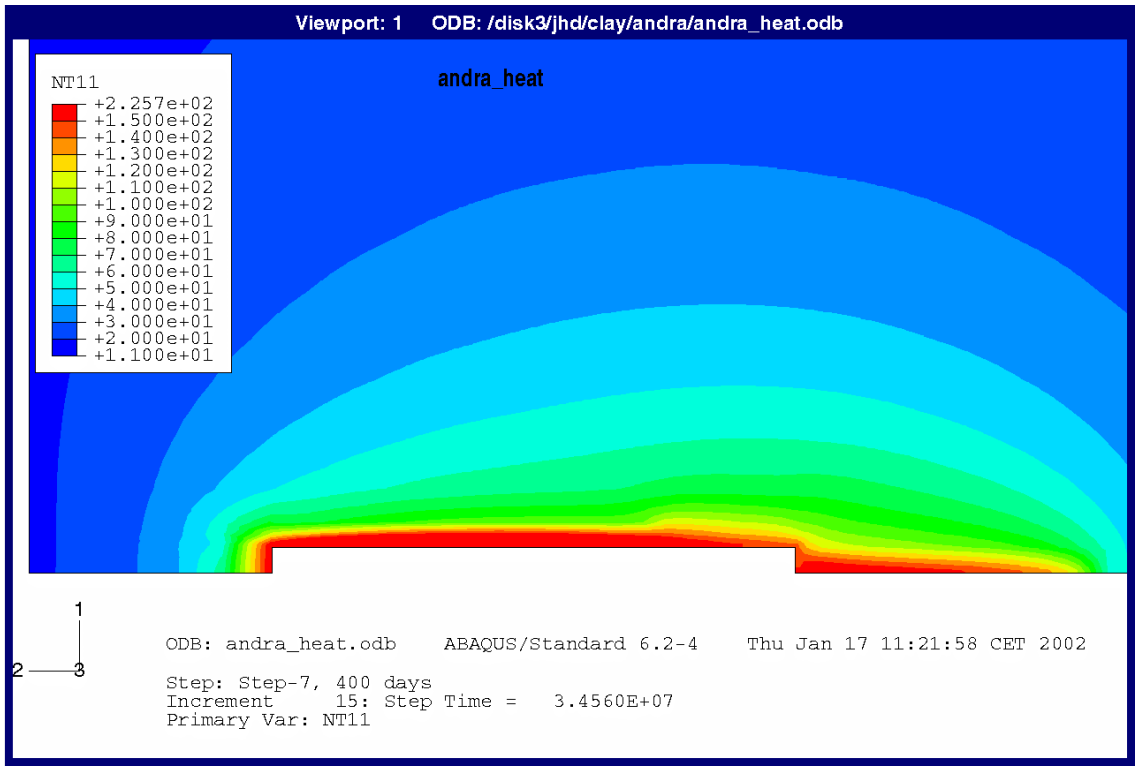

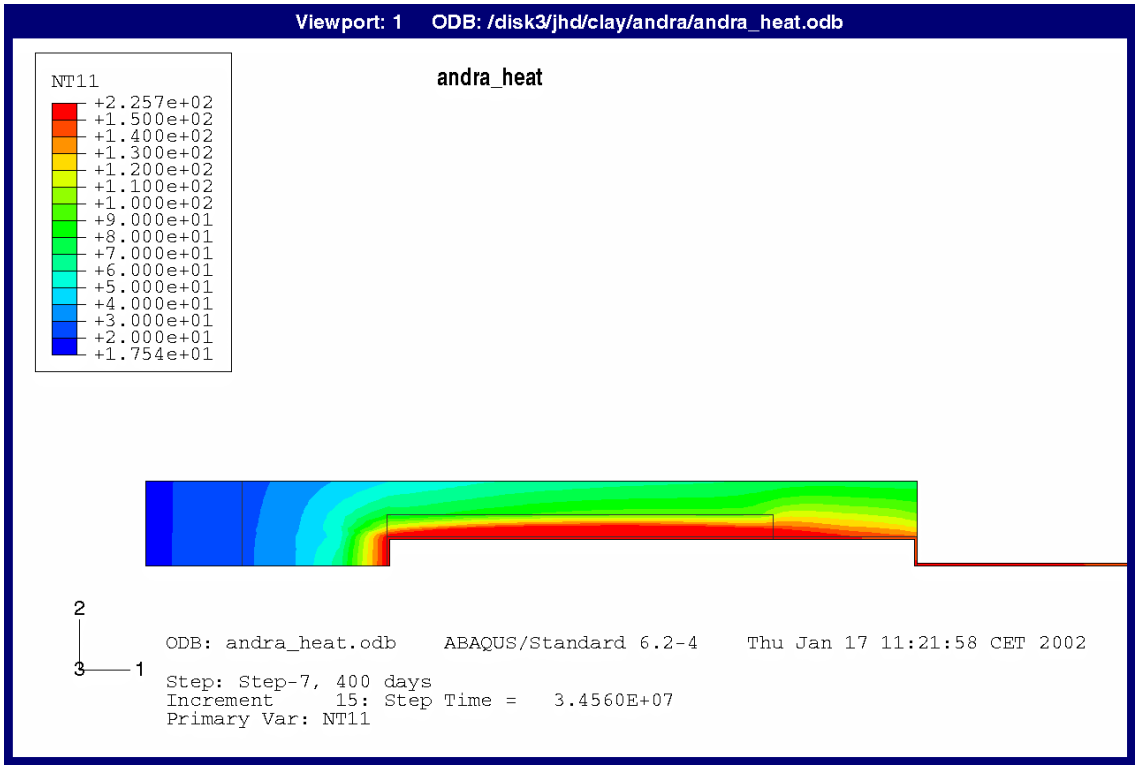

Figure 3-4. *Base case. Contour plots of the temperature (°C) distribution after 1200 days in the rock and the excavated parts (upper) and solely in the excavated parts (lower) (rotated 90 degrees)*

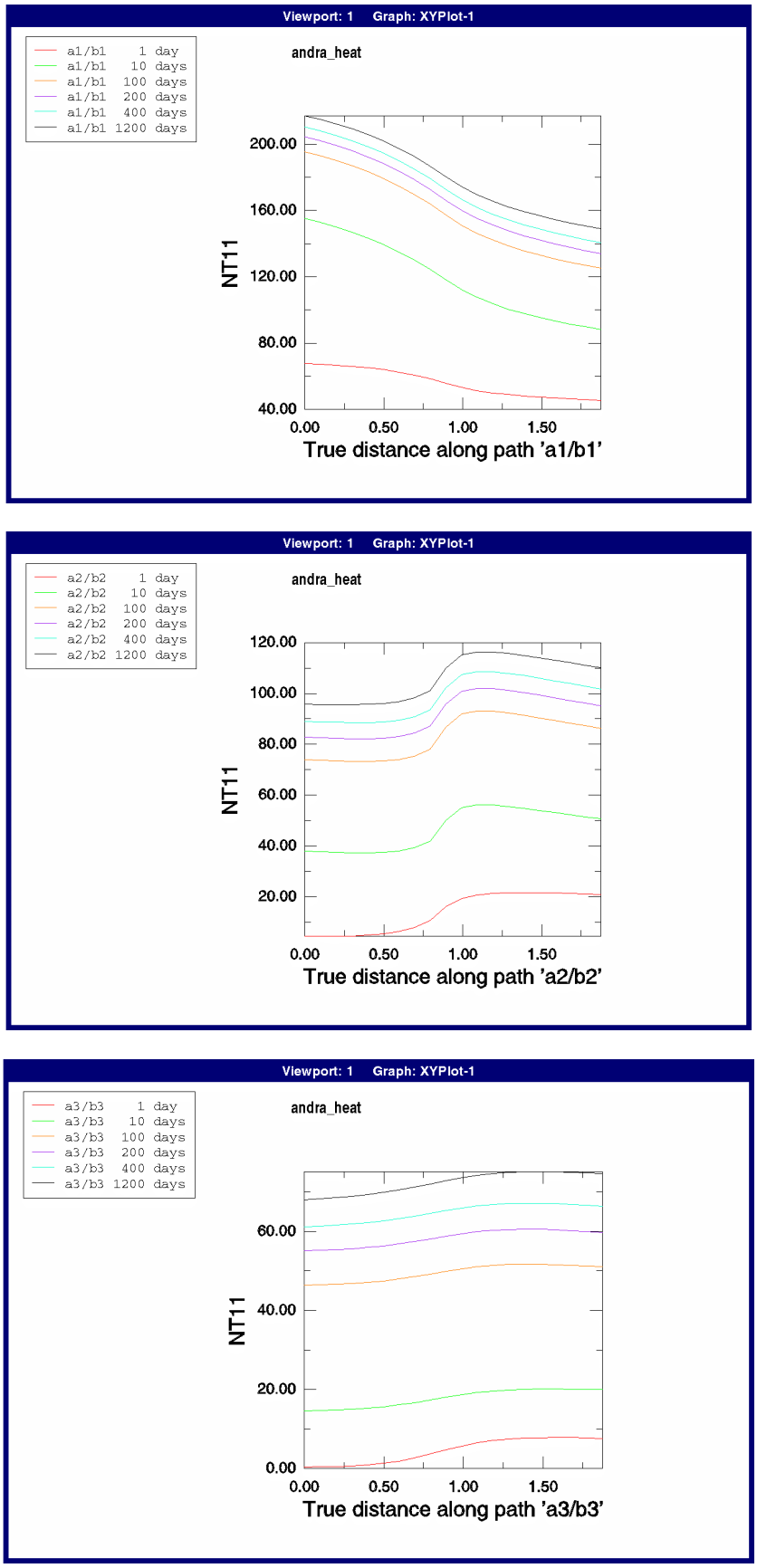

Figure 3-5. *Base case. Temperature (℃) distribution between points a1 and b1, a2 and b2, and a3 and b3 at different times*

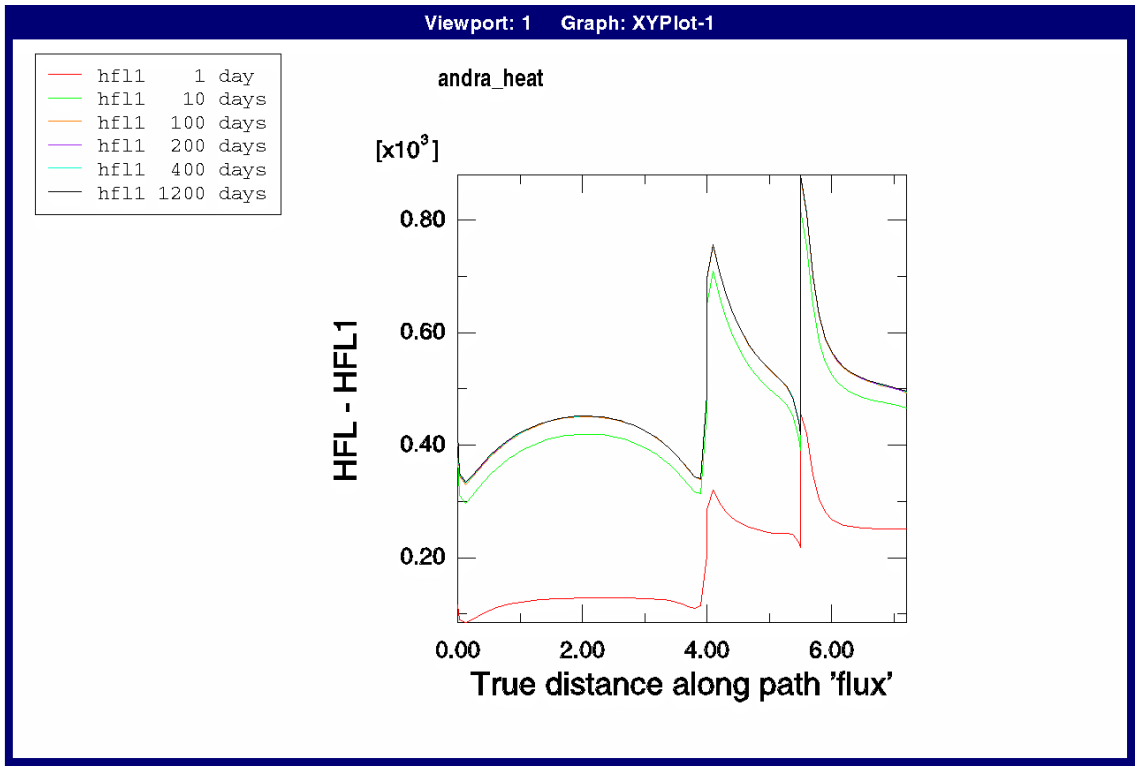

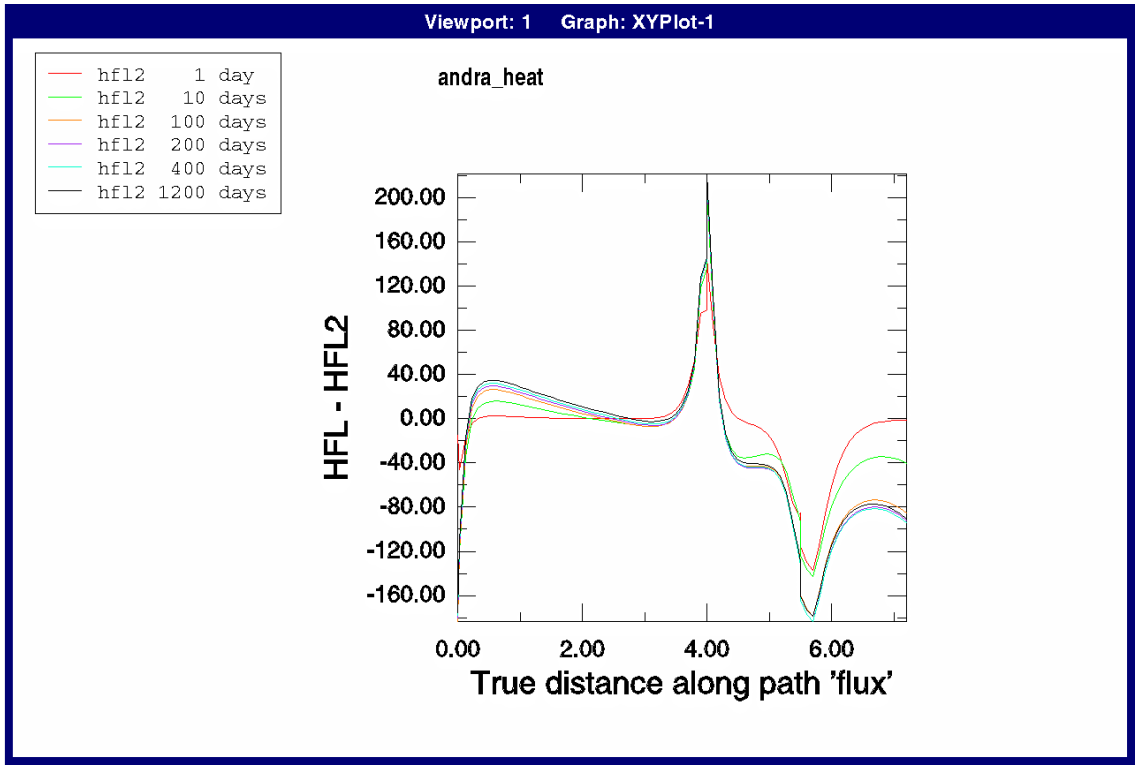

Figure 3-6. *Base case. Radial heat flux (W/m) through the surface at the radius 0.525 m (upper) and corresponding axial heat flux (lower) as a function of the distance (m) from the top of canister 1*

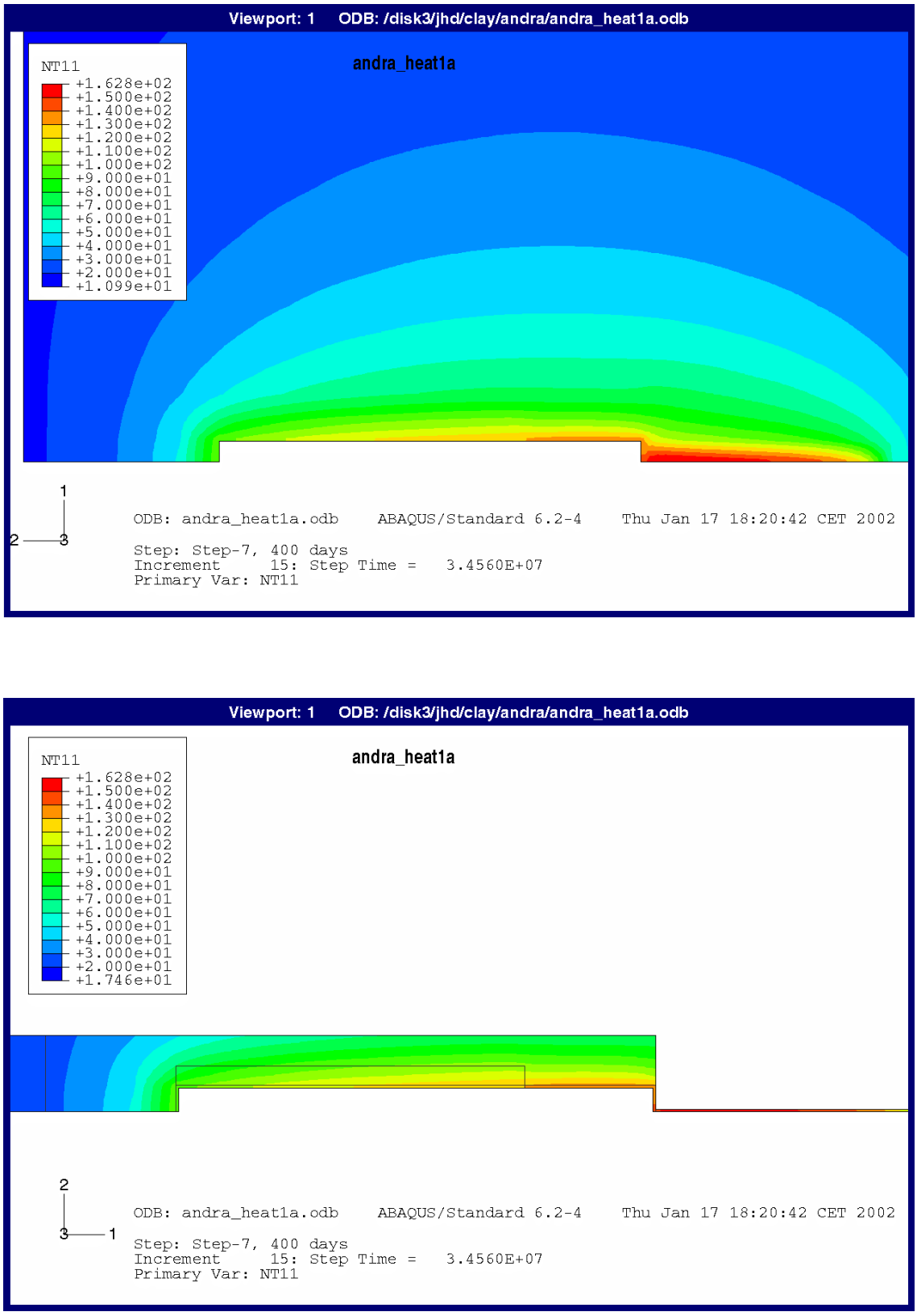

Figure 4-1. *Case 1a (increased λ_{sand}). Contour plots of the temperature (°C) distribution after 1200 days in the rock and the excavated parts (upper) and solely in the excavated parts (lower) (rotated 90 degrees)*

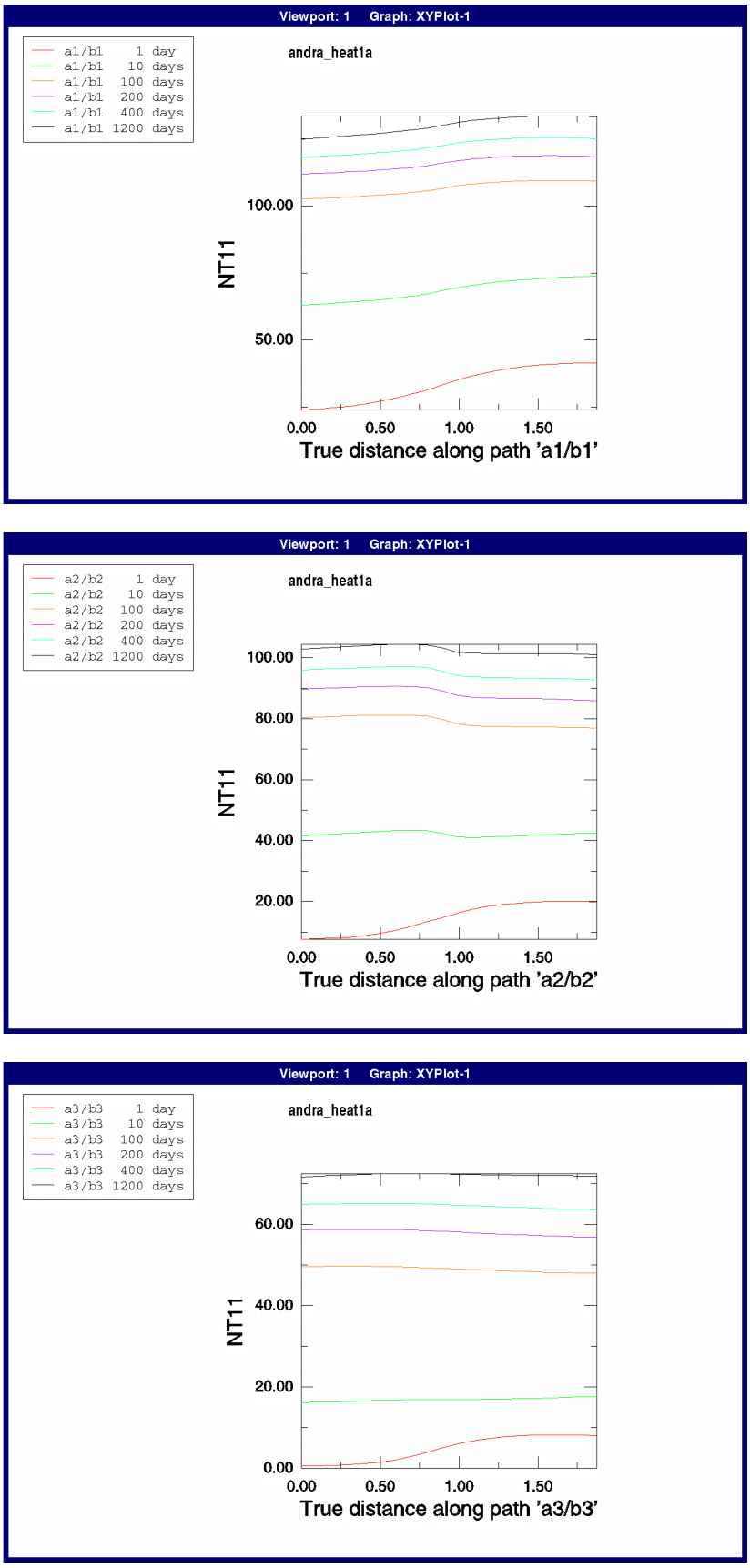

Figure 4-2. *Case 1a (increased λ_{sand}). Temperature (°C) distribution between points a1 and b1, a2 and b2, and a3 and b3 at different times*

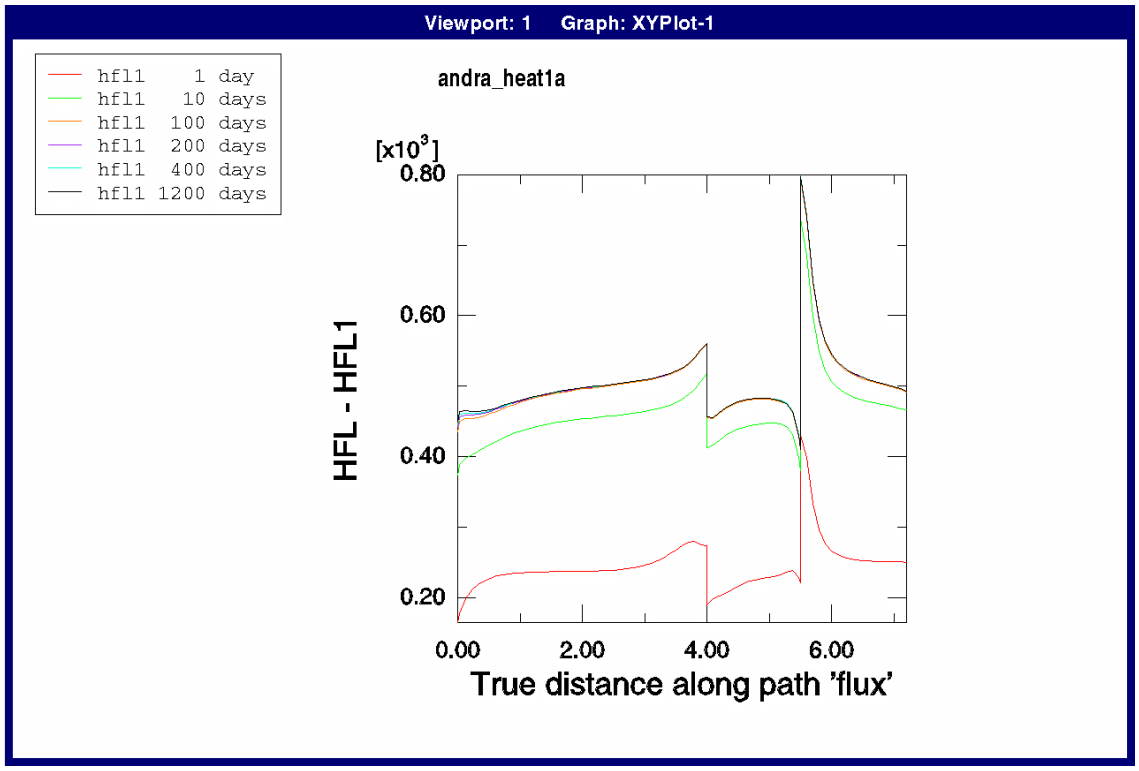

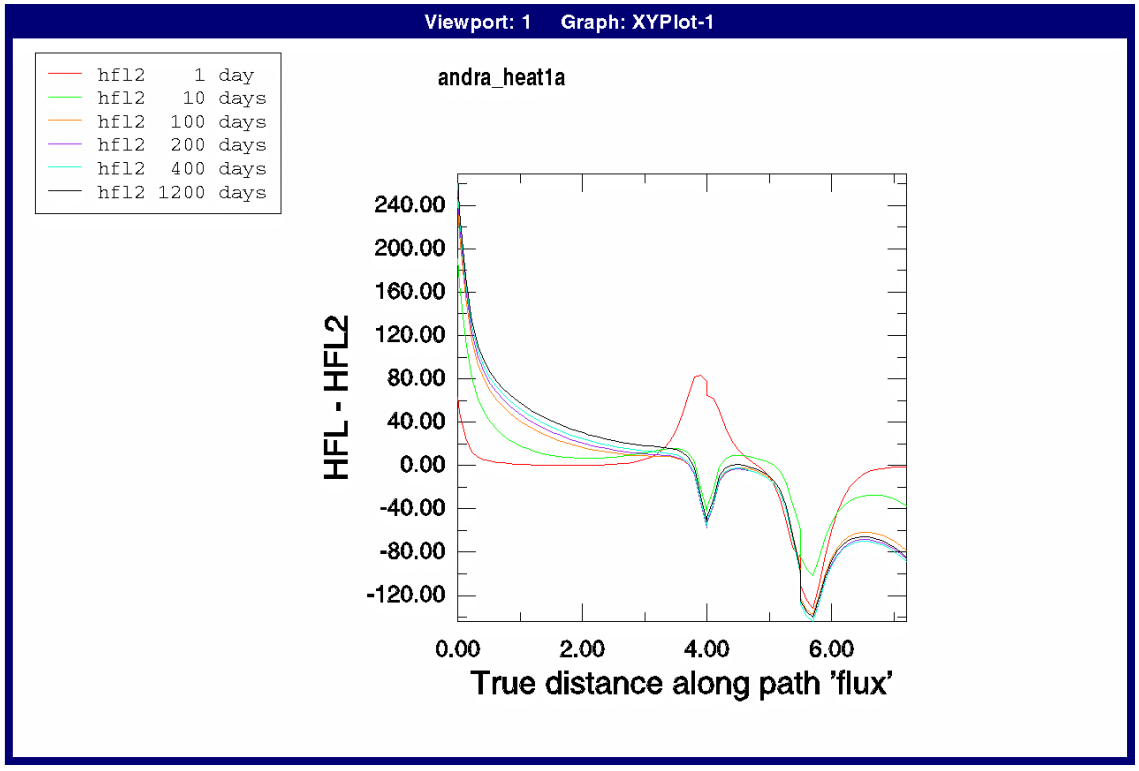

Figure 4-3. *Case 1a (increased λ_{sand}). Radial heat flux (W/m) through the surface at the radius 0.525 m (upper) and corresponding axial heat flux (lower) as a function of the distance (m) from the top of canister 1*

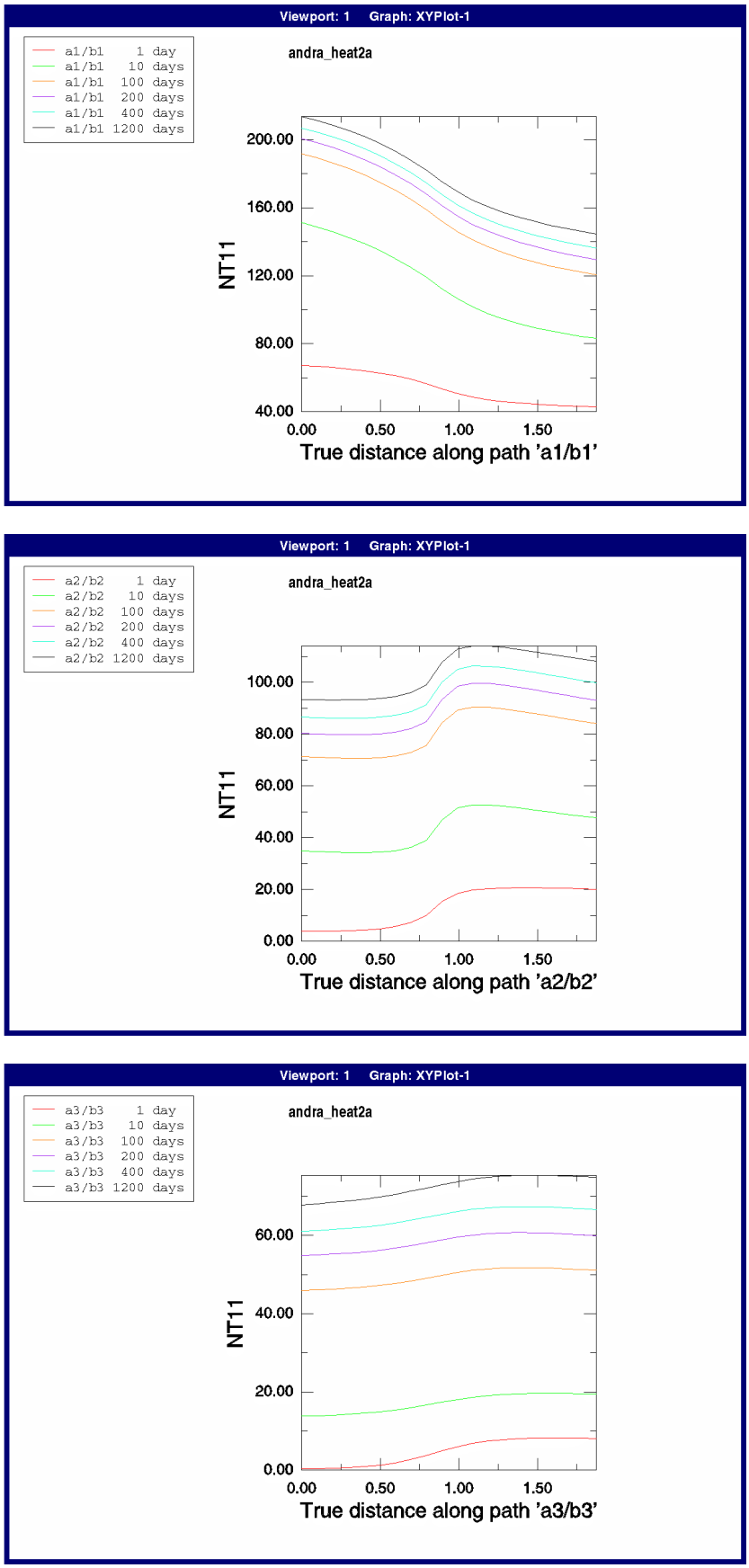

Figure 4-4. *Case 2a (wet bentonite). Temperature (°C) distribution between points a1 and b1, a2 and b2, and a3 and b3 at different times*

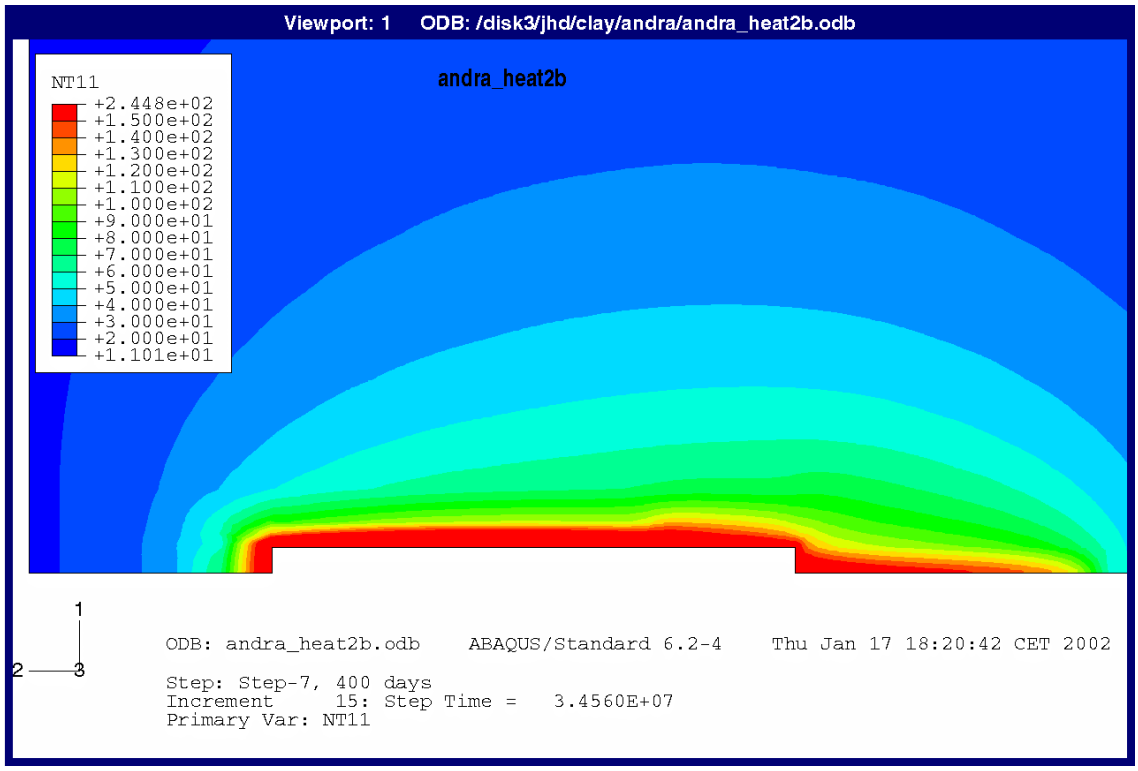

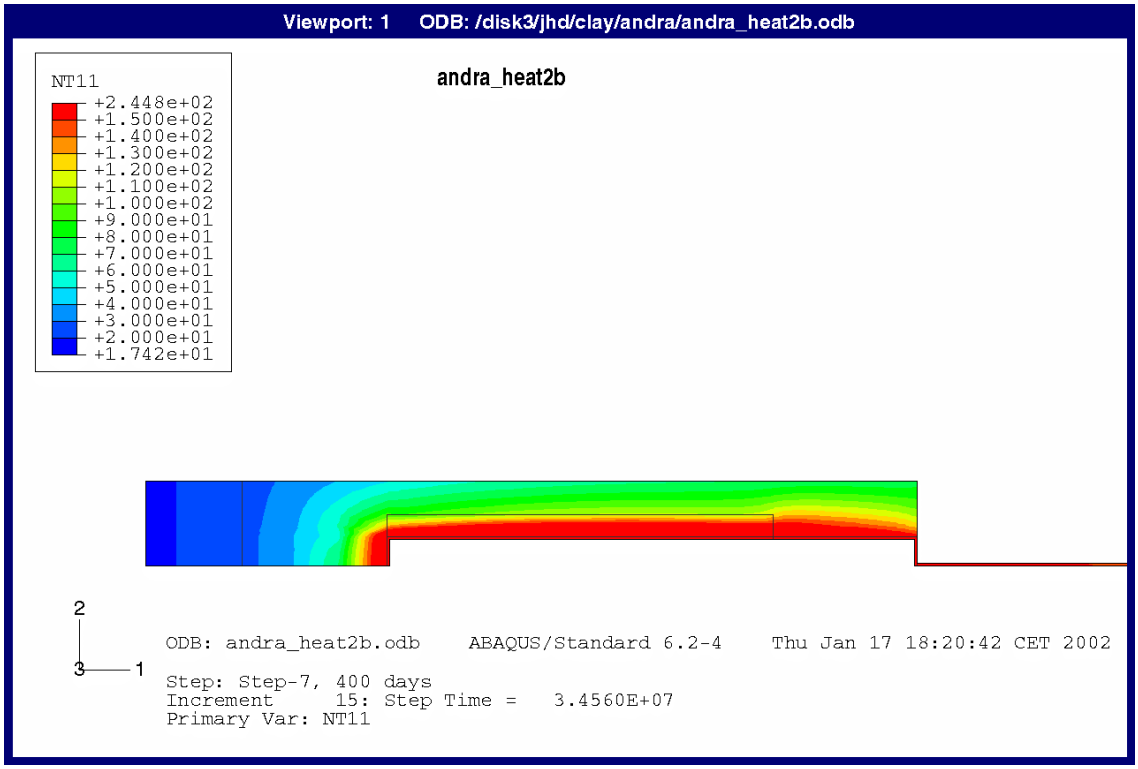

Figure 4-5. *Case 2b (dry bentonite). Contour plots of the temperature (°C) distribution after 1200 days in the rock and the excavated parts (upper) and solely in the excavated parts (lower) (rotated 90 degrees)*

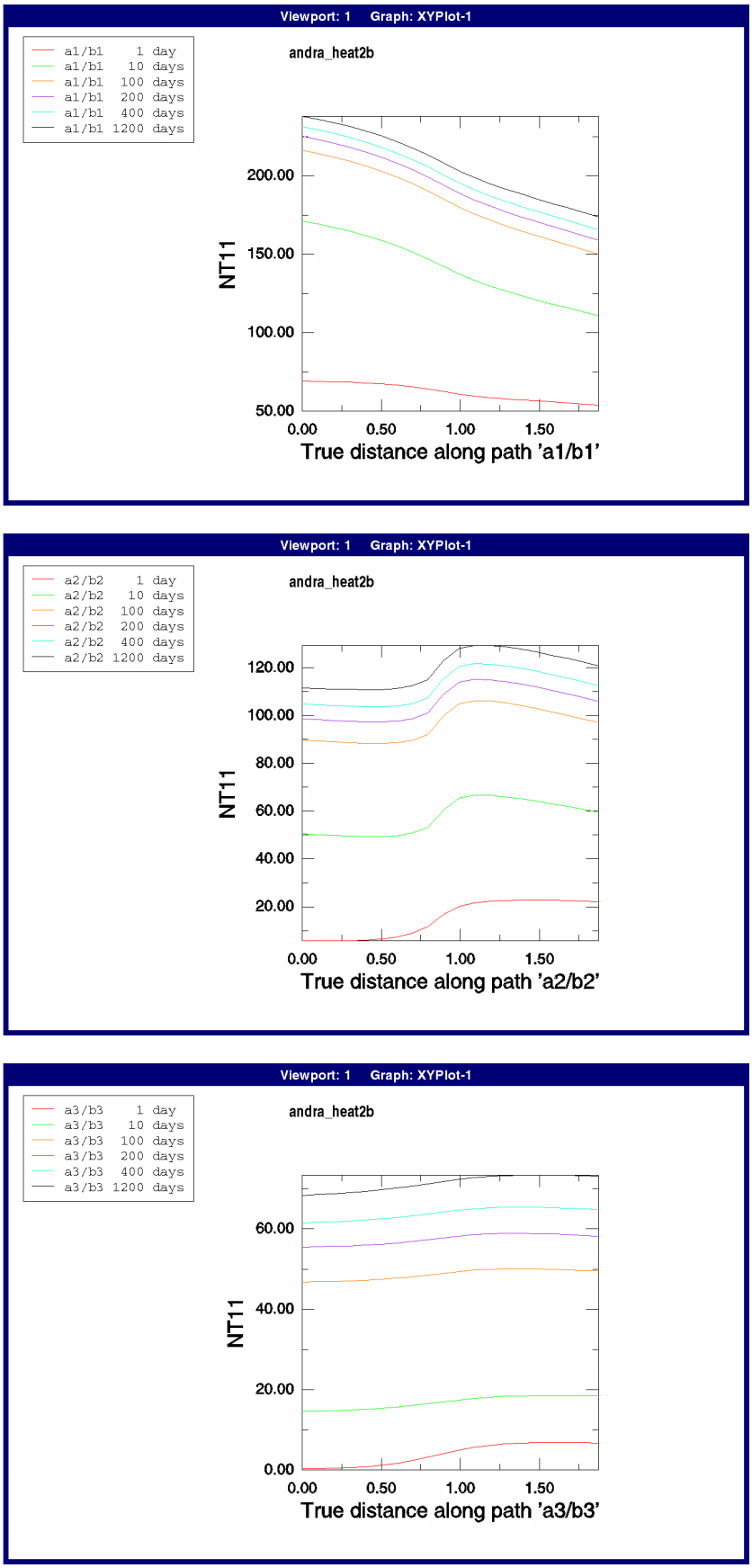

Figure 4-6. *Case 2b (dry bentonite). Temperature (°C) distribution between points a1 and b1, a2 and b2, and a3 and b3 at different times*

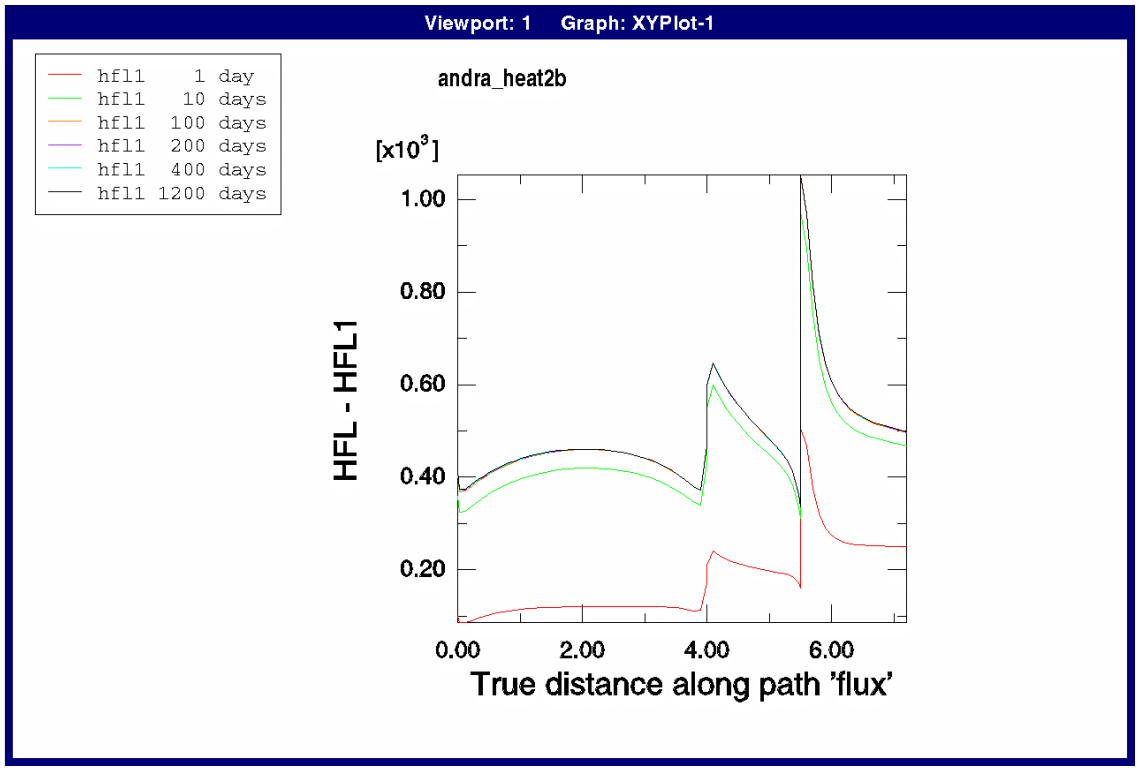

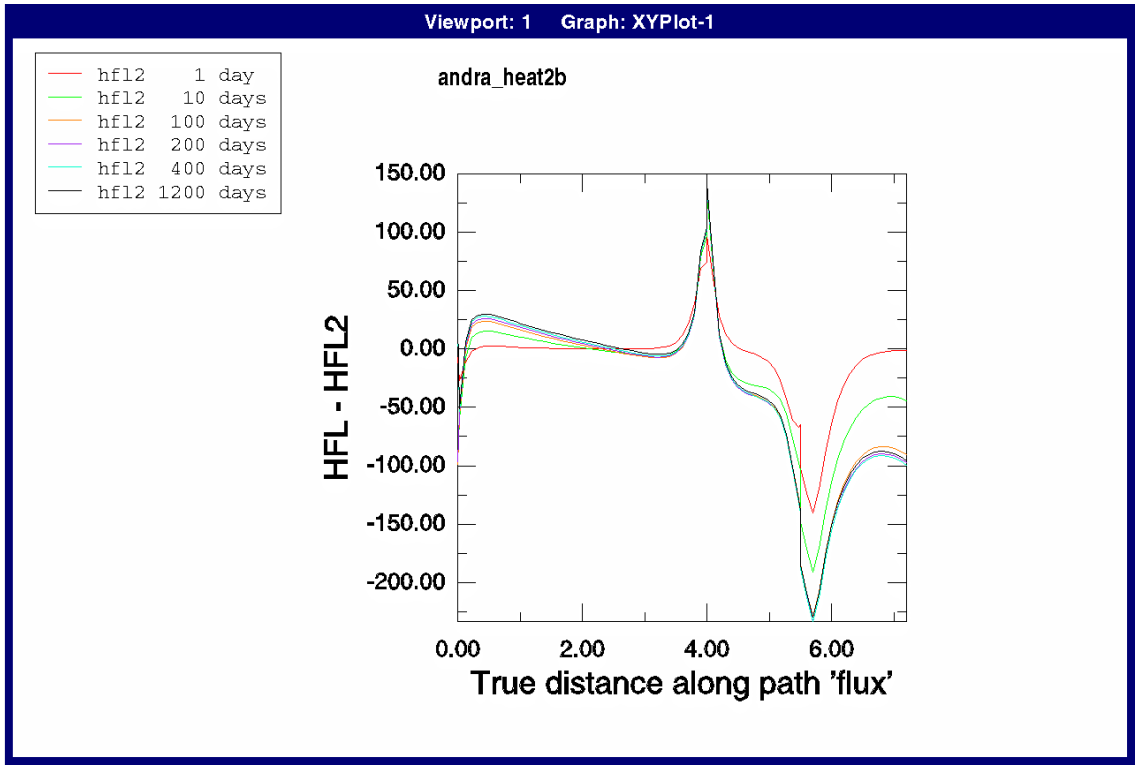

Figure 4-7. *Case 2b (dry bentonite). Radial heat flux (W/m) through the surface at the radius 0.525 m (upper) and corresponding axial heat flux (lower) as function of the distance (m) from the top of canister 1*

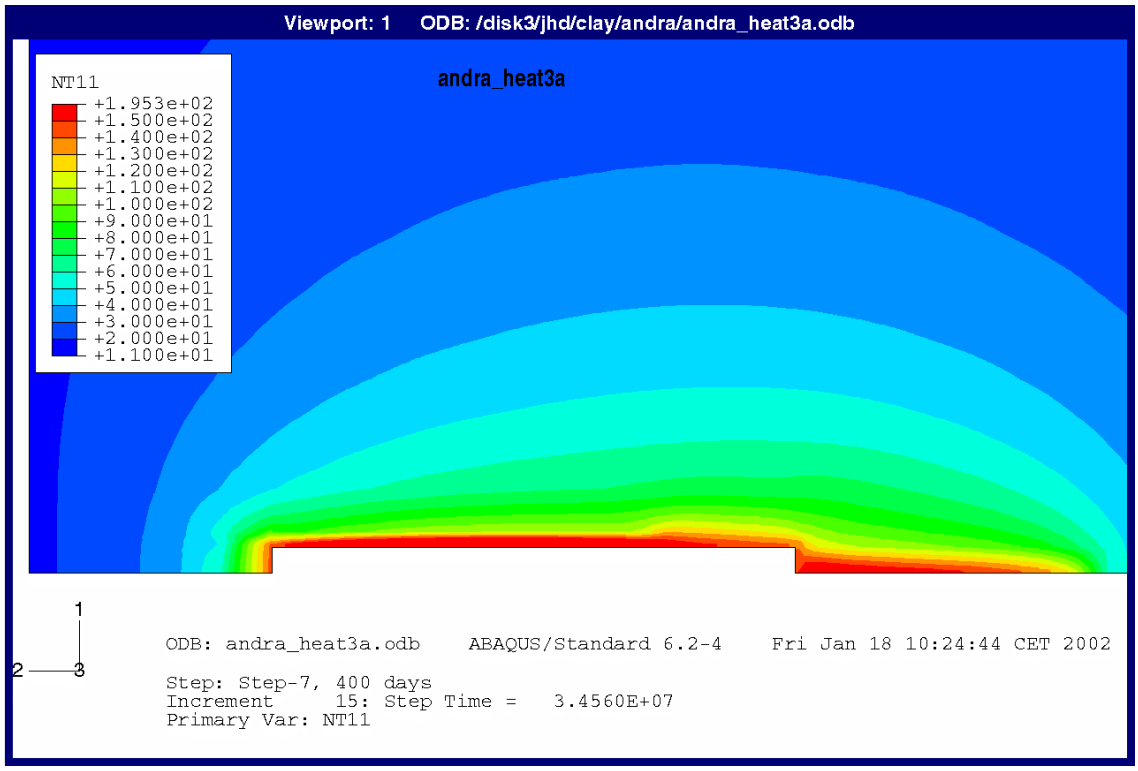

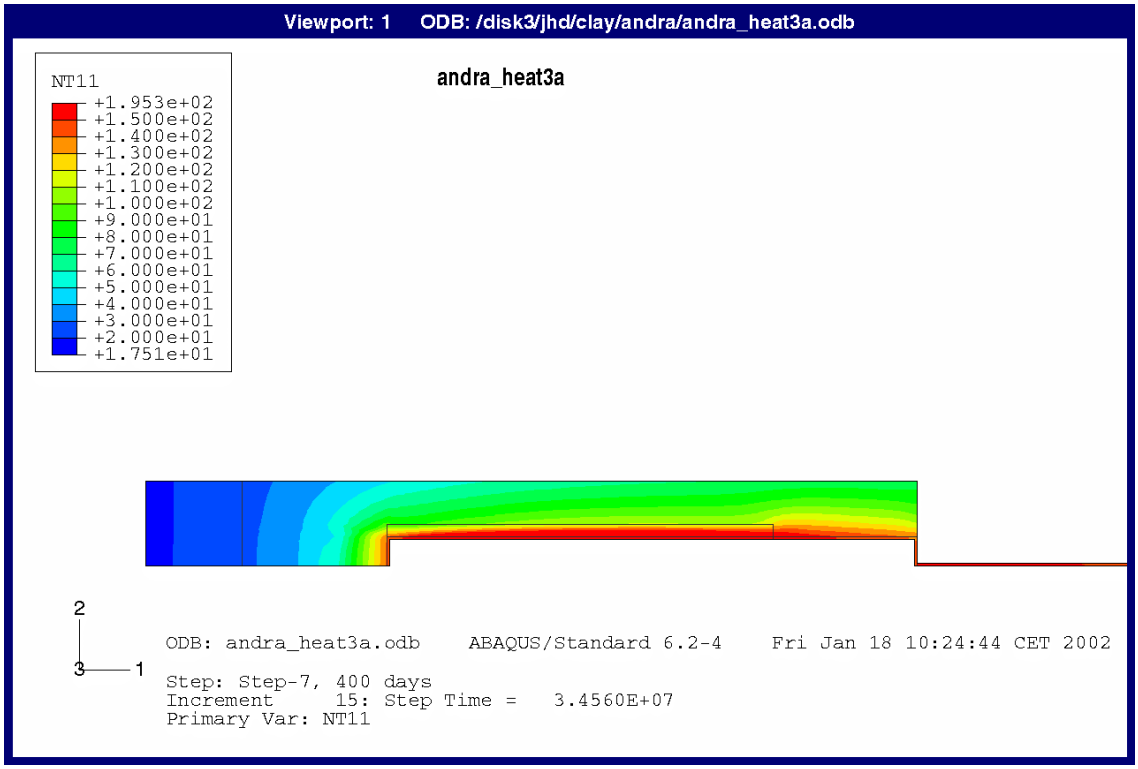

Figure 4-8. *Case 3a (thin sand layer). Contour plots of the temperature (°C) distribution after 1200 days in the rock and the excavated parts (upper) and solely in the excavated parts (lower) (rotated 90 degrees)*

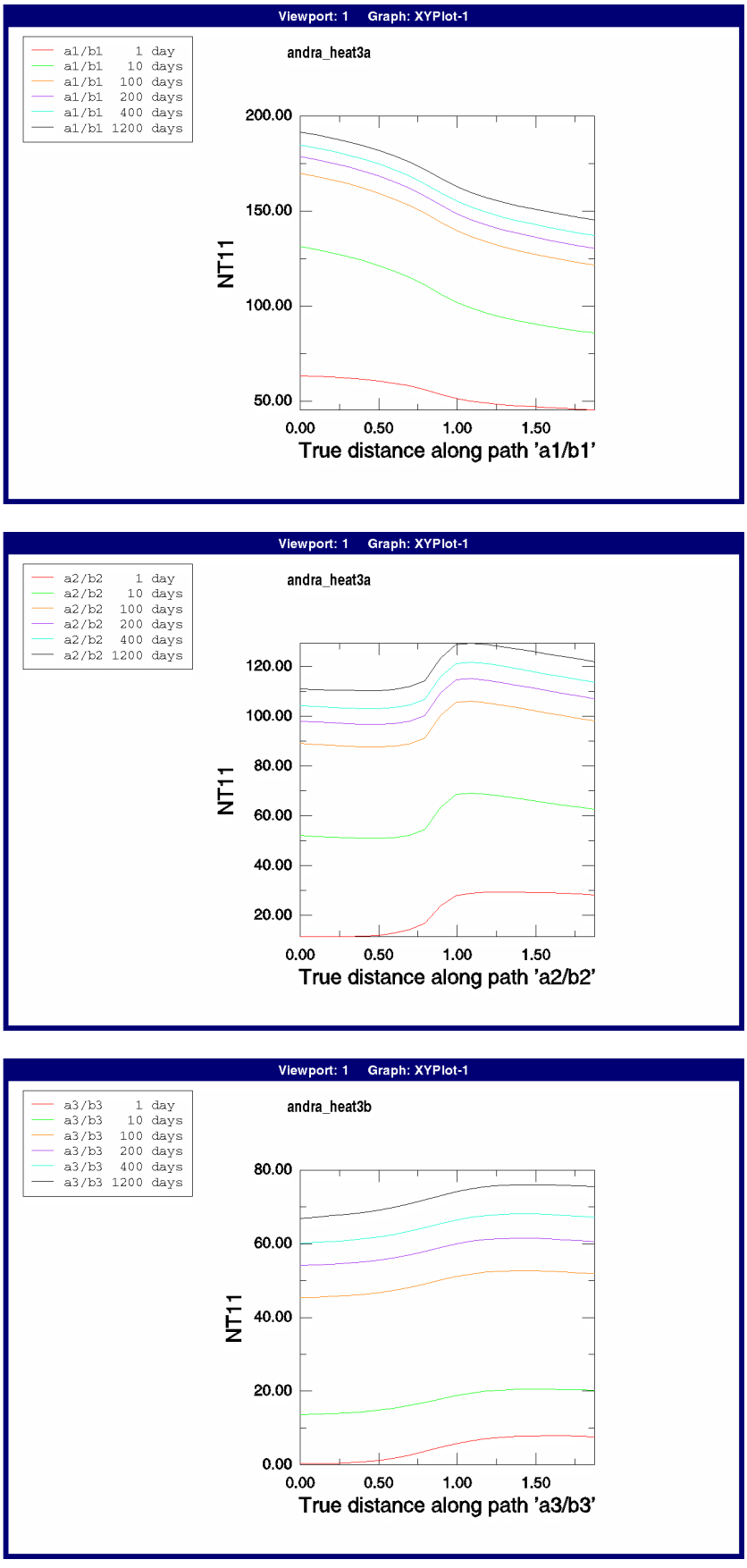

Figure 4-9. *Case 3a (thin sand layer). Temperature (°C) distribution between points a1 and b1, a2 and b2, and a3 and b3 at different times*

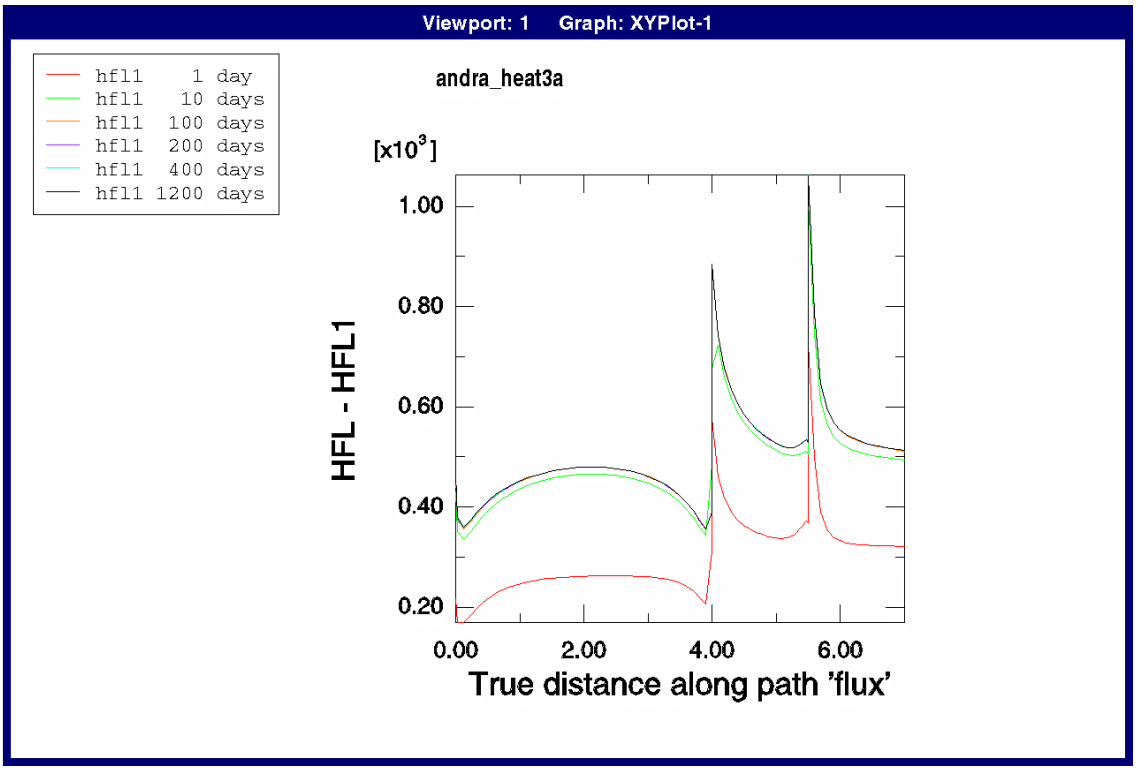

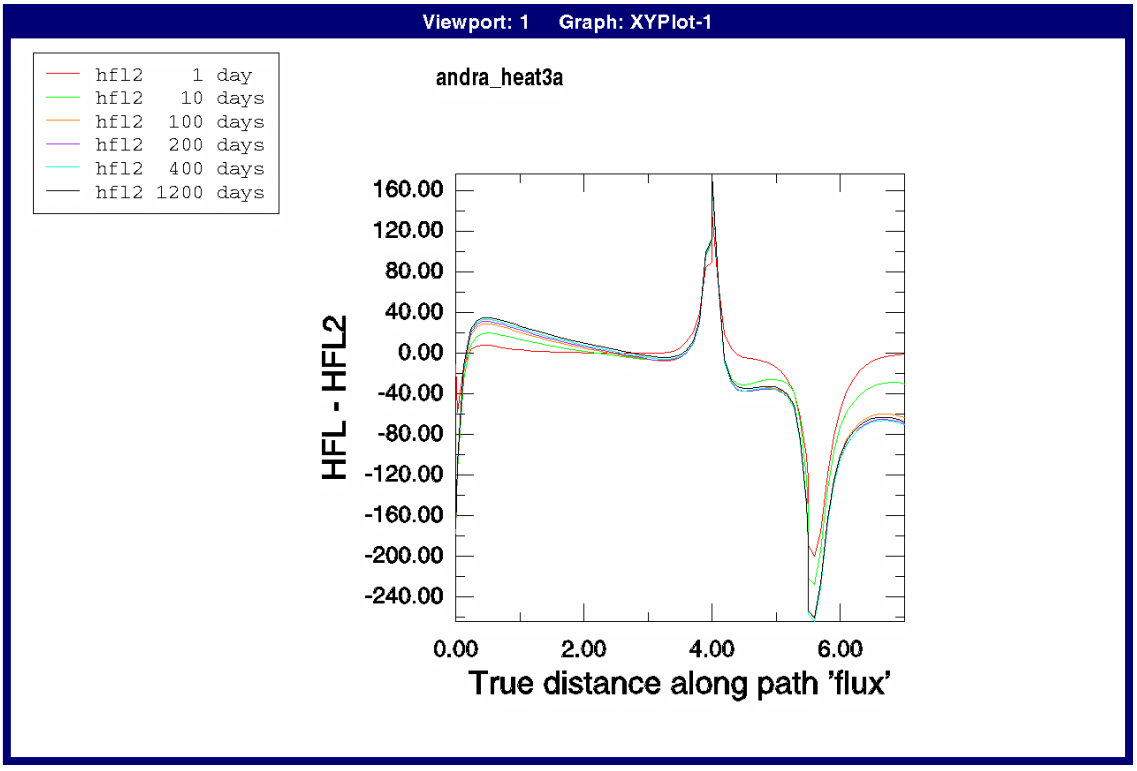

Figure 4-10. *Case 3a (thin sand layer). Radial heat flux (W/m) through the surface at the radius 0.425 m (upper) and corresponding axial heat flux (lower) as function of the distance (m) from the top of canister 1*

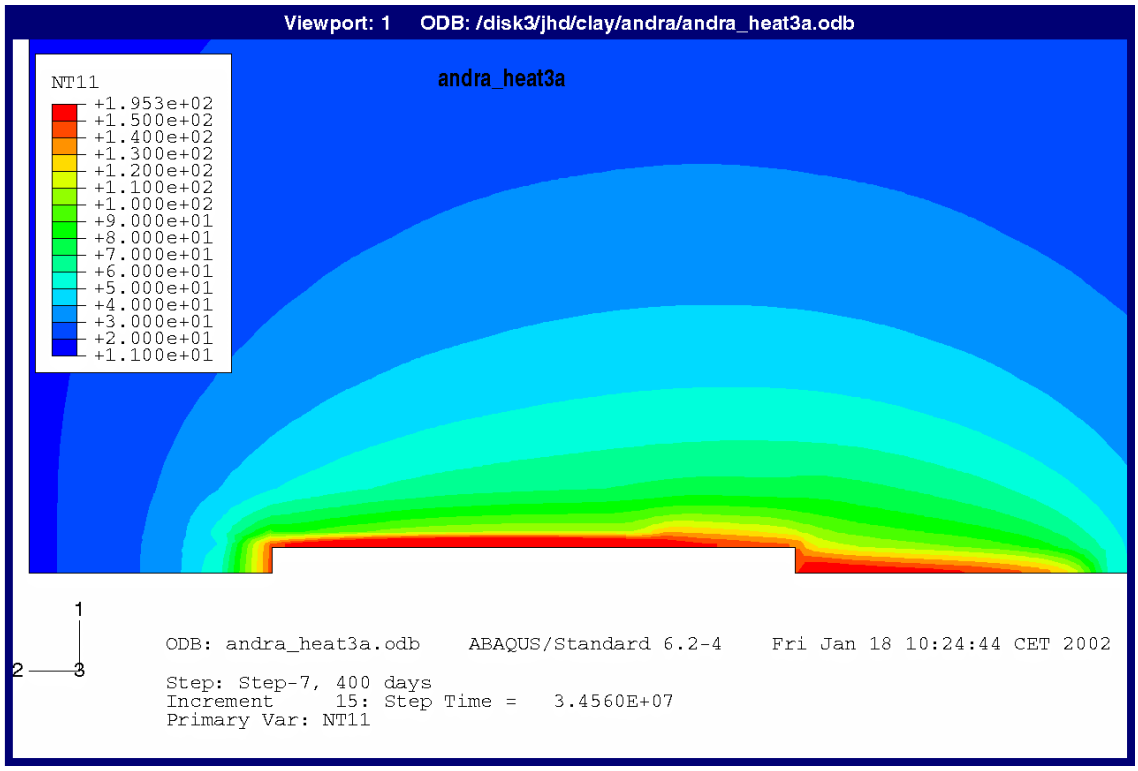

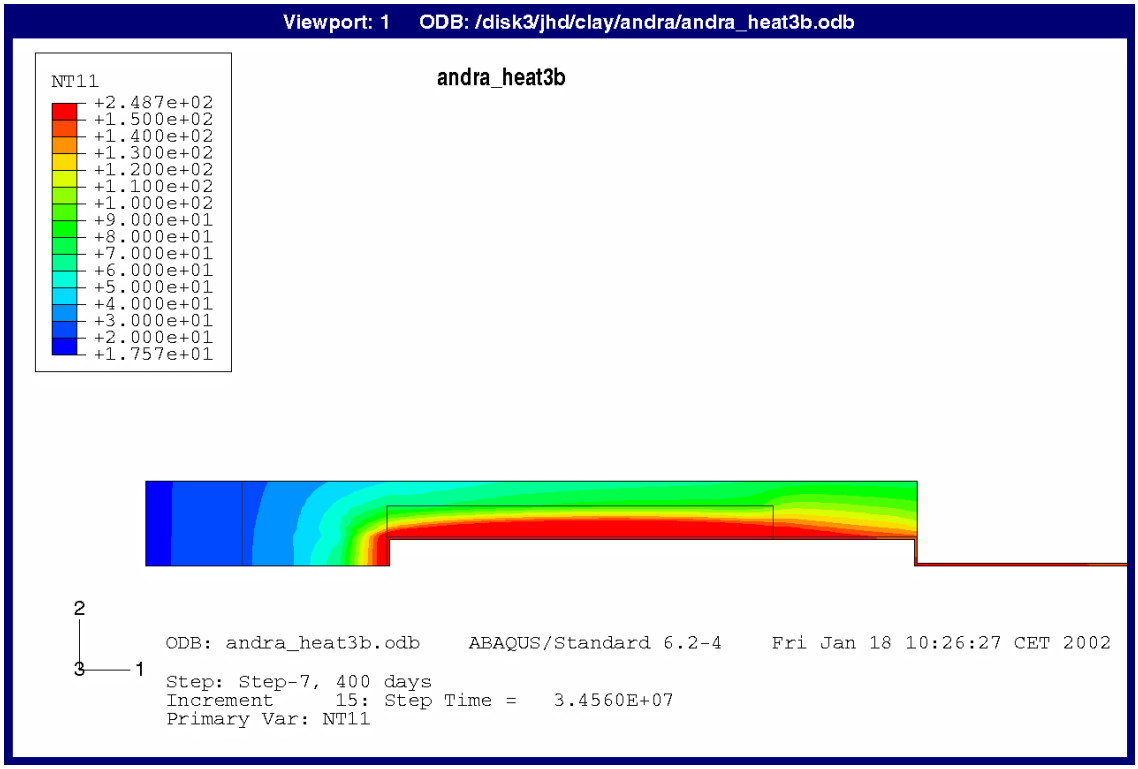

Figure 4-11. *Case 3b (thick sand layer). Contour plots of the temperature (°C) distribution after 1200 days in the rock and the excavated parts (upper) and solely in the excavated parts (lower) (rotated 90 degrees)*

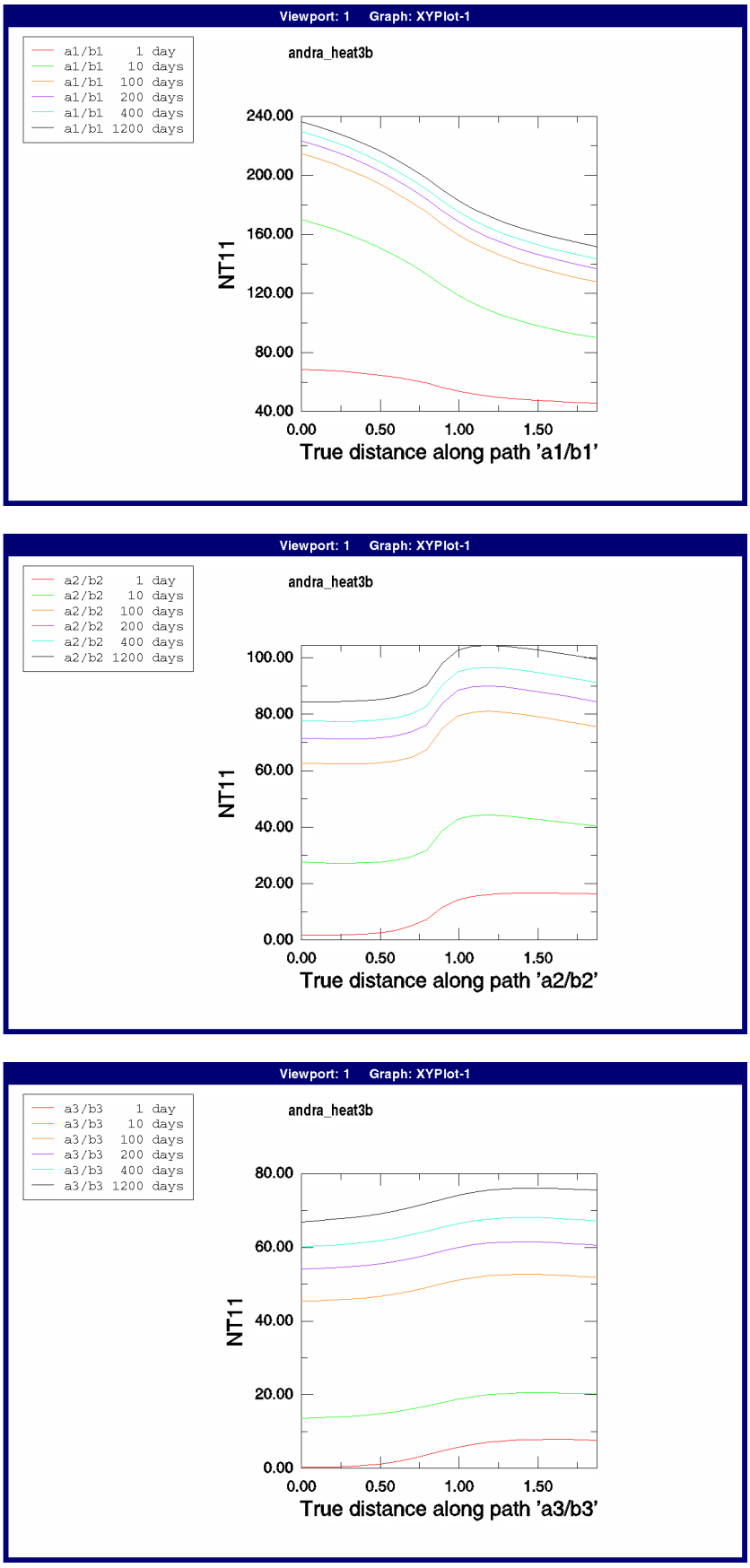

Figure 4-12. *Case 3b (thick sand layer). Temperature (°C) distribution between points a1 and b1, a2 and b2, and a3 and b3 at different times*

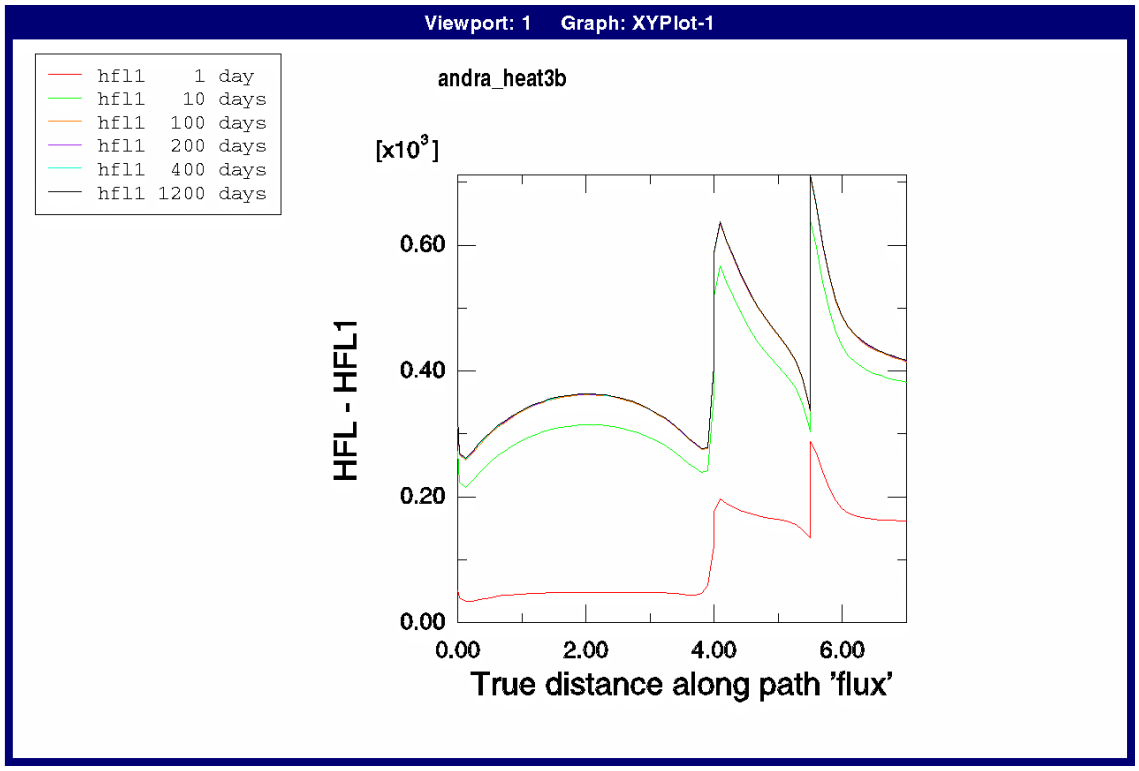

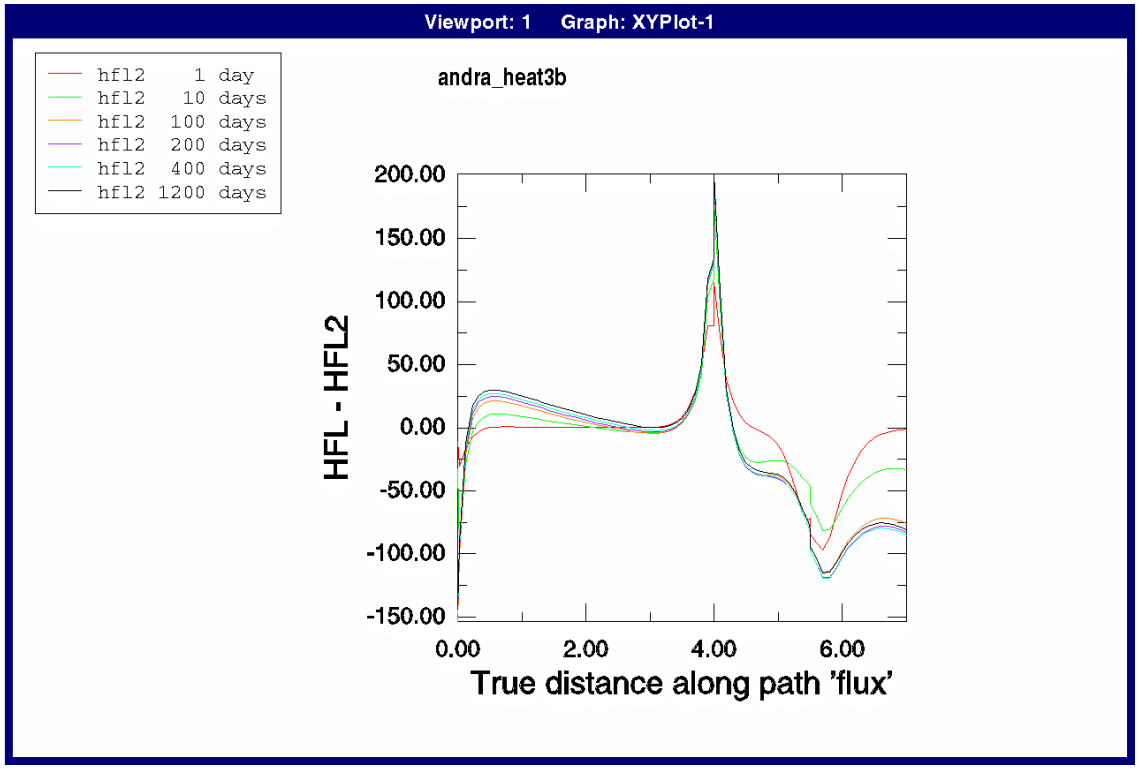

Figure 4-13. *Case 3b (thick sand layer). Radial heat flux (W/m) through the surface at the radius 0.625 m (upper) and corresponding axial heat flux (lower) as function of the distance (m) from the top of canister 1*

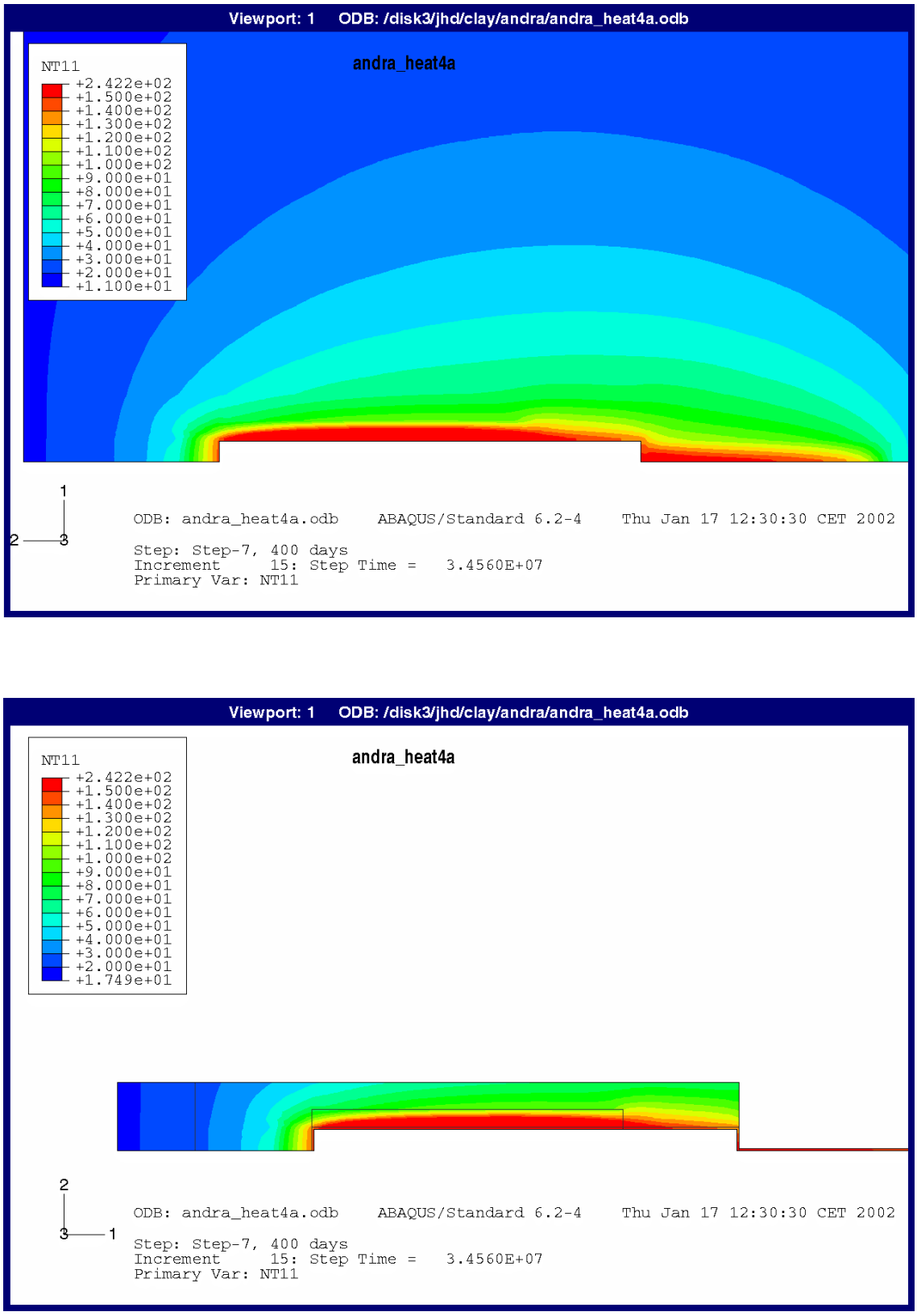

Figure 4-14. *Case 4a (thin canister). Contour plots of the temperature (°C) distribution after 1200 days in the rock and the excavated parts (upper) and solely in the excavated parts (lower) (rotated 90 degrees)*

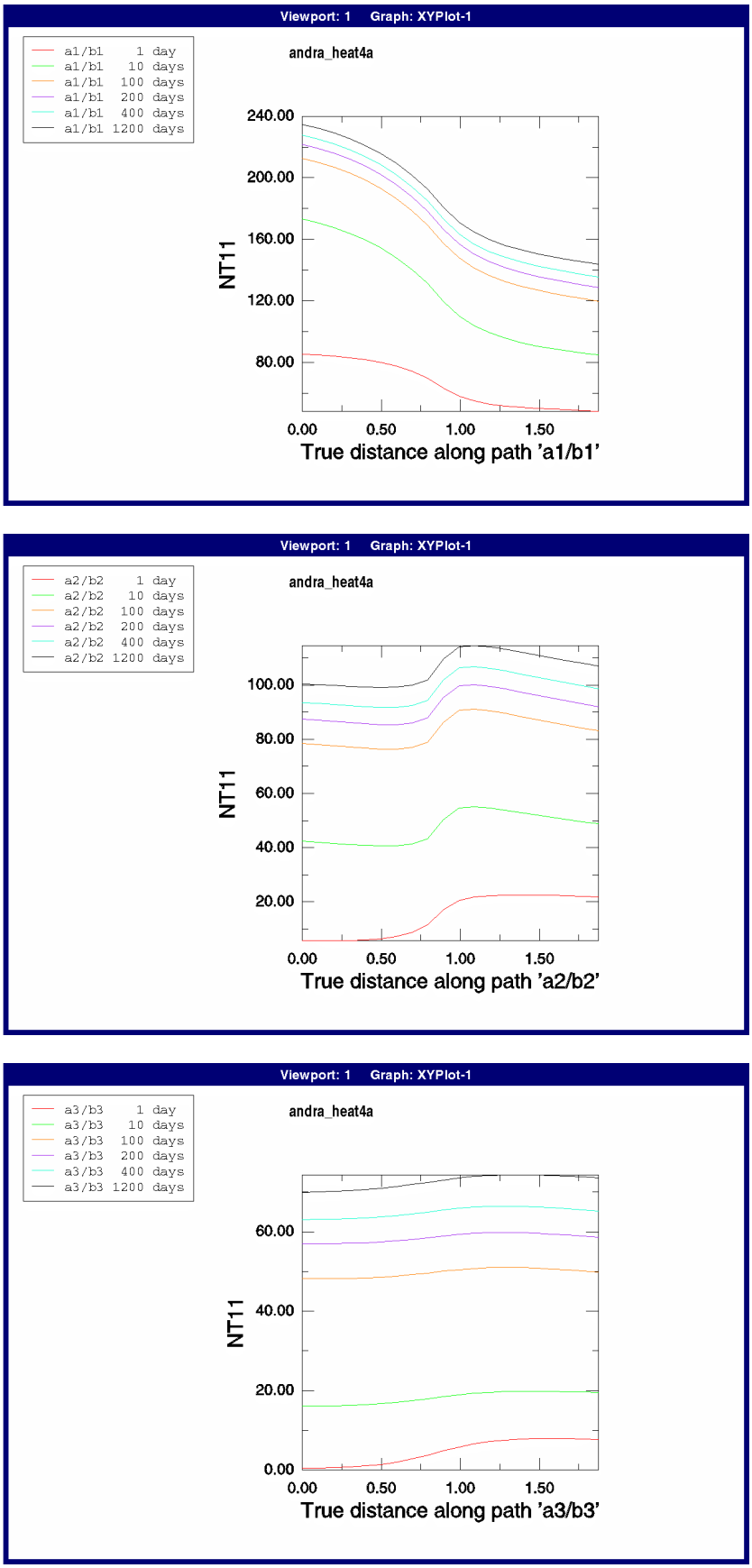

Figure 4-15. *Case 4a (thin canister). Temperature (°C) distribution between points a1 and b1, a2 and b2, and a3 and b3 at different times*

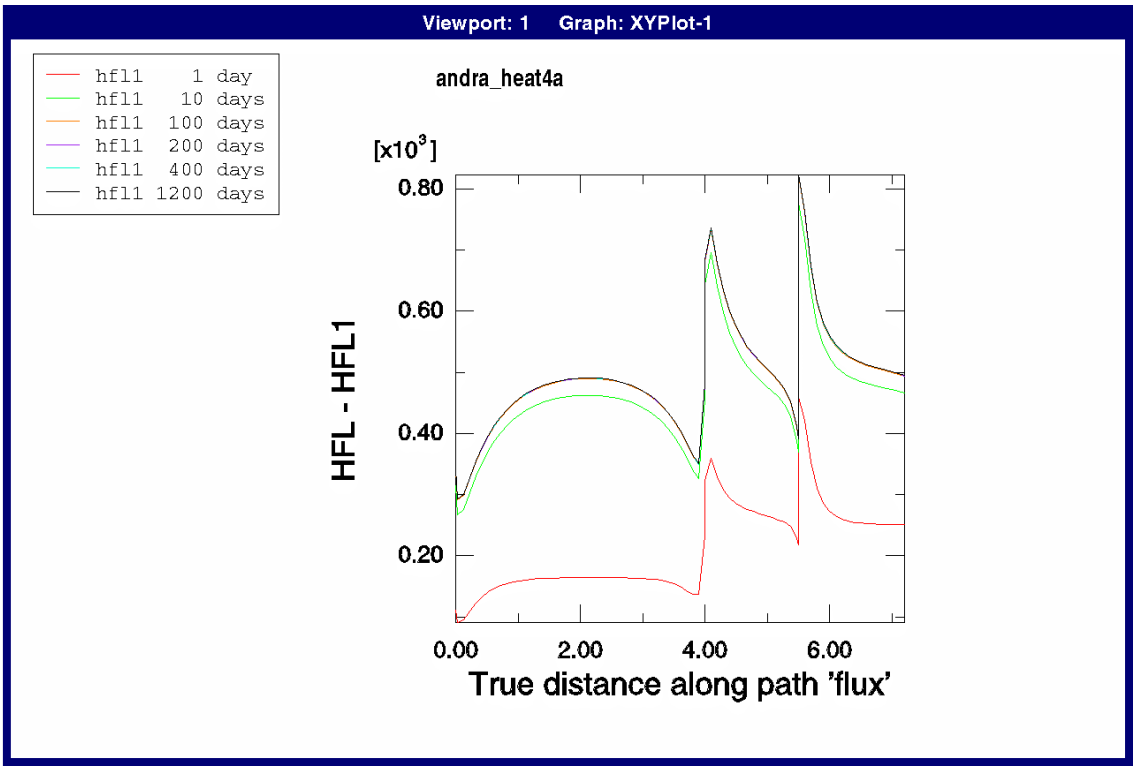

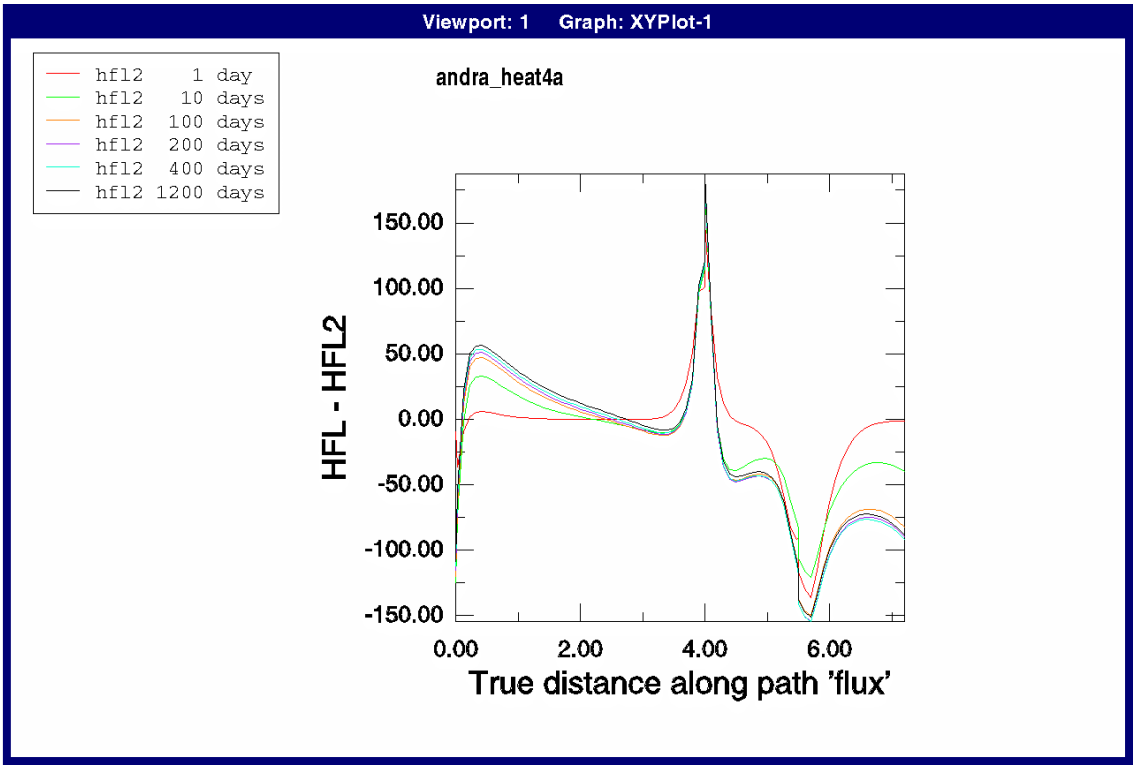

Figure 4-16. *Case 4a (thin canister). Radial heat flux (W/m) through the surface at the radius 0.525 m (upper) and corresponding axial heat flux (lower) as function of the distance (m) from the top of canister 1*

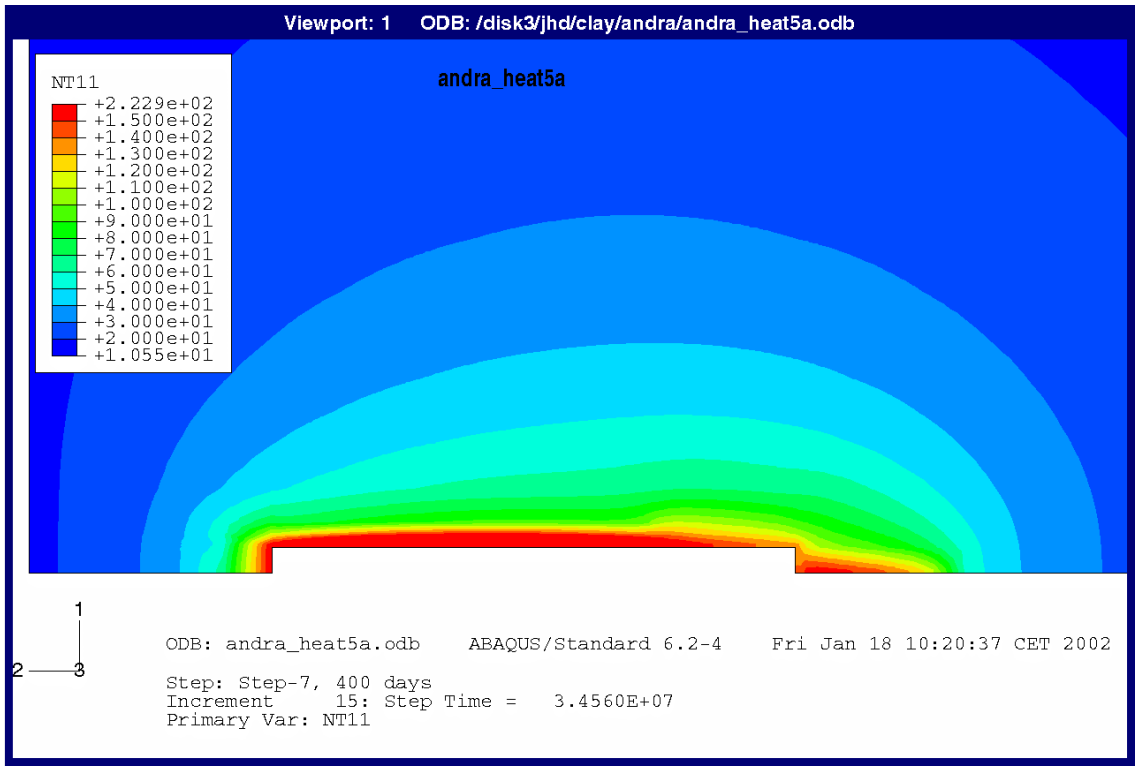

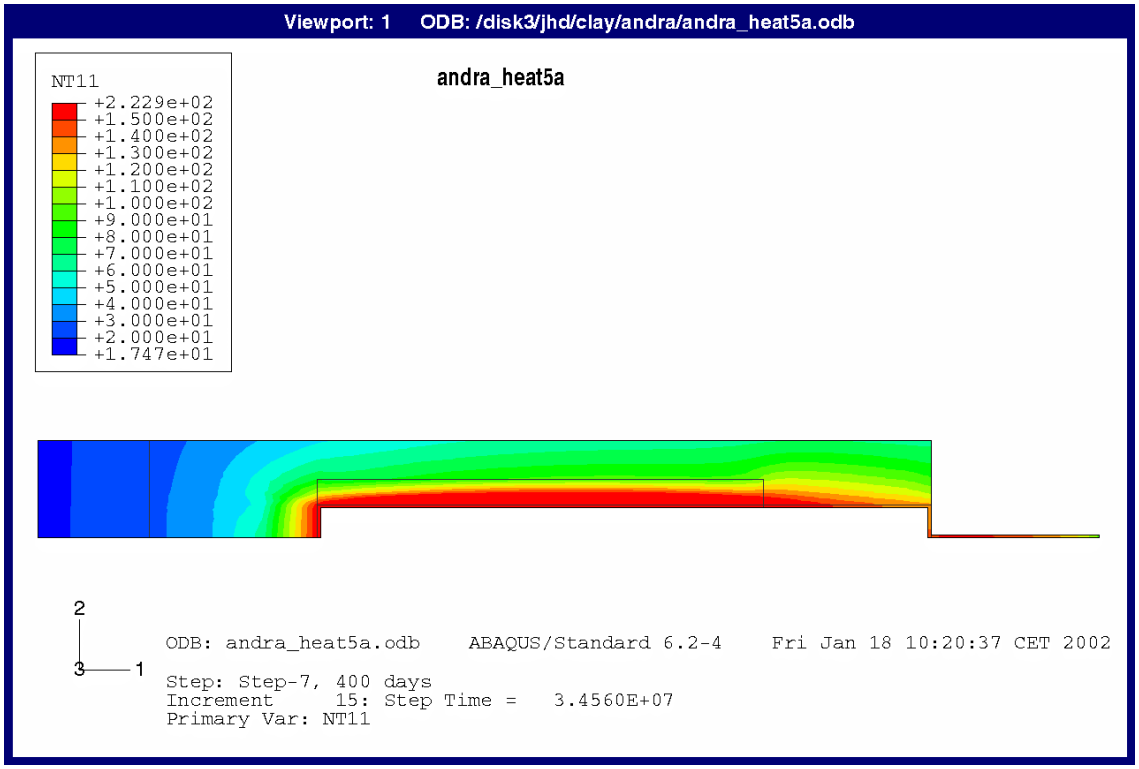

Figure 4-17. *Case 5a (short heater). Contour plots of the temperature (°C) distribution after 1200 days in the rock and the excavated parts (upper) and solely in the excavated parts (lower) (rotated 90 degrees)*

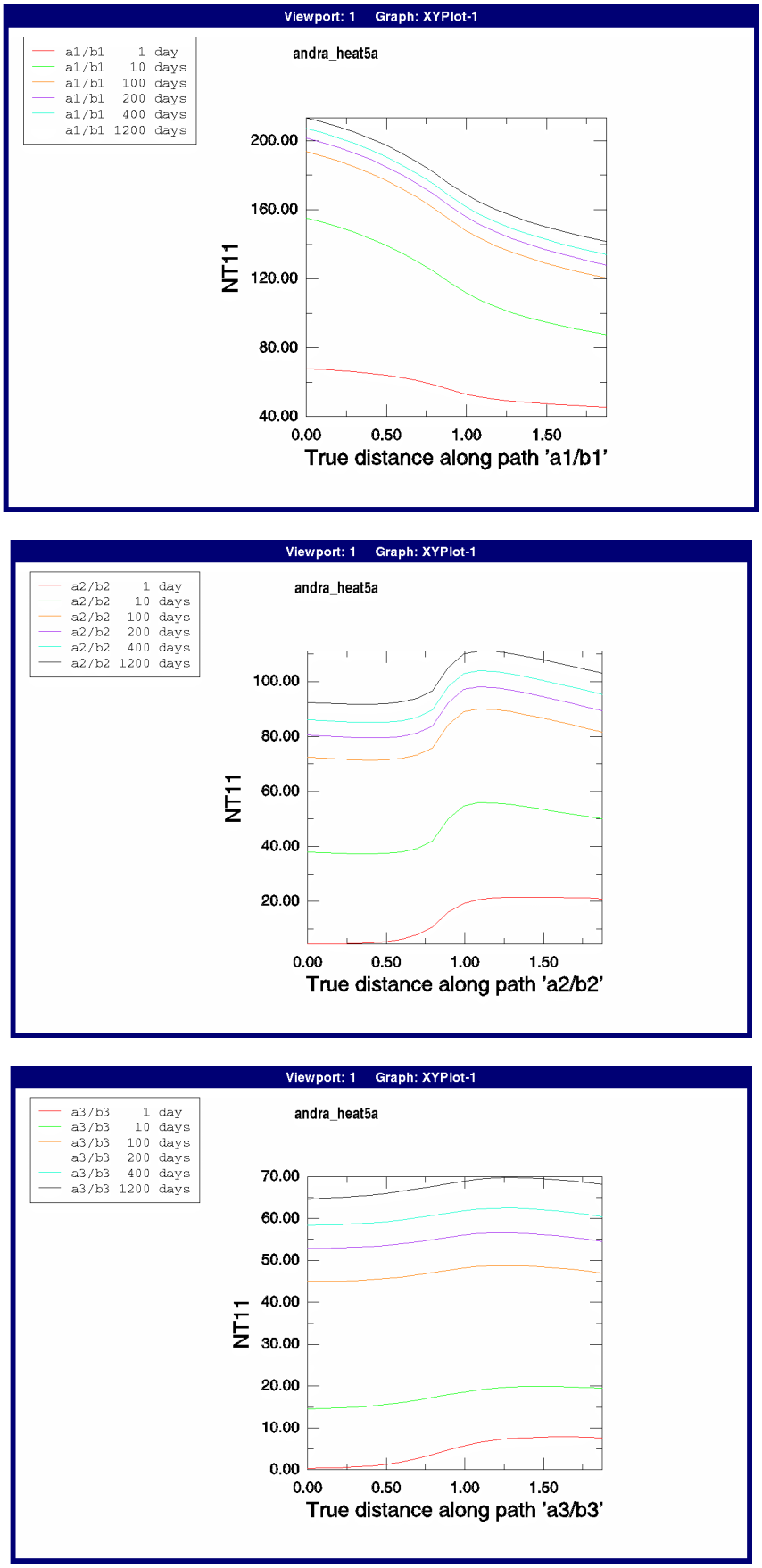

Figure 4-18. *Case 5a (short heater). Temperature (°C) distribution between points a1 and b1, a2 and b2, and a3 and b3 at different times*

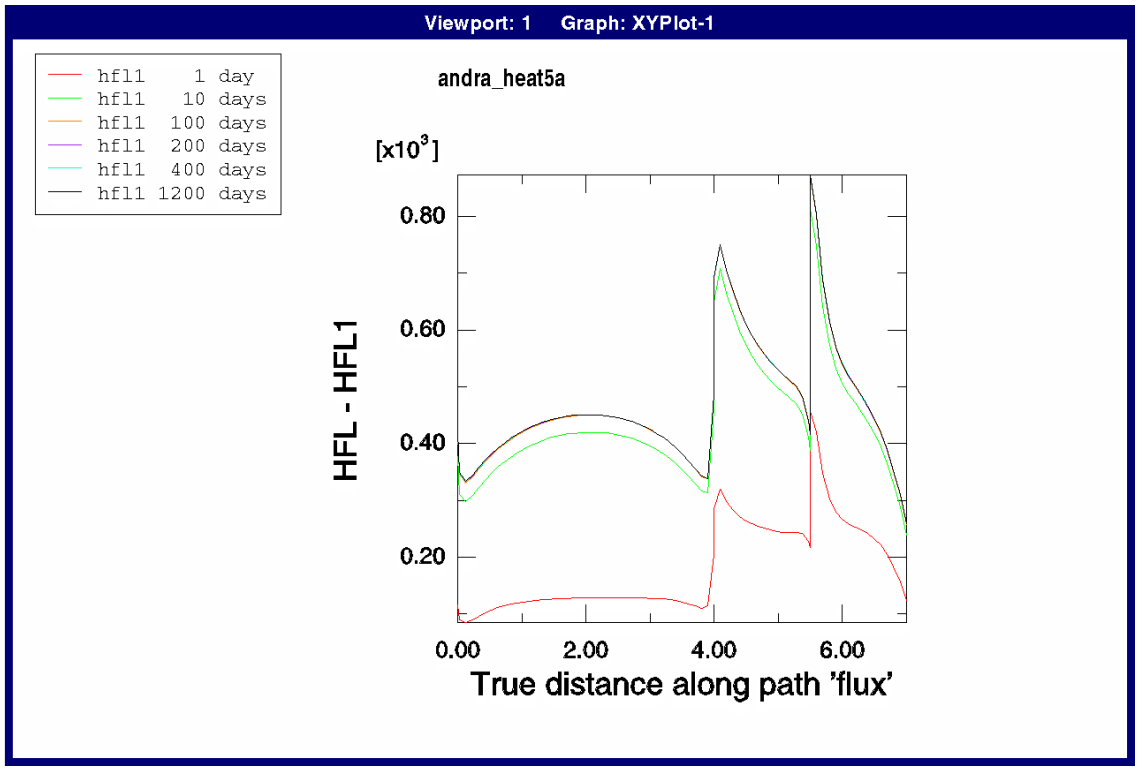

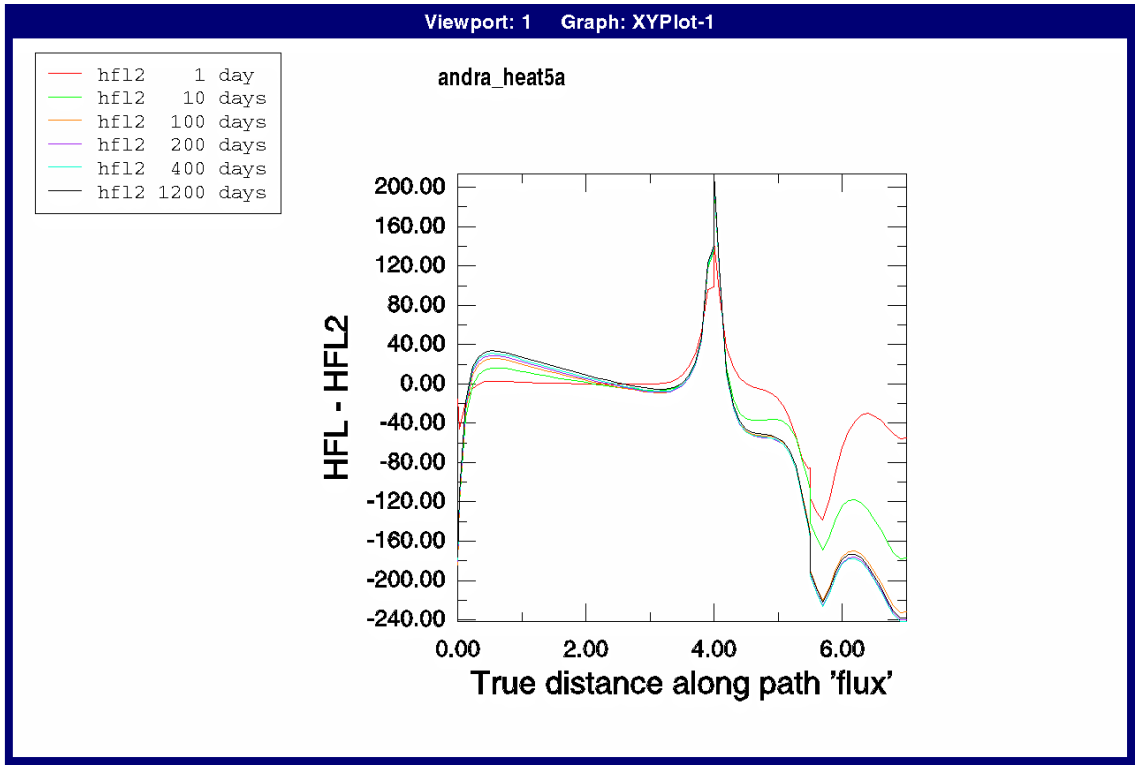

Figure 4-19. *Case 5a (short heater). Radial heat flux (W/m) through the surface at the radius 0.525 m (upper) and corresponding axial heat flux (lower) as function of the distance (m) from the top of canister 1*

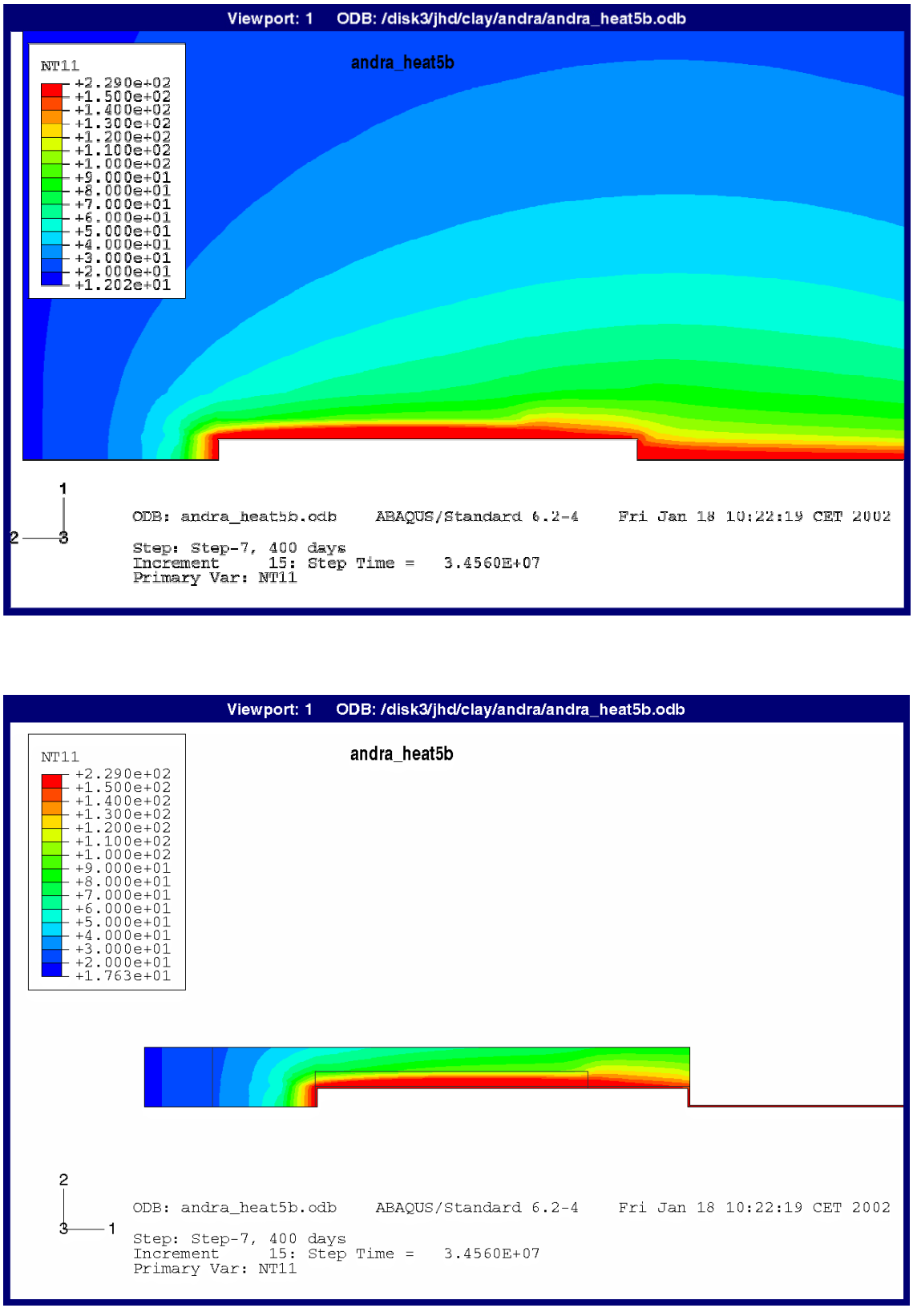

Figure 4-20. *Case 5b (long heater). Contour plots of the temperature (°C) distribution after 1200 days in the rock and the excavated parts (upper) and solely in the excavated parts (lower) (rotated 90 degrees)*

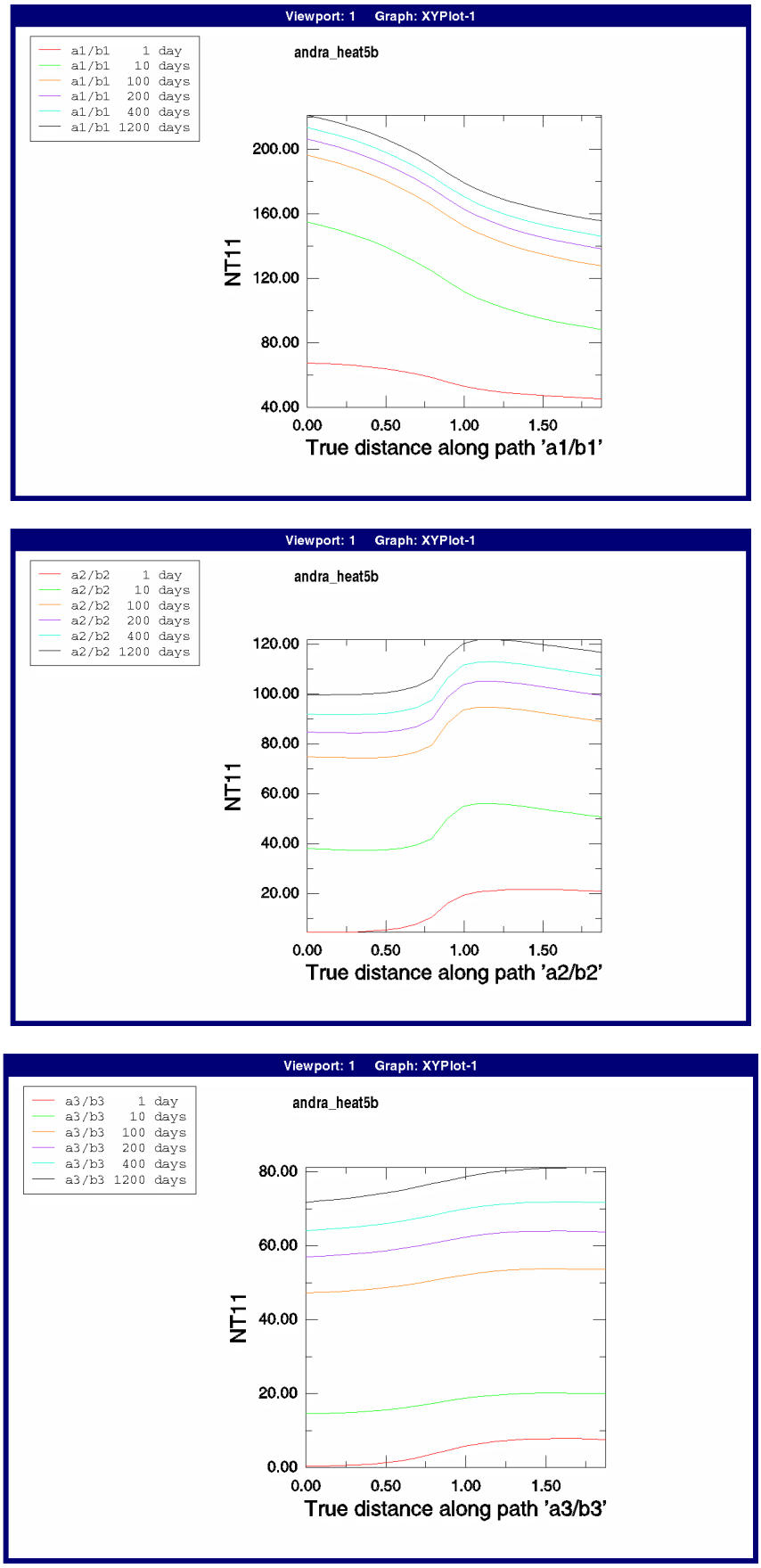

Figure 4-21. *Case 5b (long heater). Temperature (°C) distribution between points a1 and b1, a2 and b2, and a3 and b3 at different times*

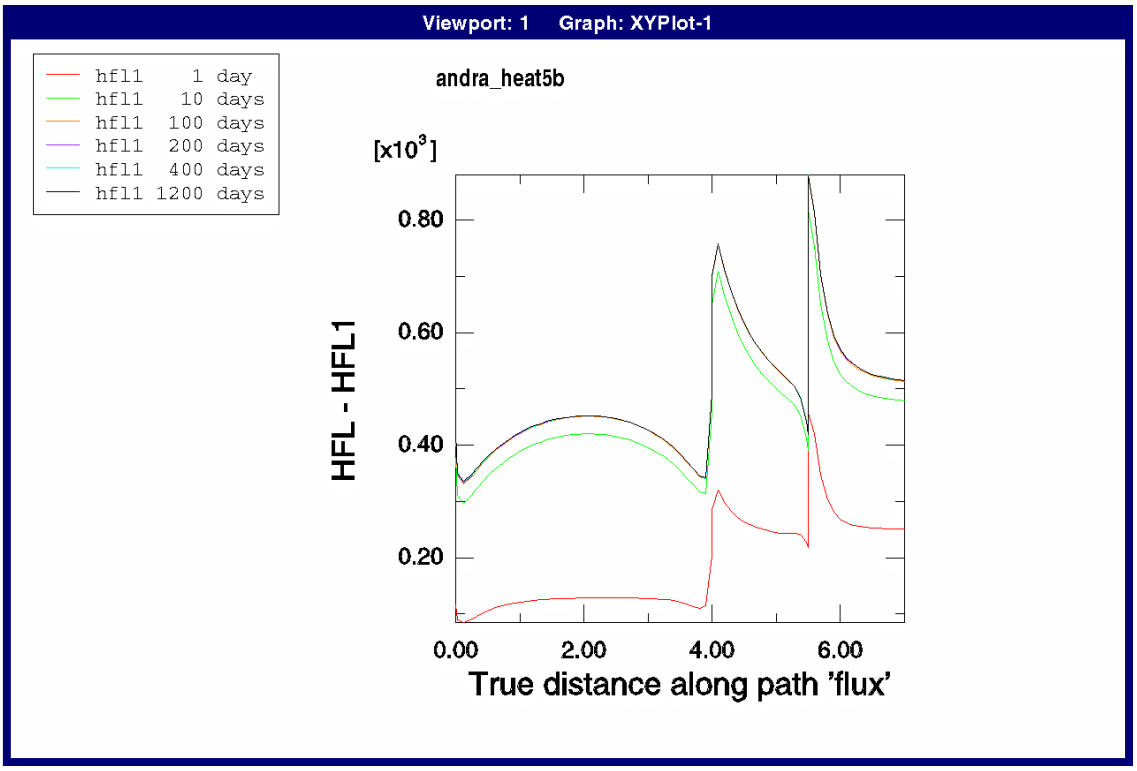

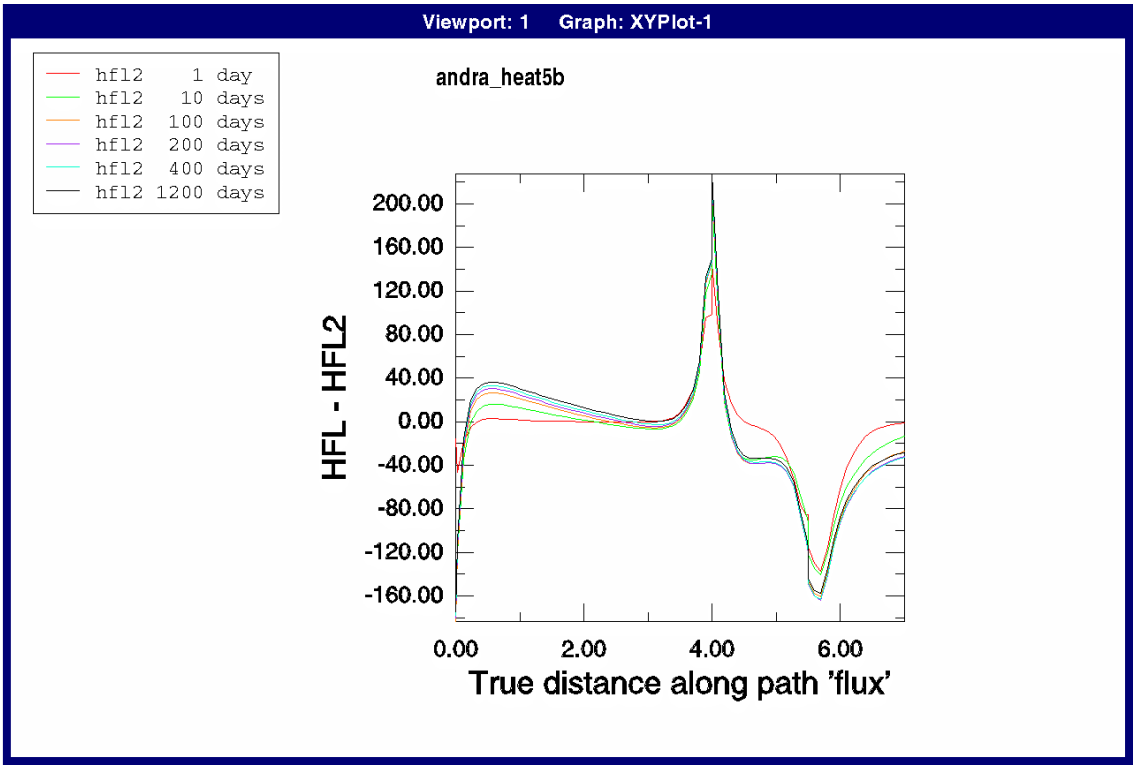

Figure 4-22. *Case 5b (long heater). Radial heat flux (W/m) through the surface at the radius 0.525 m (upper) and corresponding axial heat flux (lower) as function of the distance (m) from the top of canister 1*

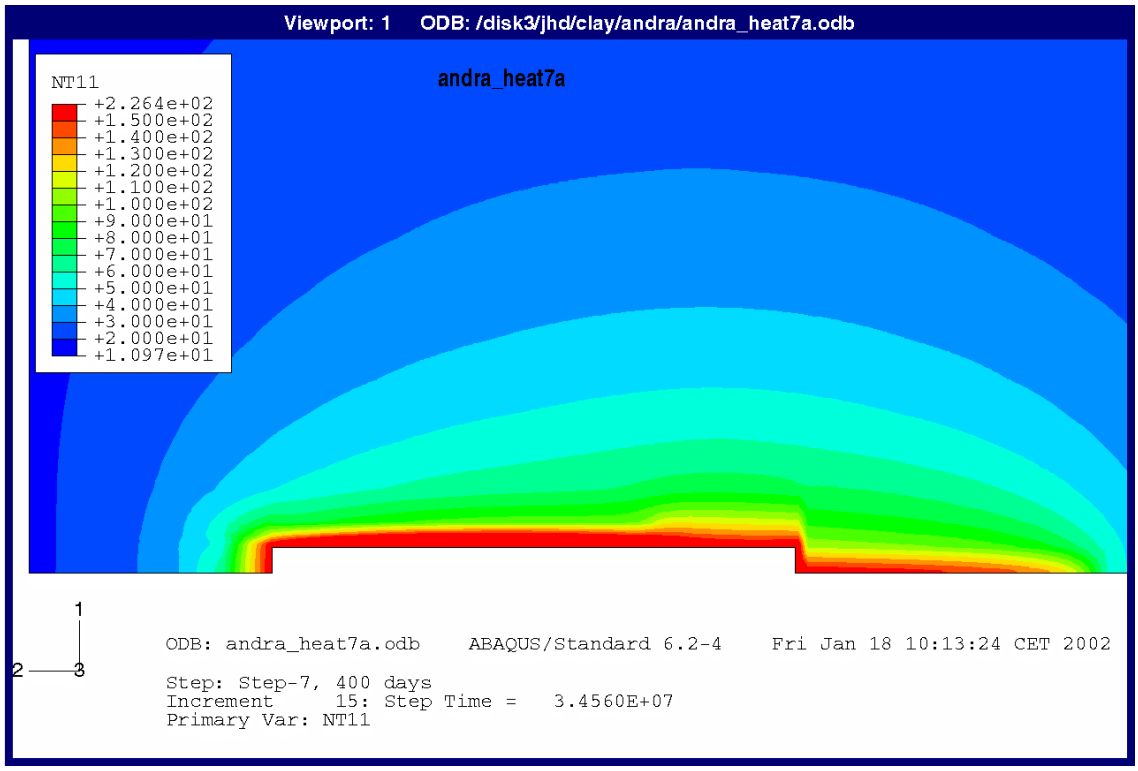

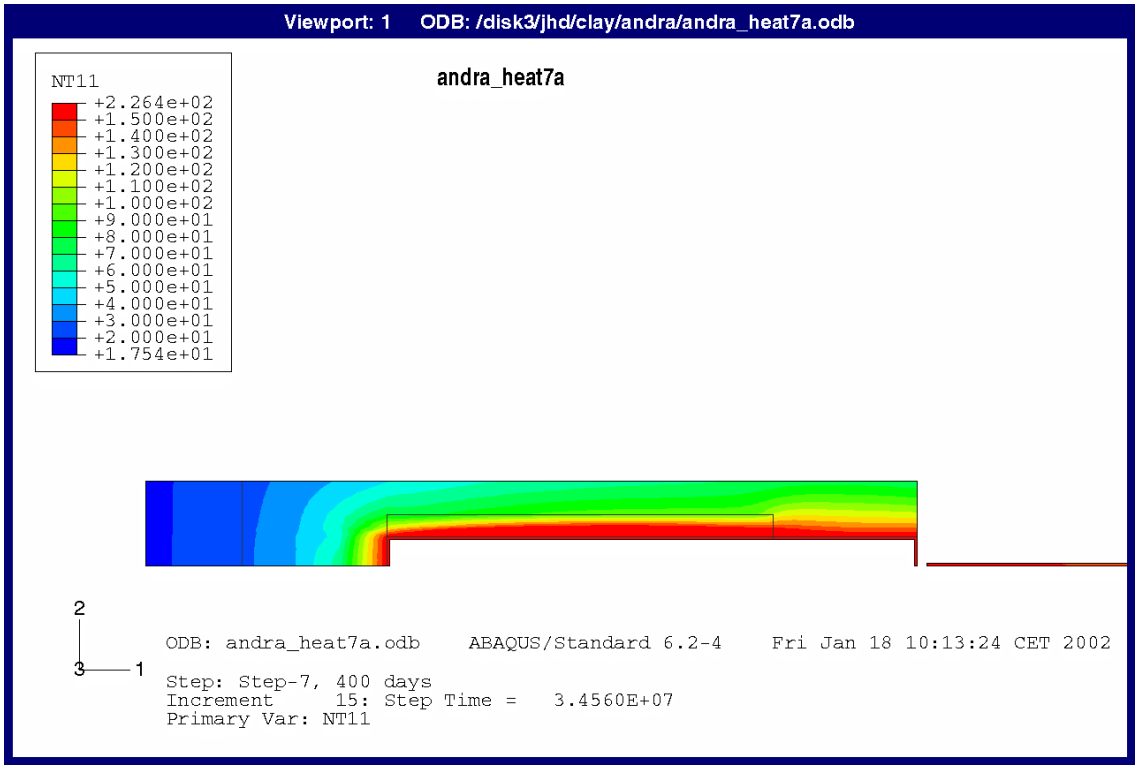

Figure 4-23. *Case 7a (bottom isolation). Contour plots of the temperature (°C) distribution after 1200 days in the rock and the excavated parts (upper) and solely in the excavated parts (lower) (rotated 90 degrees)*

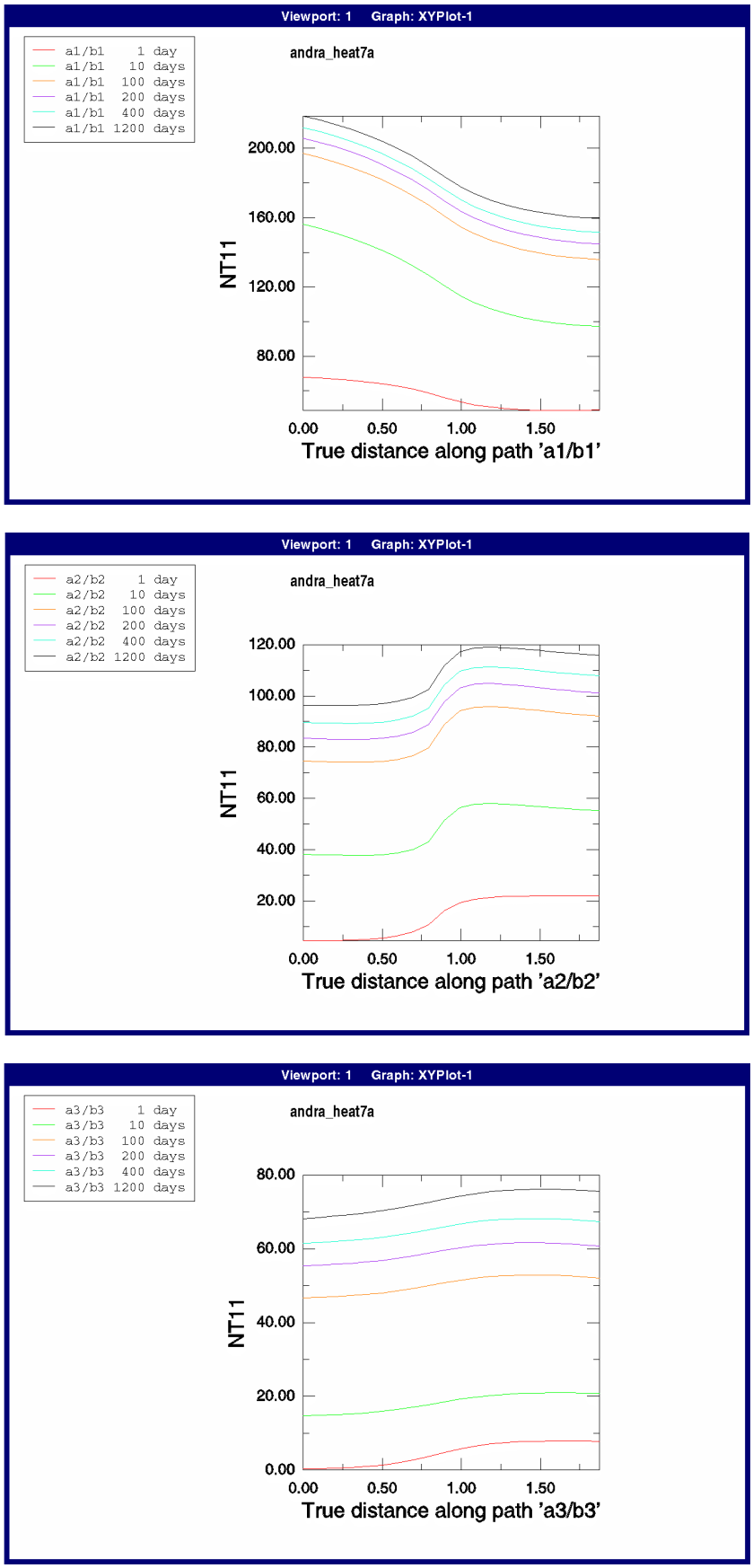

Figure 4-24. *Case 7a (bottom isolation). Temperature (°C) distribution between points a1 and b1, a2 and b2, and a3 and b3 at different times*

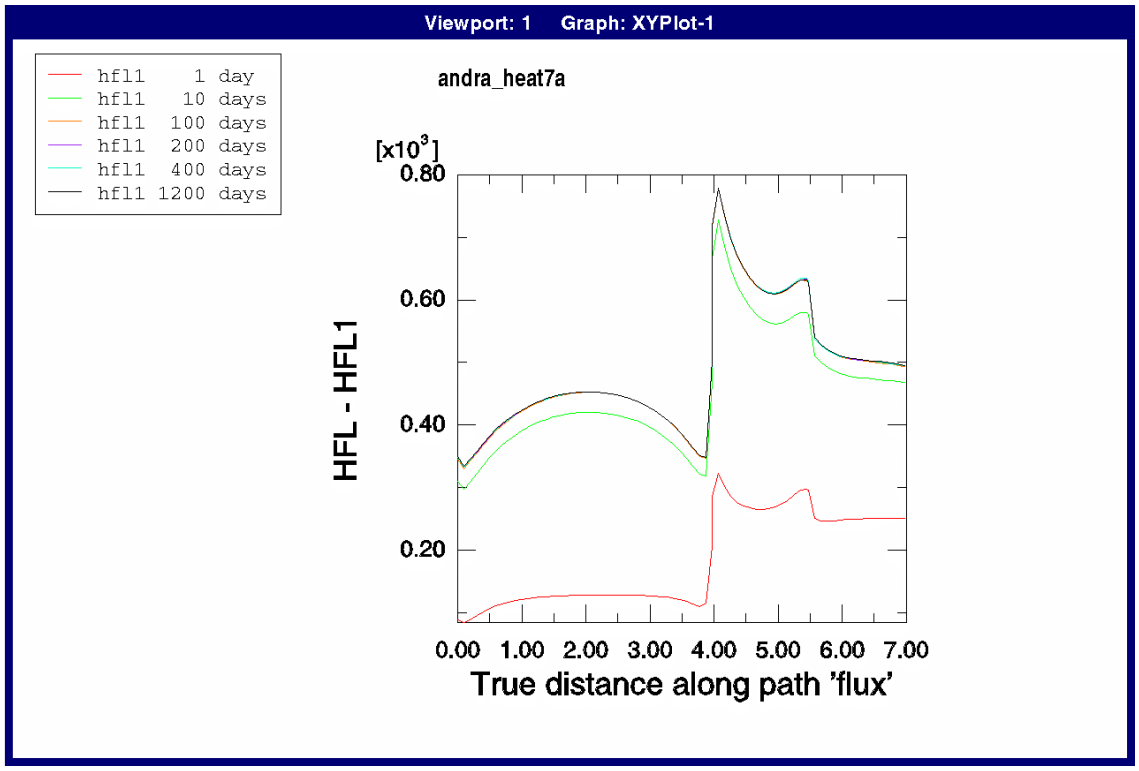

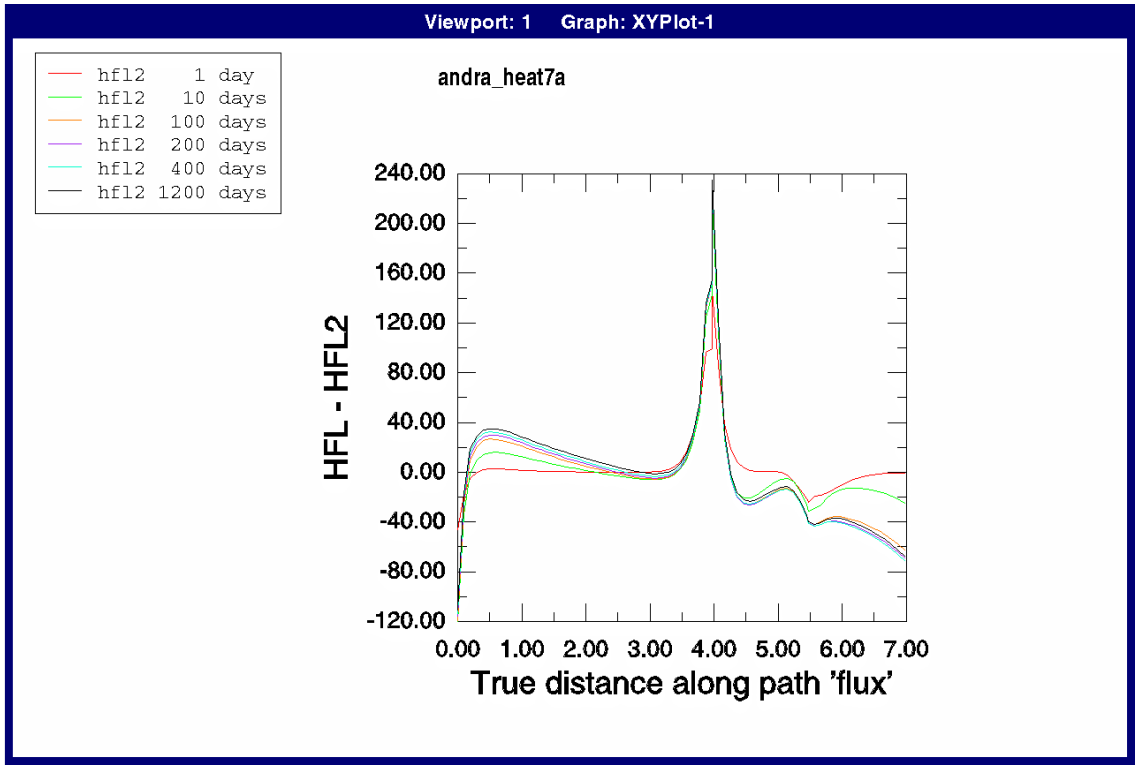

Figure 4-25. *Case 7a (bottom isolation). Radial heat flux (W/m) through the surface at the radius 0.525 m (upper) and corresponding axial heat flux (lower) as function of the distance (m) from the top of canister 1*

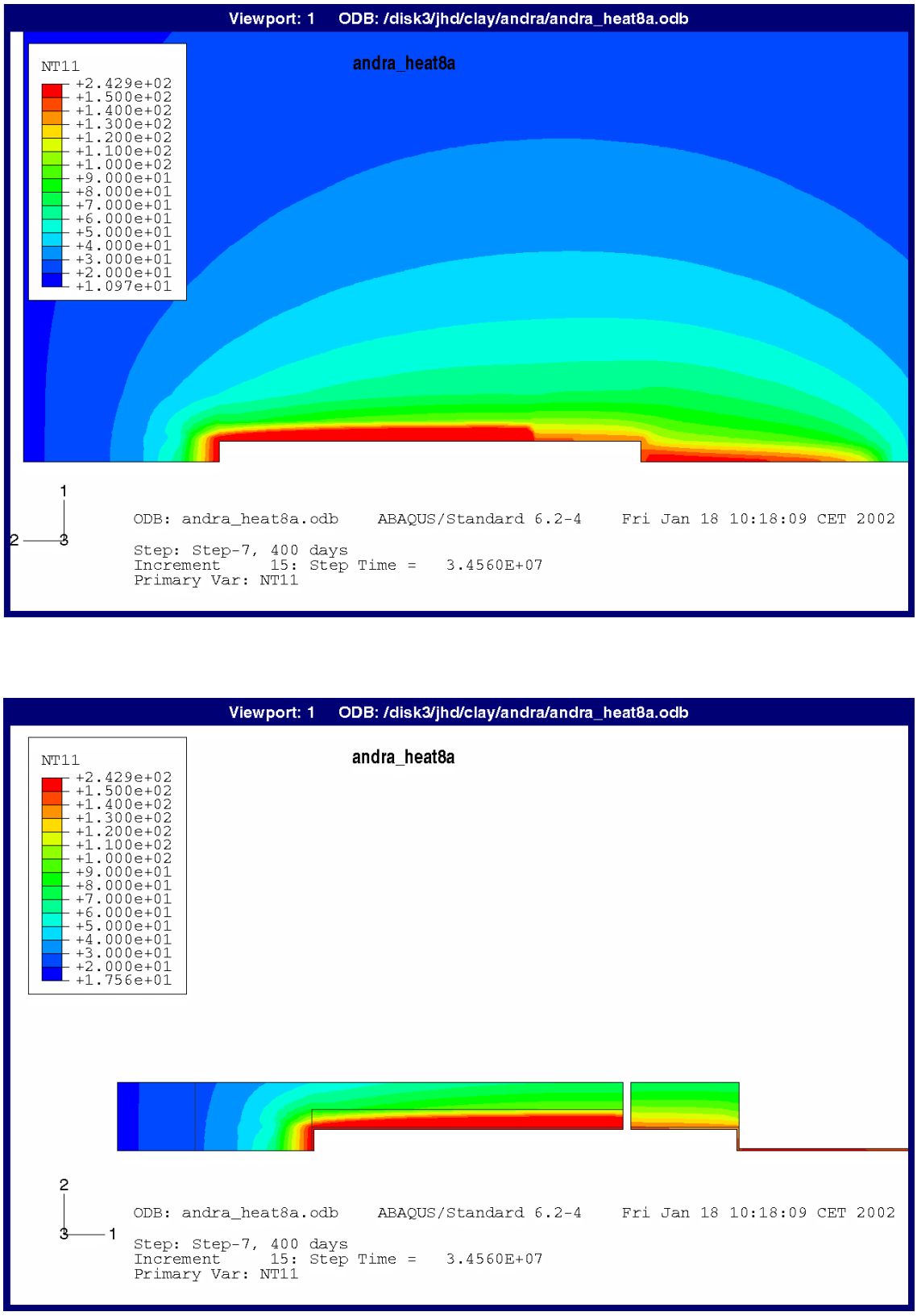

Figure 4-26. *Case 8a (central isolation). Contour plots of the temperature (°C) distribution after 1200 days in the rock and the excavated parts (upper) and solely in the excavated parts (lower) (rotated 90 degrees)*

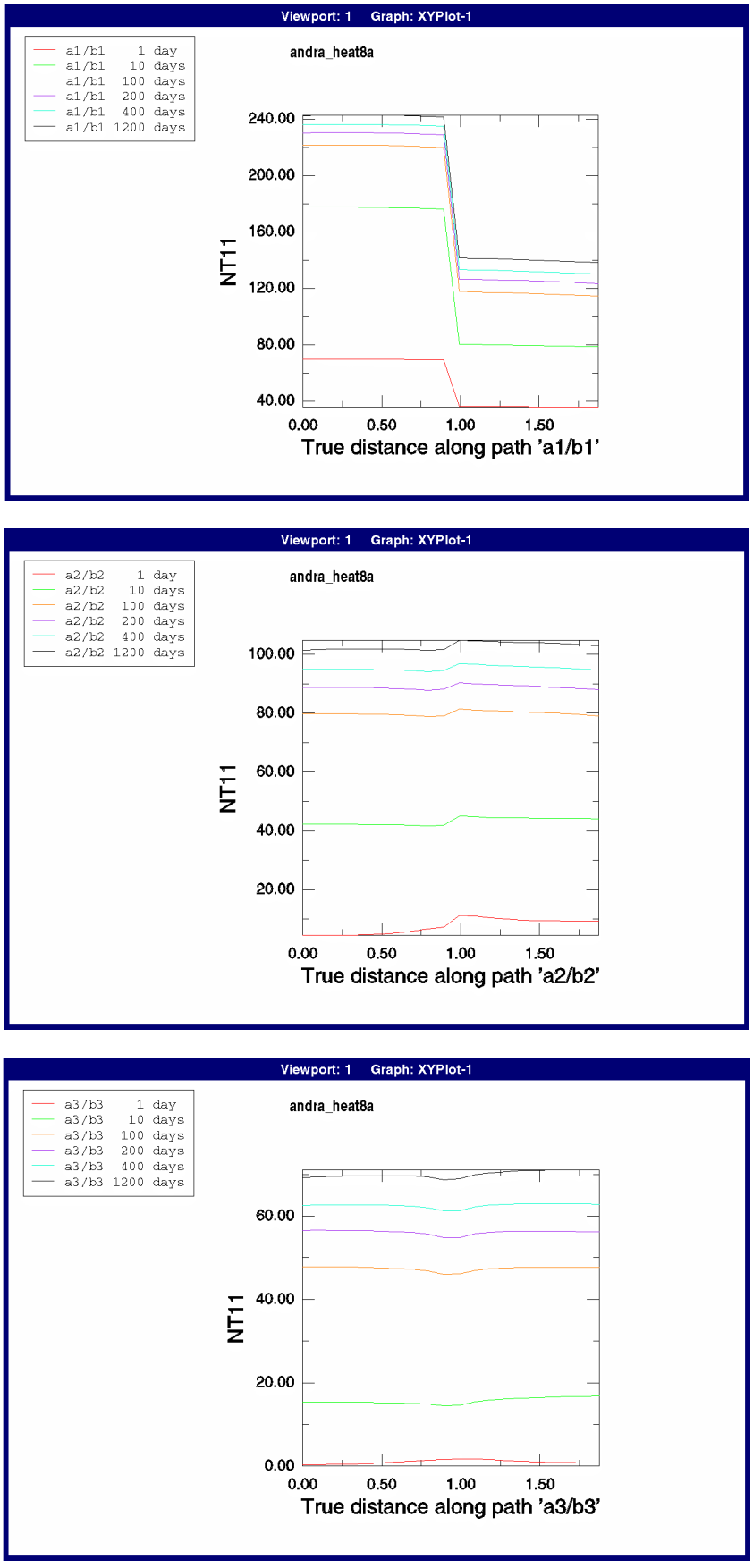

Figure 4-27. *Case 8a (central isolation). Temperature (°C) distribution between points a1 and b1, a2 and b2, and a3 and b3 at different times*

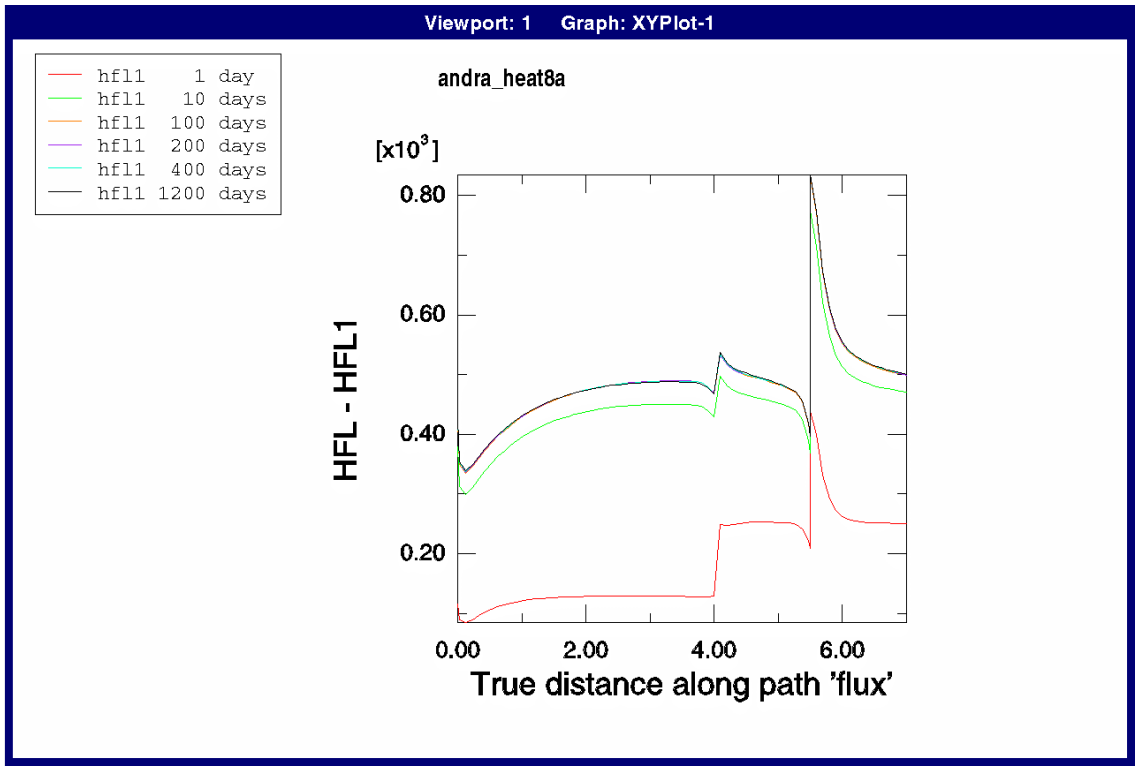

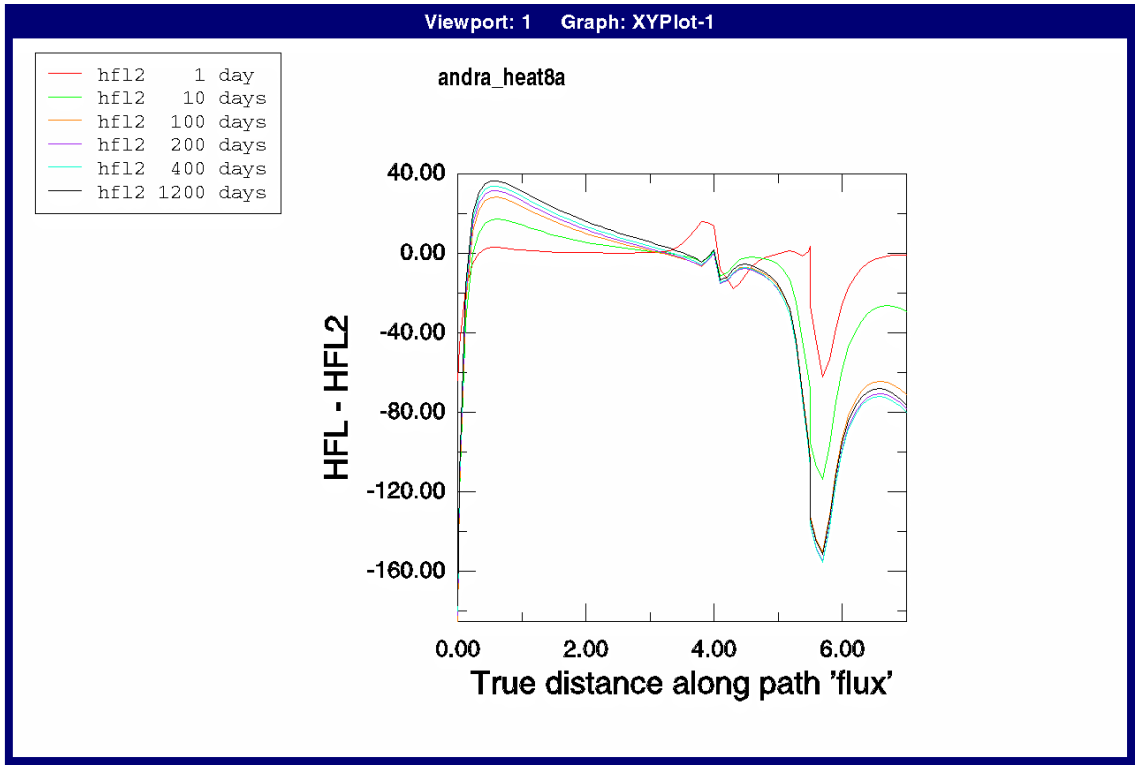

Figure 4-28. *Case 8a (central isolation). Radial heat flux (W/m) through the surface at the radius 0.525 m (upper) and corresponding axial heat flux (lower) as function of the distance (m) from the top of canister 1*

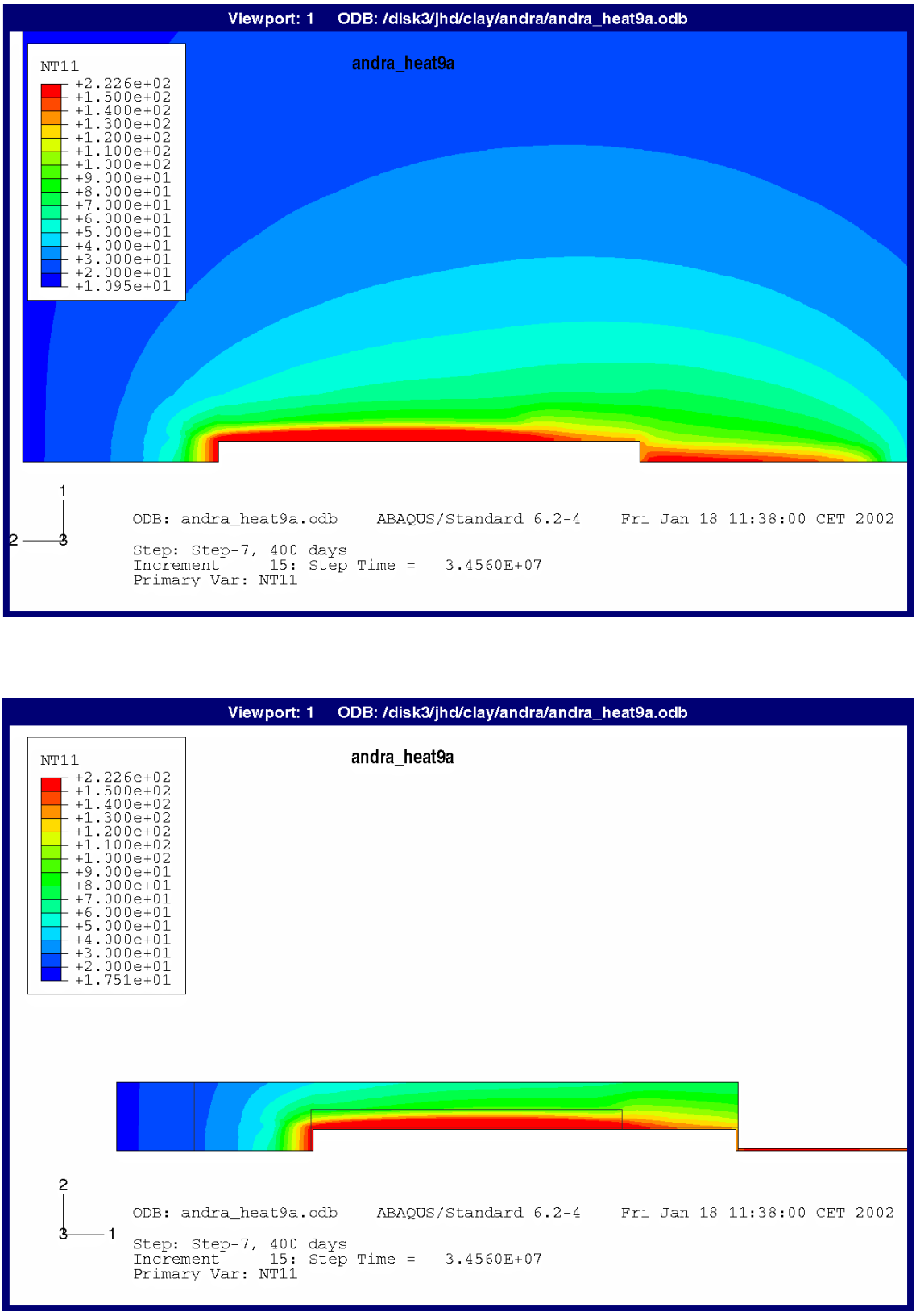

Figure 4-29. *Case 9a (reduced power in canister 2). Contour plots of the temperature (°C) distribution after 1200 days in the rock and the excavated parts (upper) and solely in the excavated parts (lower) (rotated 90 degrees)*

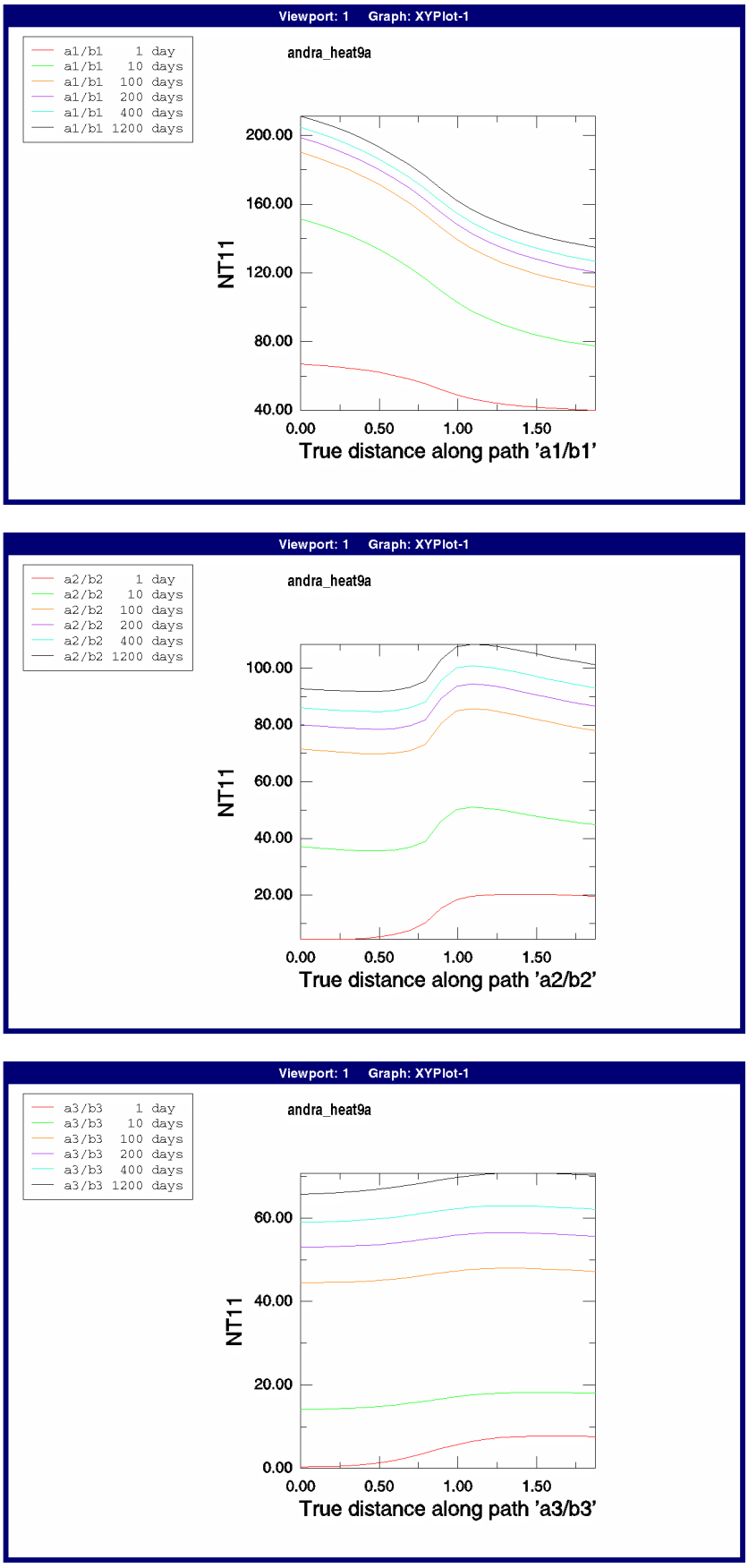

Figure 4-30. *Case 9a (reduced power in canister 2). Temperature (°C) distribution between points a1 and b1, a2 and b2, and a3 and b3 at different times*

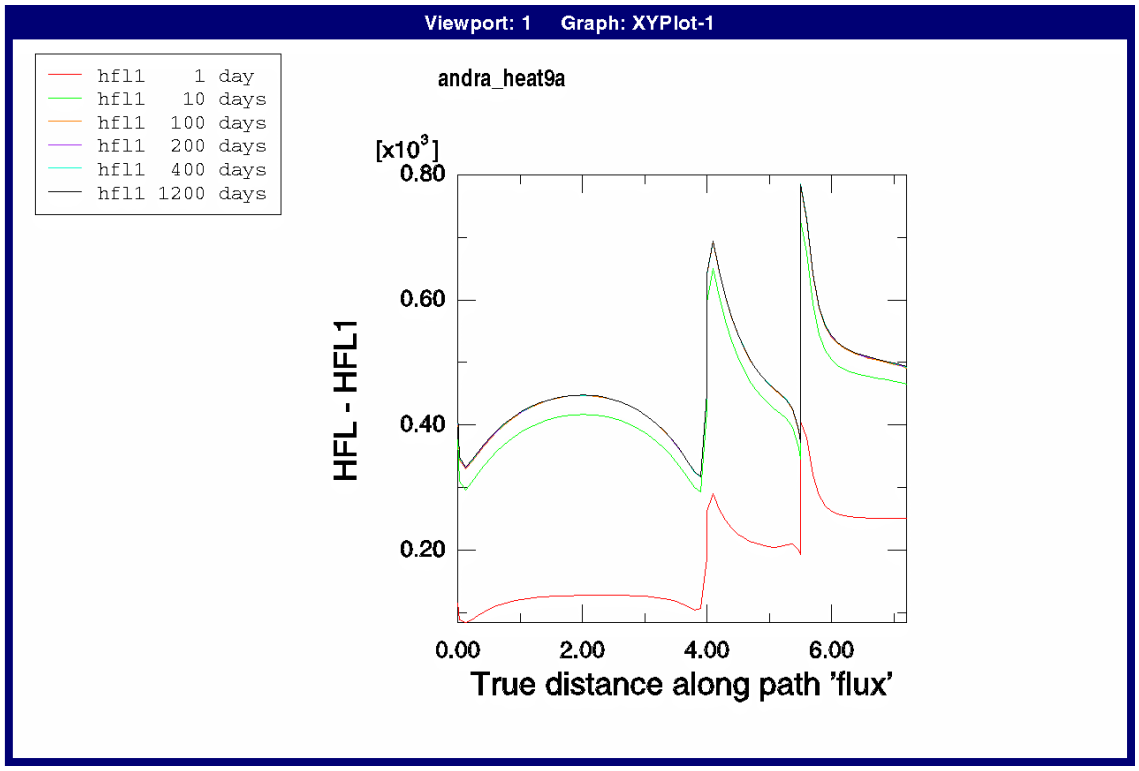

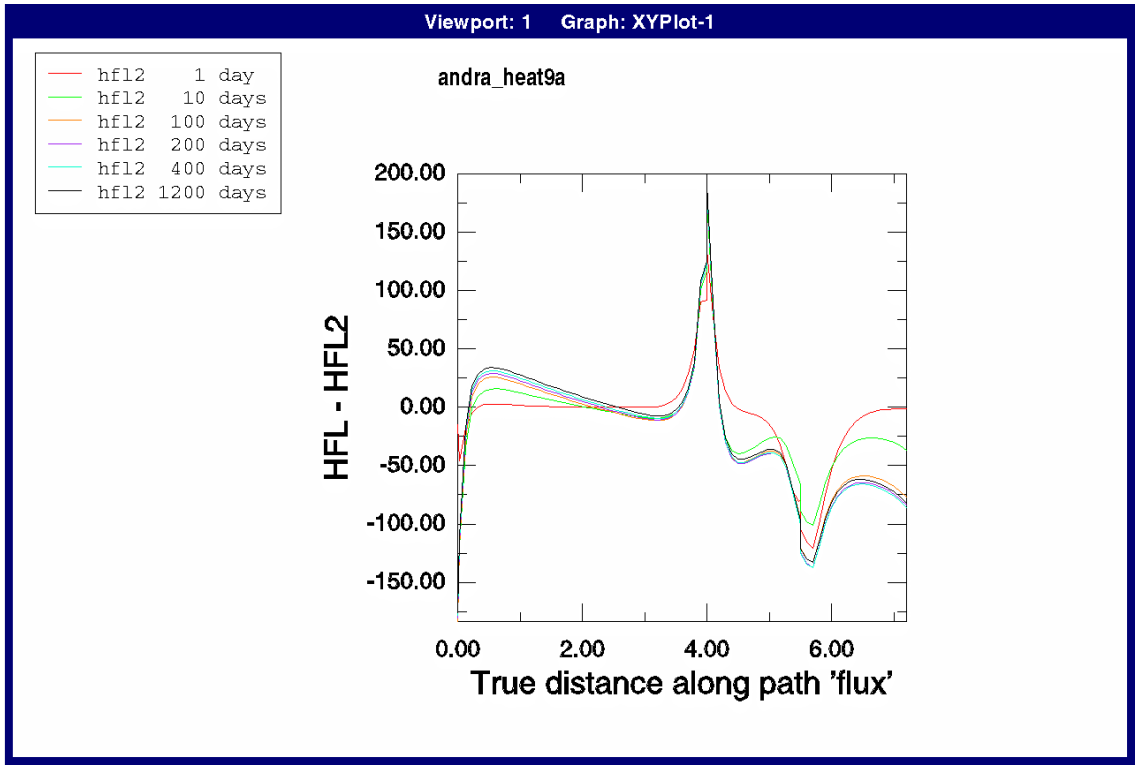

Figure 4-31. *Case 9a (reduced power in canister 2). Radial heat flux (W/m) through the surface at the radius 0.525 m (upper) and corresponding axial heat flux (lower) as function of the distance (m) from the top of canister 1*

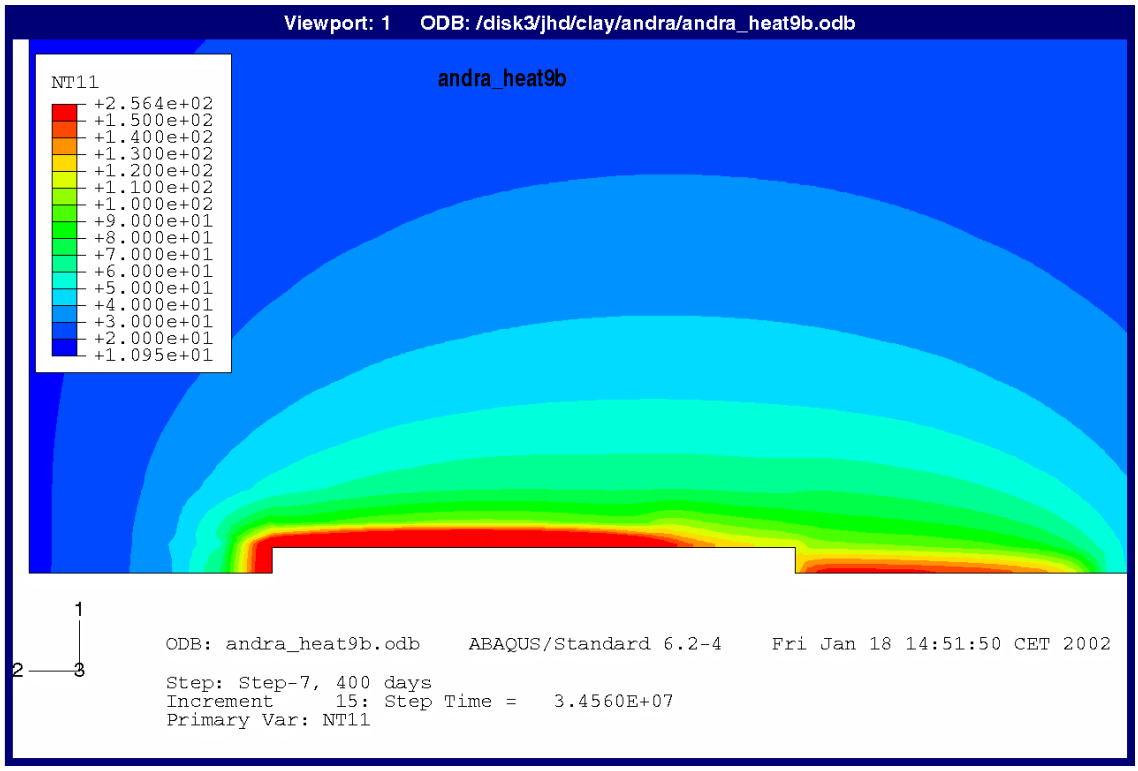

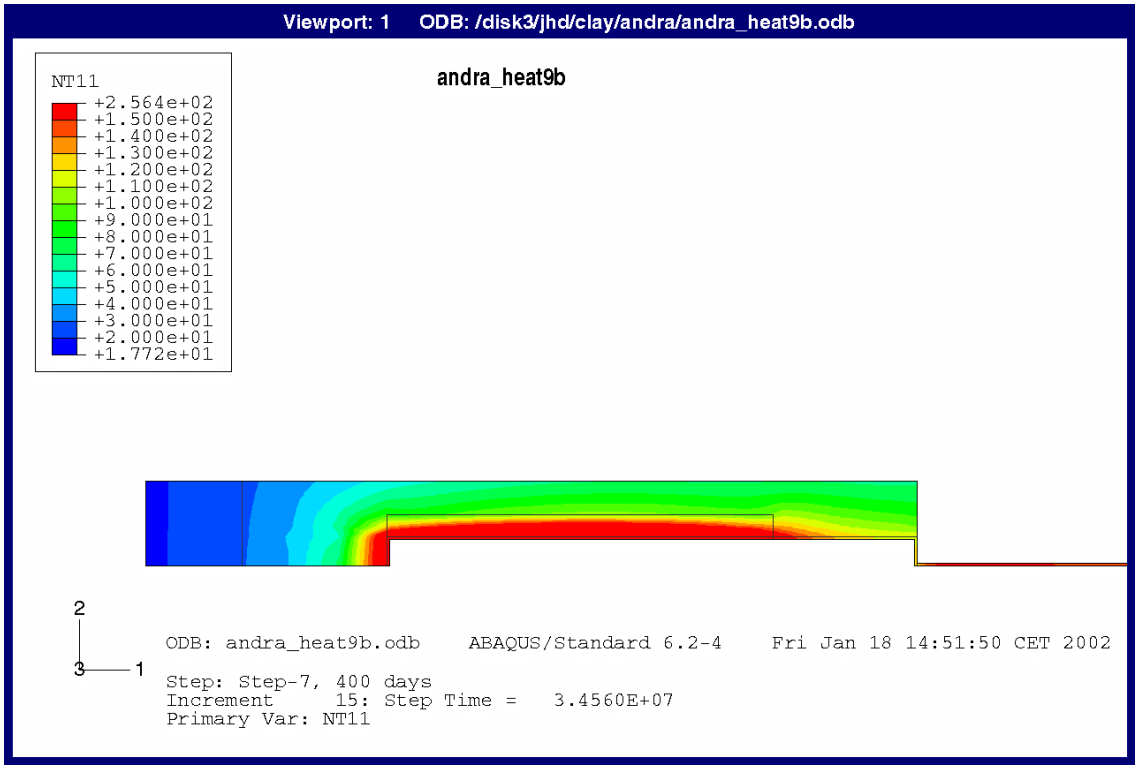

Figure 4-32. *Case 9b (differentiated power). Contour plots of the temperature (°C) distribution after 1200 days in the rock and the excavated parts (upper) and solely in the excavated parts (lower) (rotated 90 degrees)*

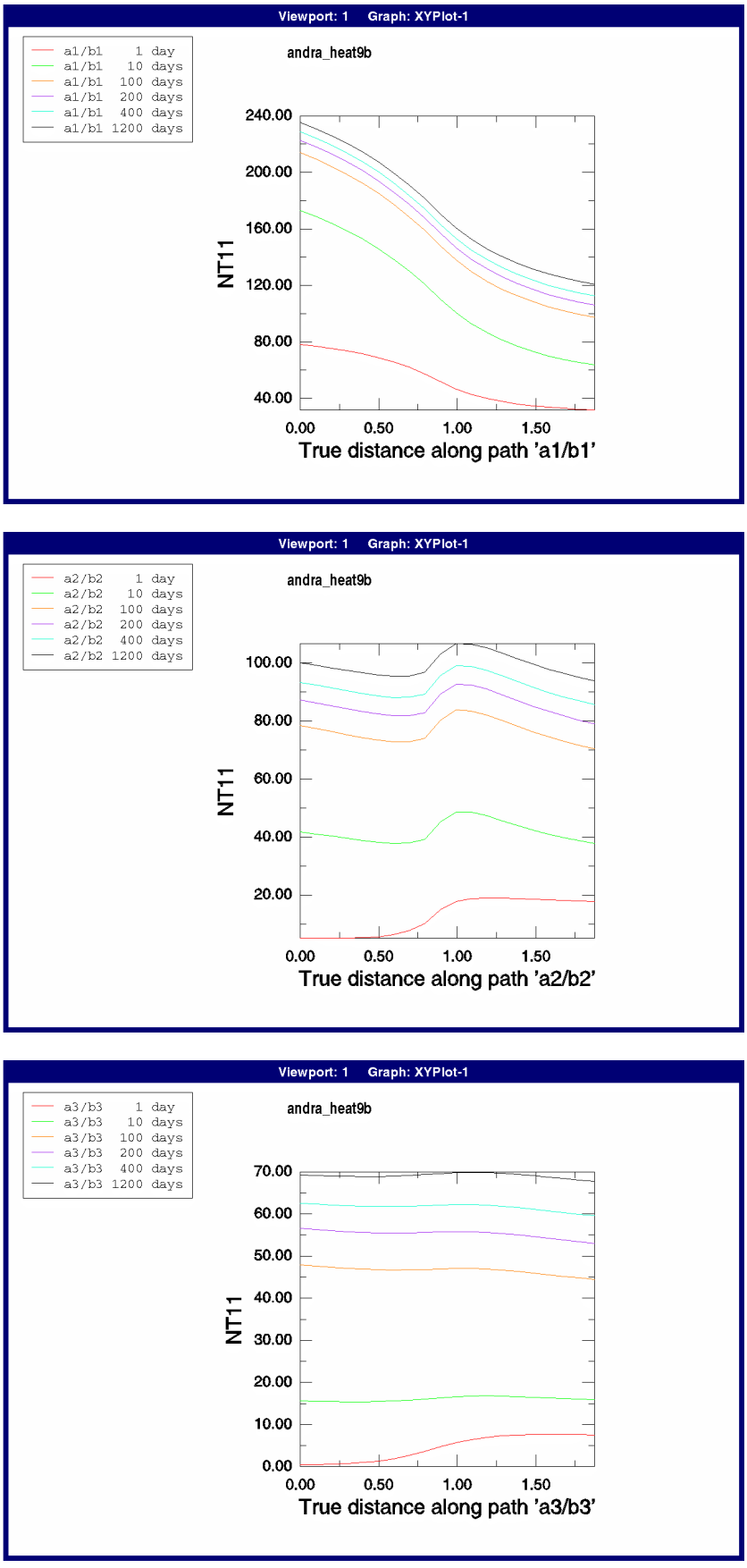

Figure 4-33. *Case 9b (differentiated power). Temperature (°C) distribution between points a1 and b1, a2 and b2, and a3 and b3 at different times*

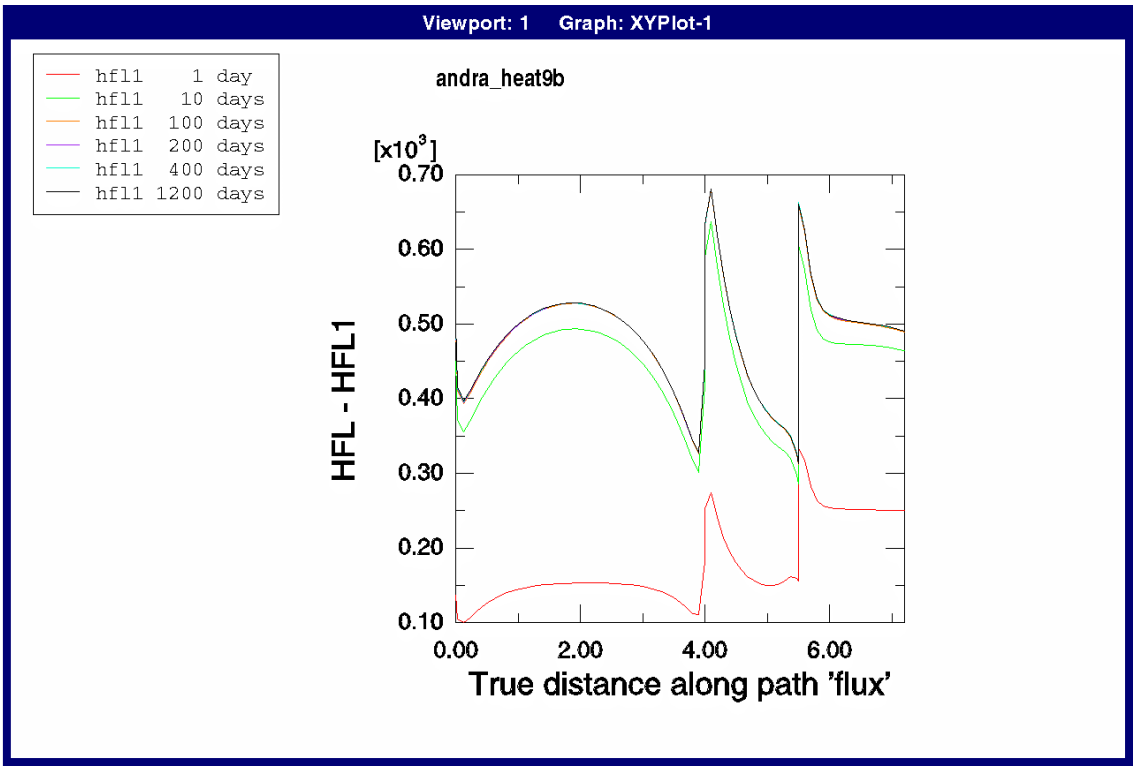

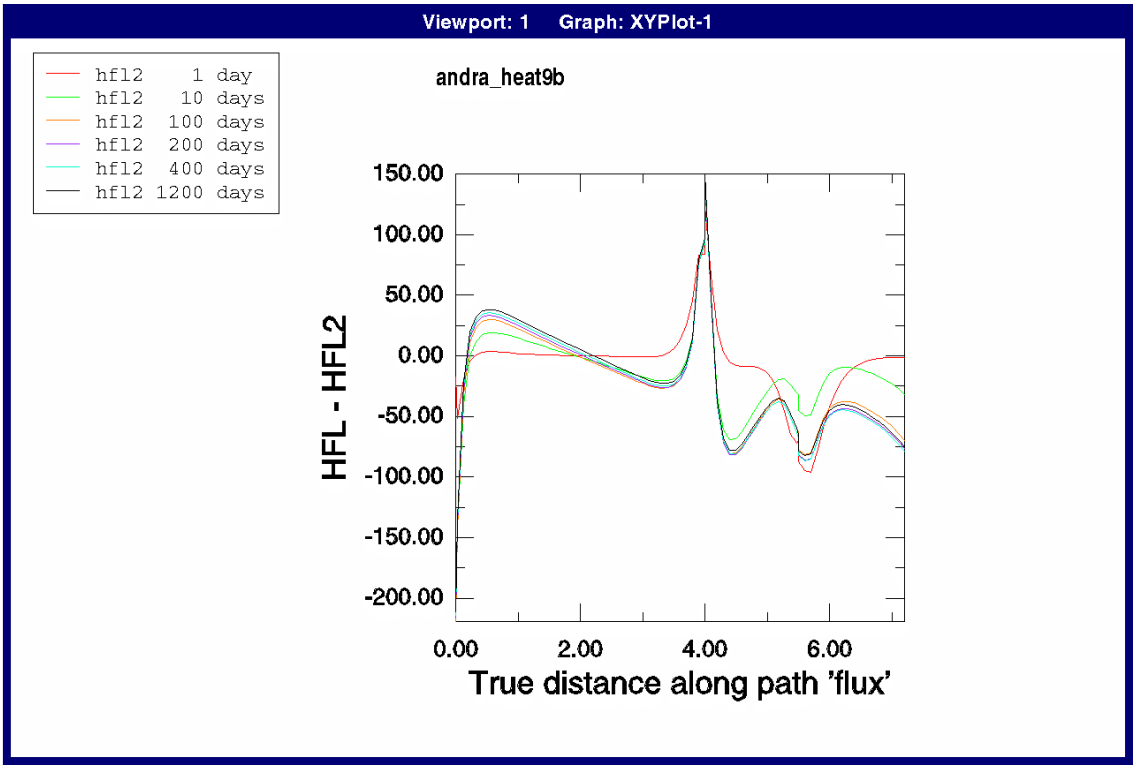

Figure 4-34. *Case 9b (differentiated power). Radial heat flux (W/m) through the surface at the radius 0.525 m (upper) and corresponding axial heat flux (lower) as function of the distance (m) from the top of canister 1*

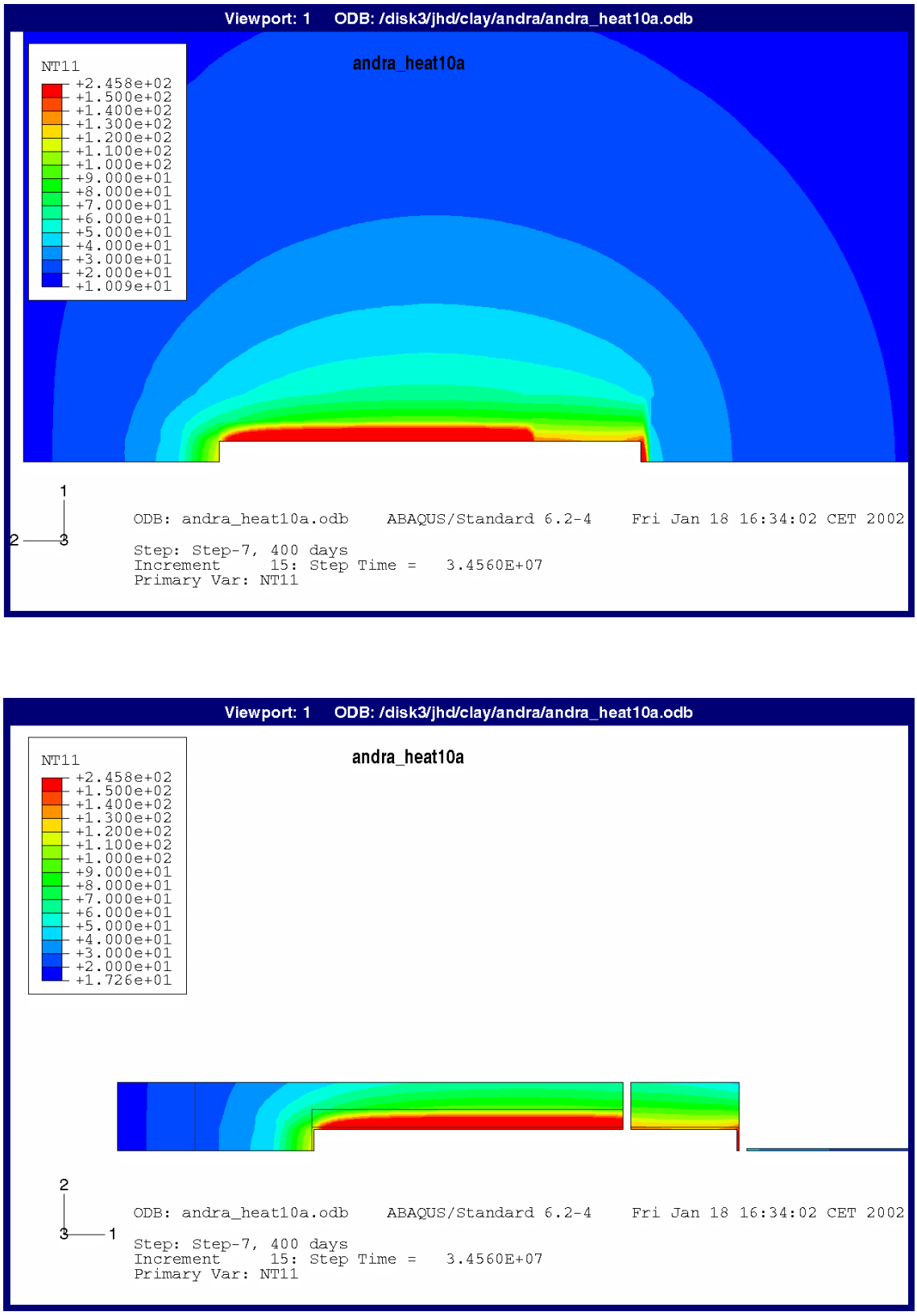

Figure 4-35. *Case 10a (double isolation). Contour plots of the temperature (°C) distribution after 1200 days in the rock and the excavated parts (upper) and solely in the excavated parts (lower) (rotated 90 degrees)*

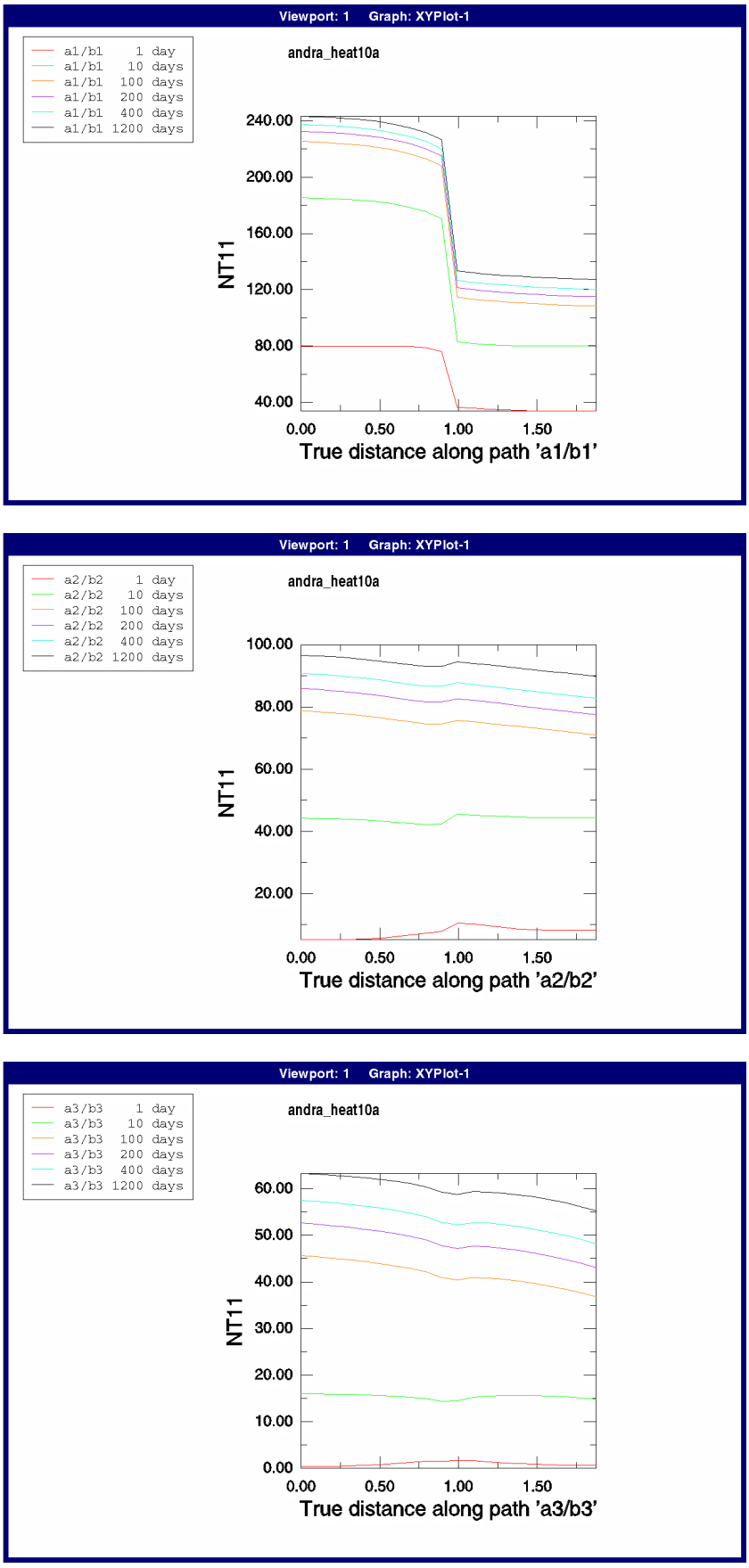

Figure 4-36. *Case 10a (double isolation). Temperature (°C) distribution between points a1 and b1, a2 and b2, and a3 and b3 at different times*

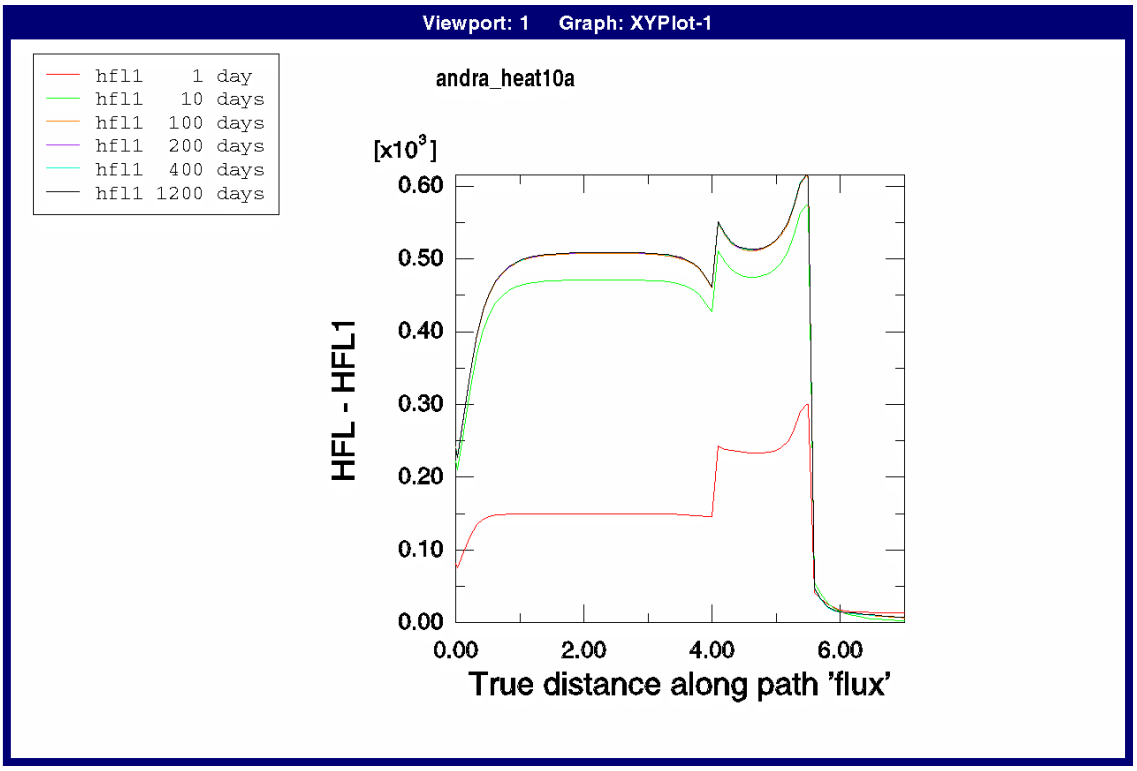

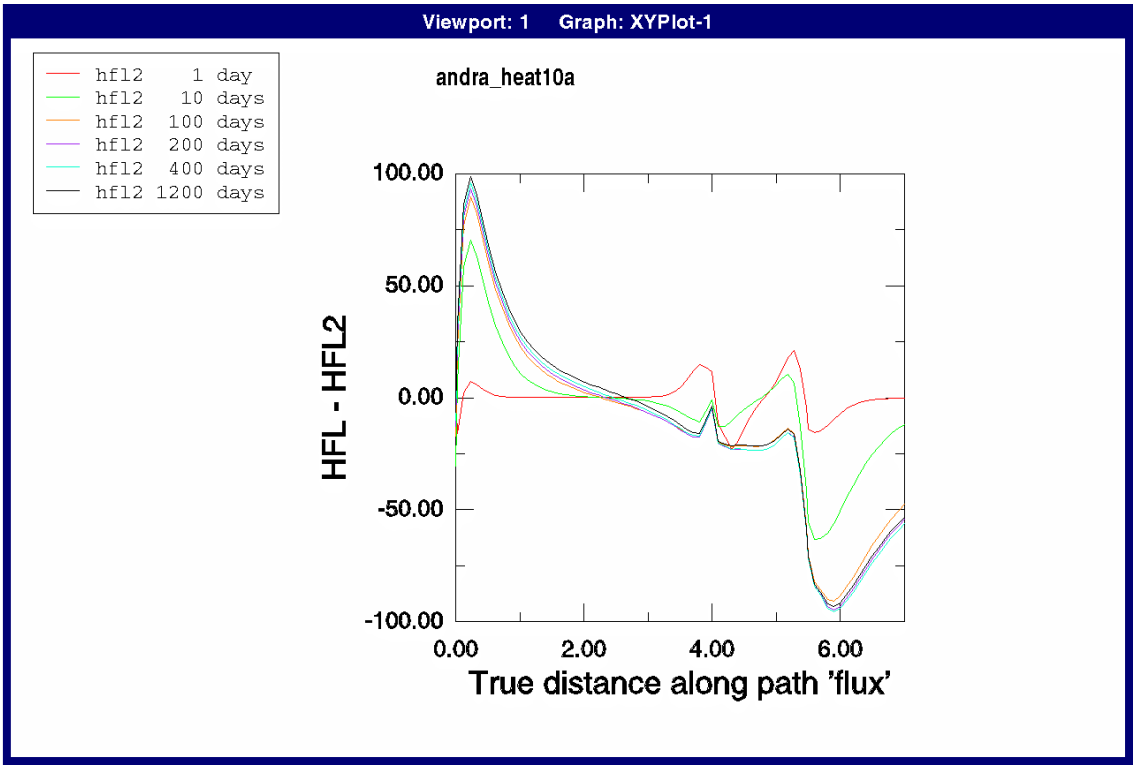

Figure 4-37. *Case 10a (double isolation). Radial heat flux (W/m) through the surface at the radius 0.525 m (upper) and corresponding axial heat flux (lower) as function of the distance (m) from the top of canister 1*

APPENDIX IIb

PM regarding TBT in ÄHRL

Design calculations for the geometry and test concept dated June 2002.

Lennart Börgesson

Clay Technology AB

Jan Hernelind

FEM-Tech AB

General

A revised design of the TBT-test with bentonite blocks instead of isolation at the heater ends has been proposed. This PM is a brief description of the results from FEM-calculations of the temperature development in a test with that new design.

The geometry is shown in Figure 1. All data of included material are the same as the base case described in the report of study 2 (*Test of vitrified waste; Study 2, temperature field* by Börgesson and Hernelind). The calculation sequence, boundary conditions etc. are also described in that report.

The element mesh is shown in Figure 2. The steel plate below the upper heater has not been included in the model.

Results

The temperature distribution along the vertical lines a1/b1, a2/b2 and a3/b3 are shown in Figures 2 to 4. Line a1/b1 goes from the center of the upper heater to the center of the lower heater at the radius 0.3 m (heater surface), line a2/b2 goes from the center of the upper heater to the center of the lower heater at the radius 0.525 m (sand/bentonite interface) and line a3/b3 goes from the center of the upper heater to the center of the lower heater at the radius 0.875 m (rock surface).

Figures 6 and 7 show the radial and axial heat flux at the radius 0.525 (sand/bentonite interface) as a function of the vertical distance from 0.1 m above the upper lid of the upper heater.

Figures 8 to 11 show the temperature distribution (no rock) at different times while Figures 13 and 14 show the temperature distribution including some of the rock.

Figure 15 shows the temperature as a function of time in the points a1, b1, a2, b2, a3 and b3.

Comments

The results clearly show that an ideal radial heat flux is not achieved since the isolation from the bentonite is not good enough. Because of drying the isolation properties are expected to be improved during a large part of the test period before wetting of those blocks. The calculations are representative for the initial stage (about a year) and the end stage after saturation.

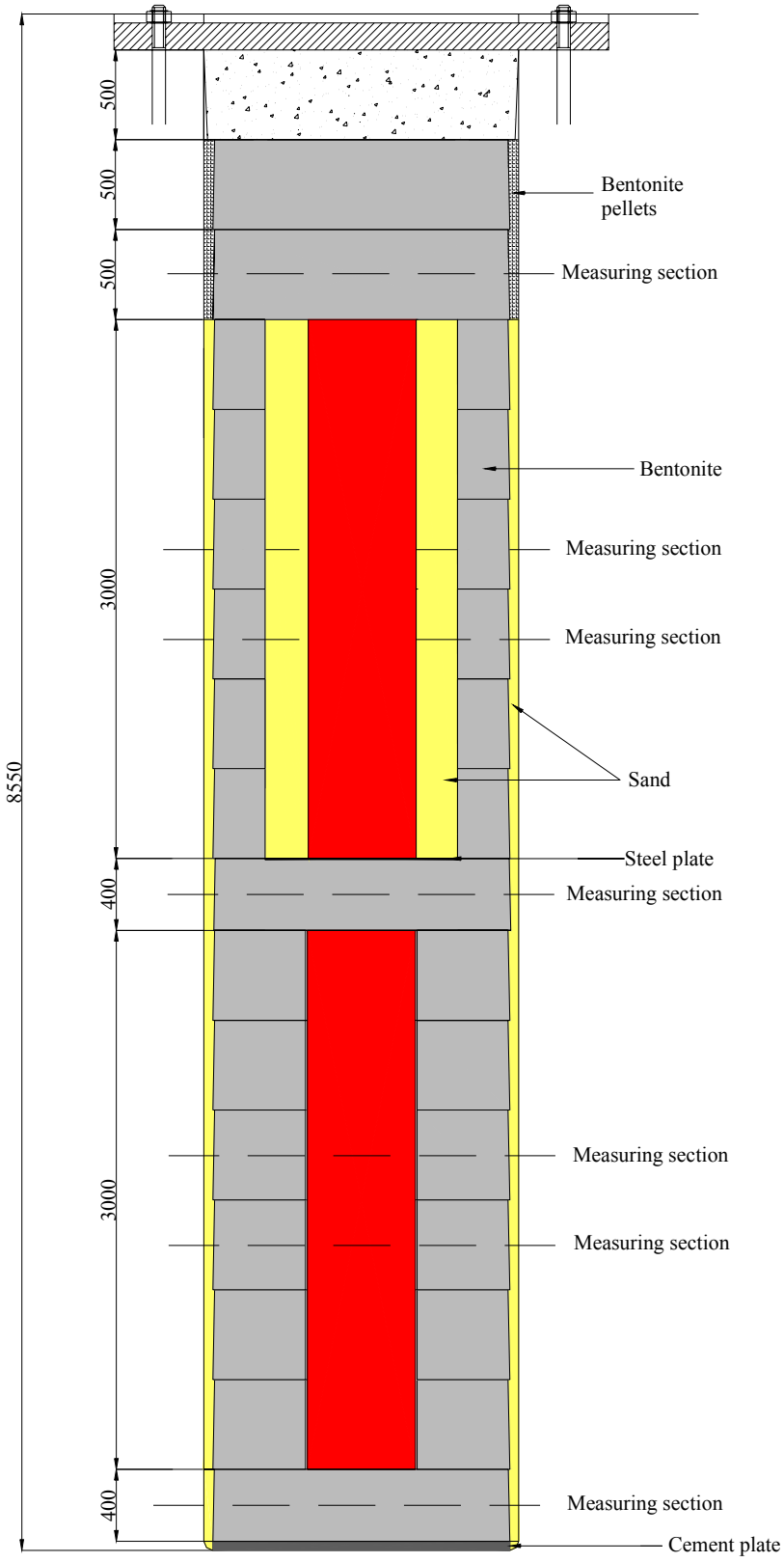

Figure 1. *New design of TBT*

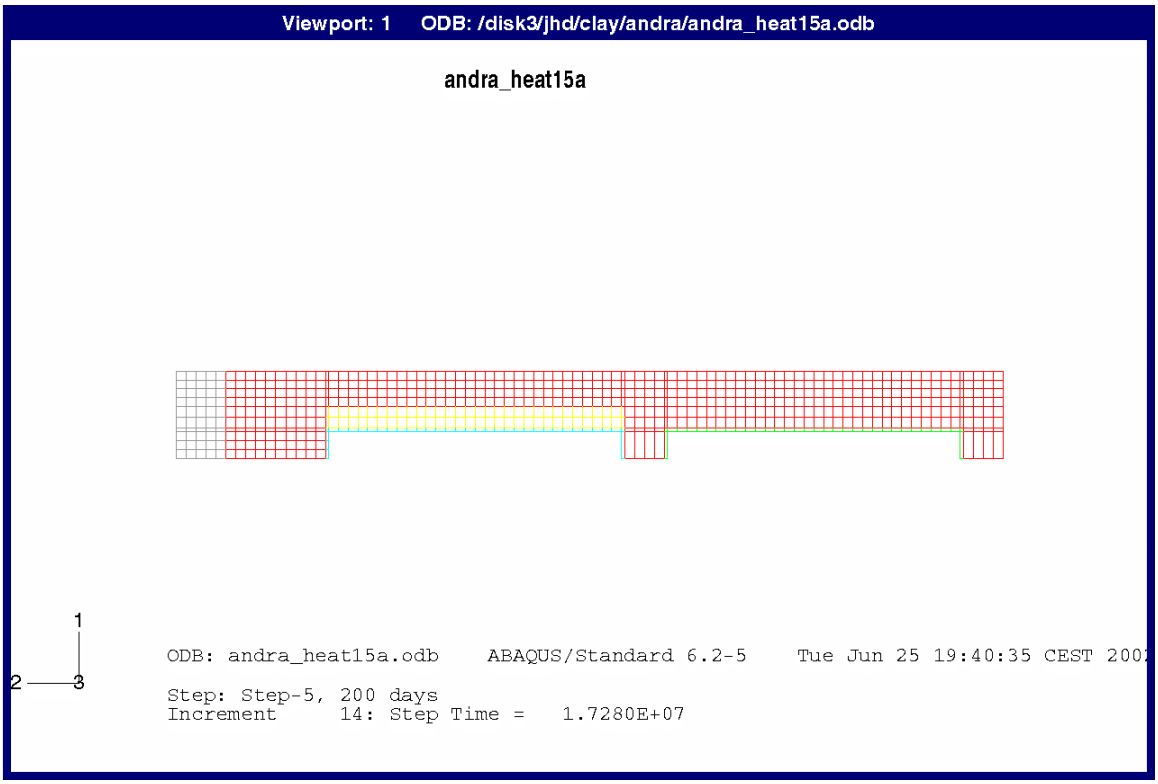

Figure 2. *Element mesh of all parts except the rock*

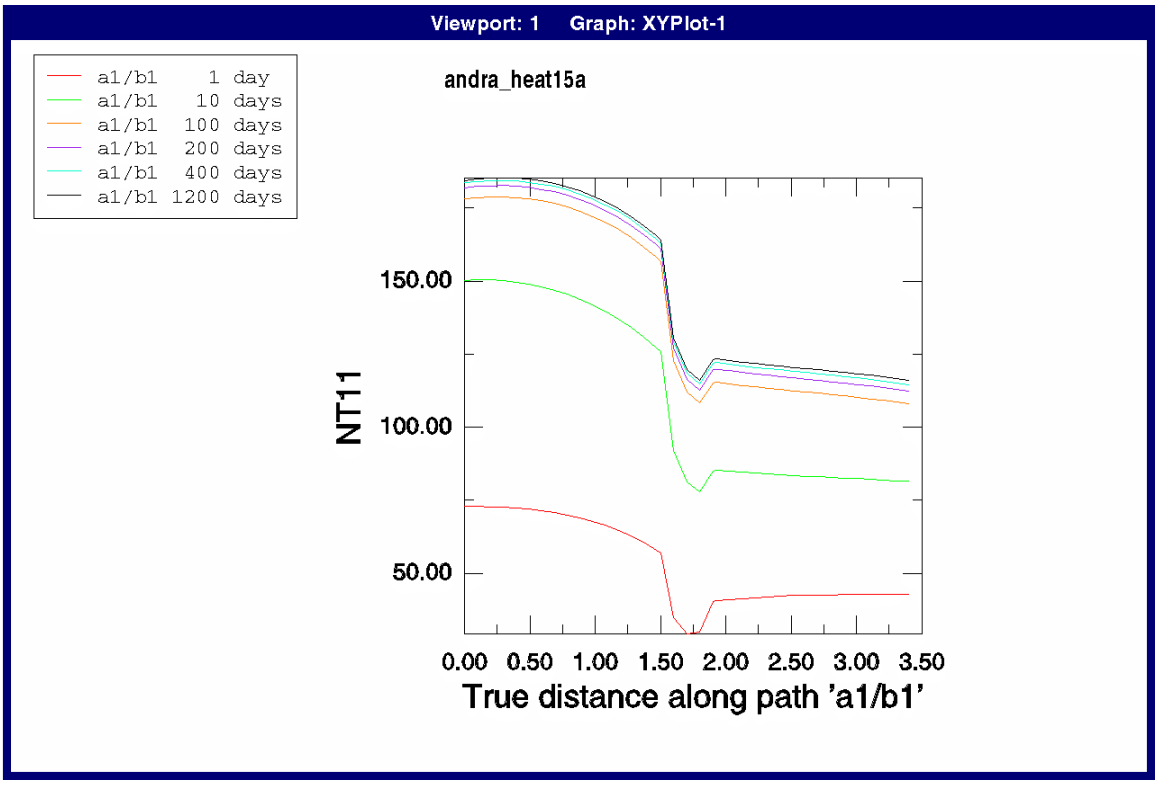

Figure 3. *Temperature along path a1/b1 (canister surface)*

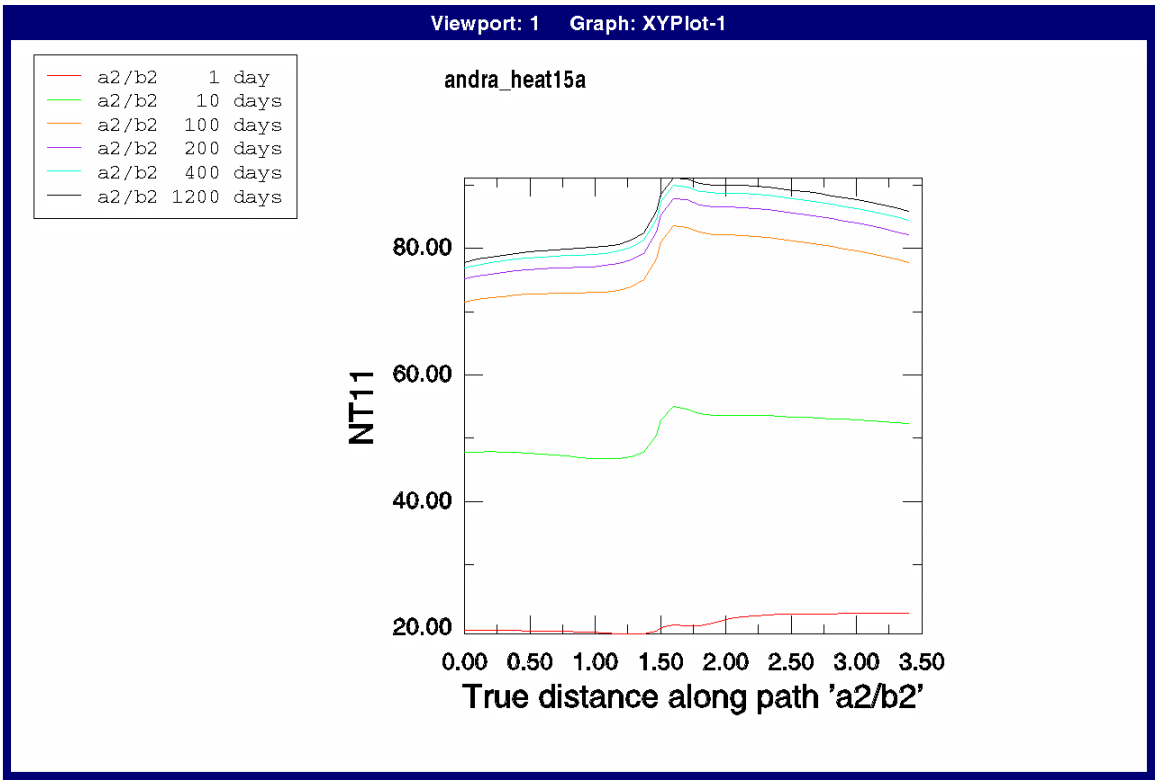

Figure 4. *Temperature along path a2/b2 (sand/bentonite interface)*

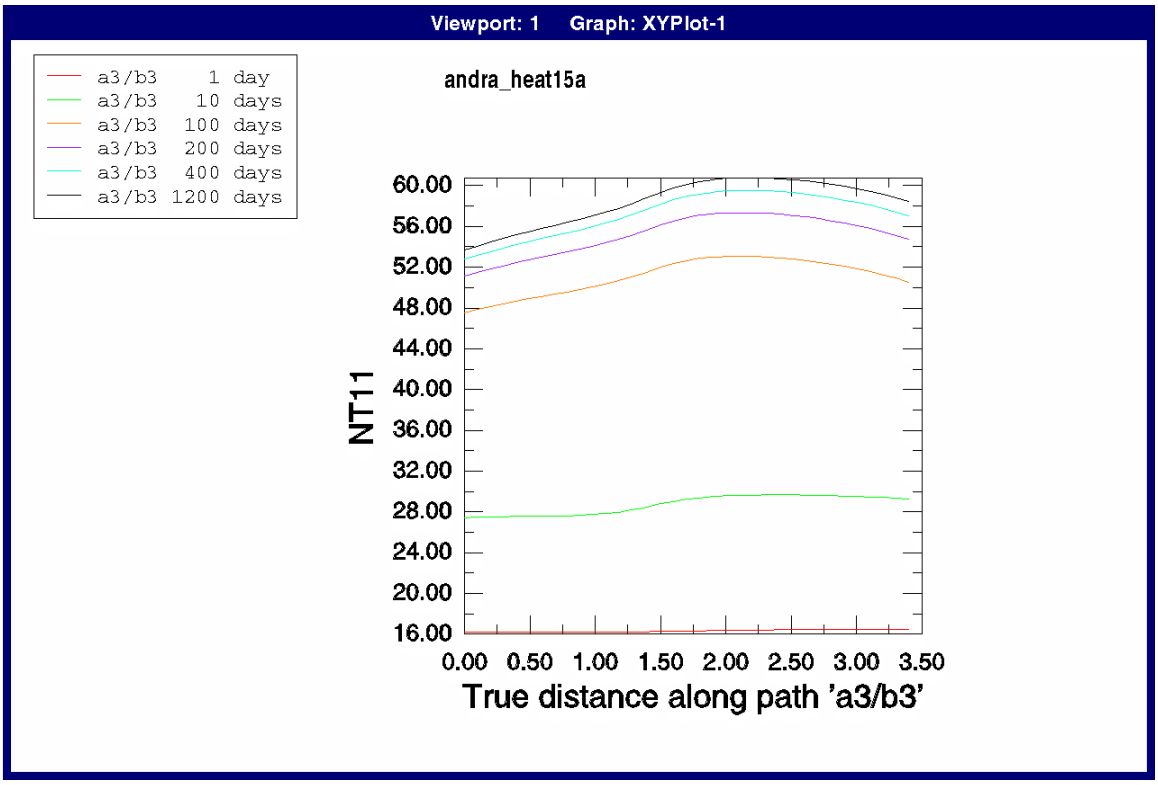

Figure 5. *Temperature along path a3/b3 (rock/bentonite)*

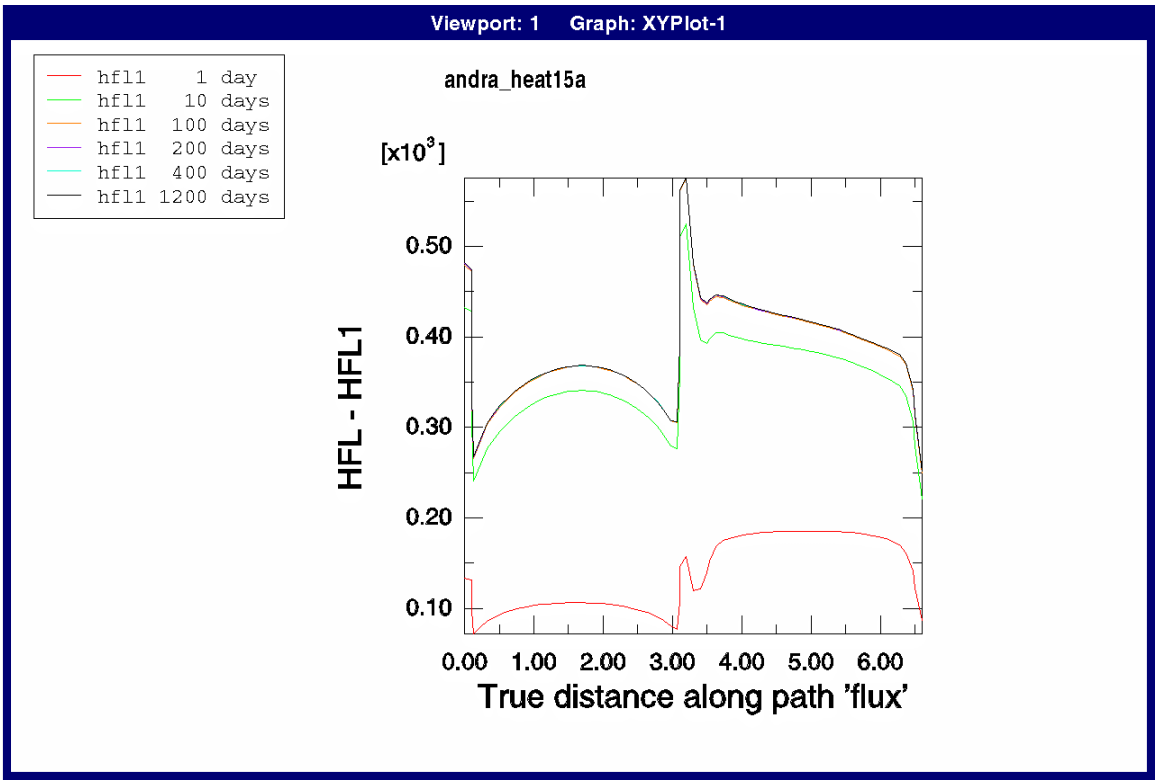

Figure 6. *Radial heat flux (W/m) along vertical line located at sand/bentonite interface*

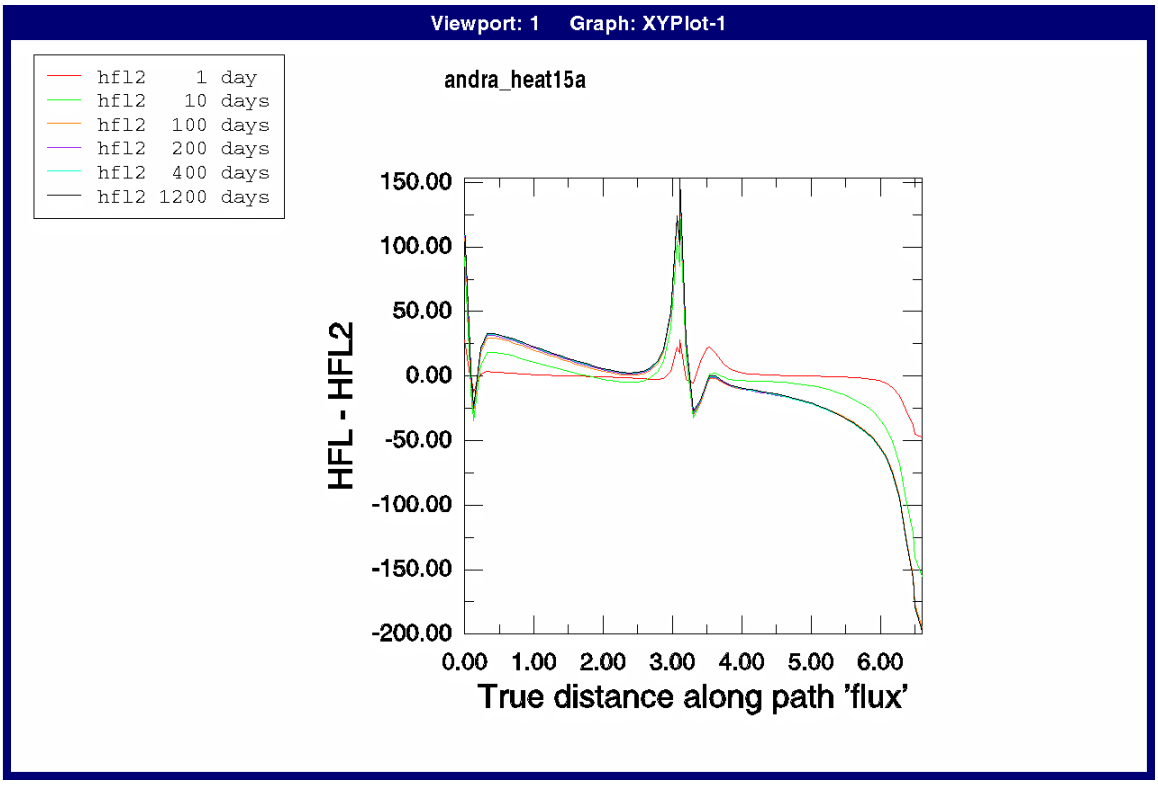

Figure 7. *Axial heat flux (W/m) along vertical line located at sand/bentonite interface*

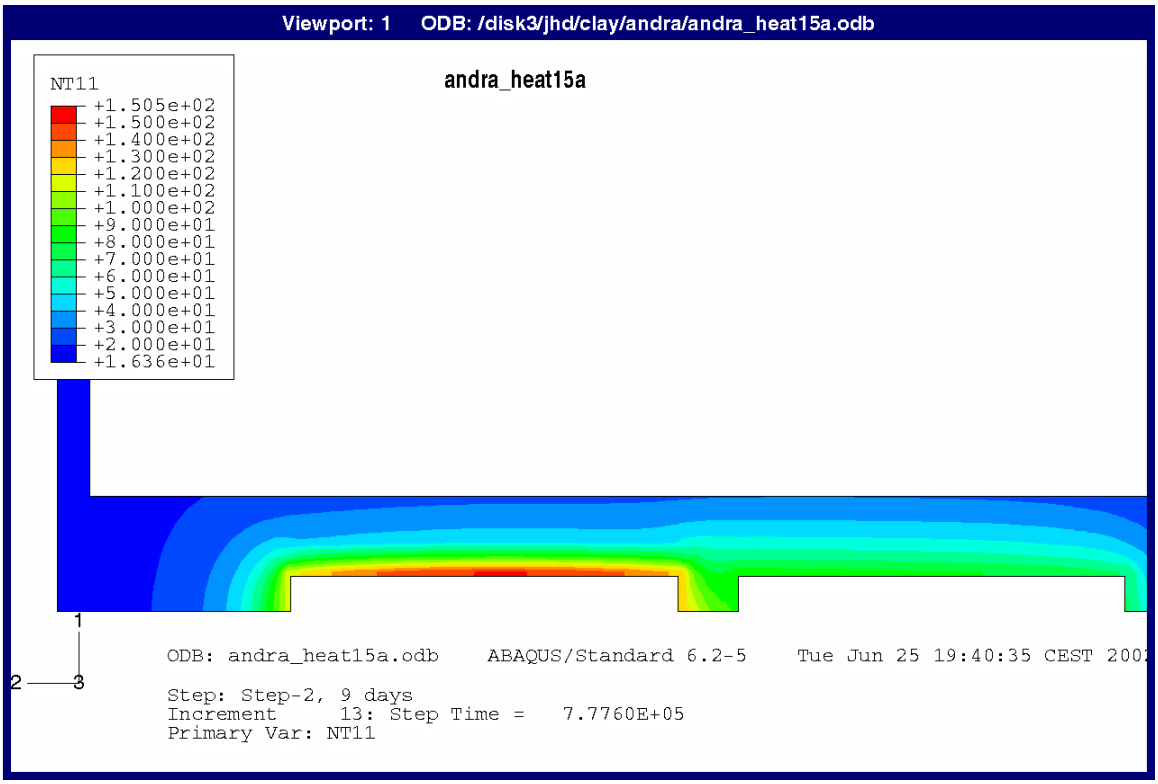

Figure 8. *Temperature after 10 days*

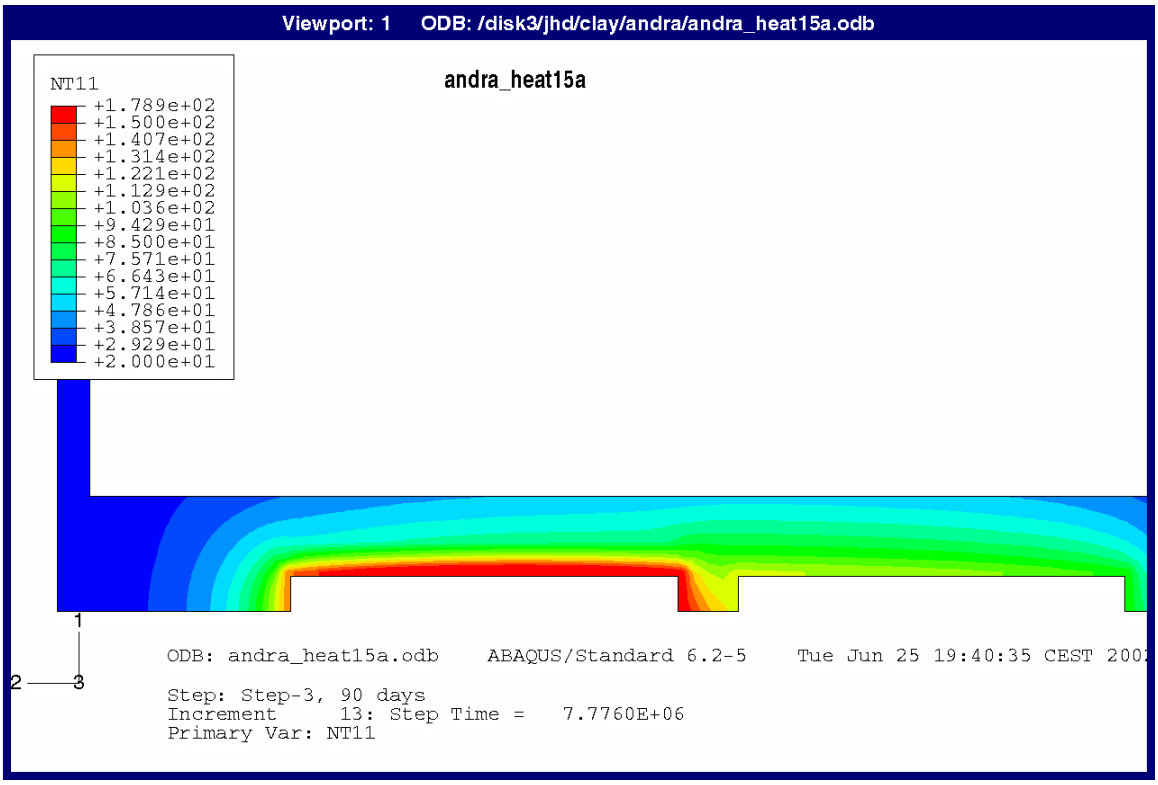

Figure 9. *Temperature after 100 days*

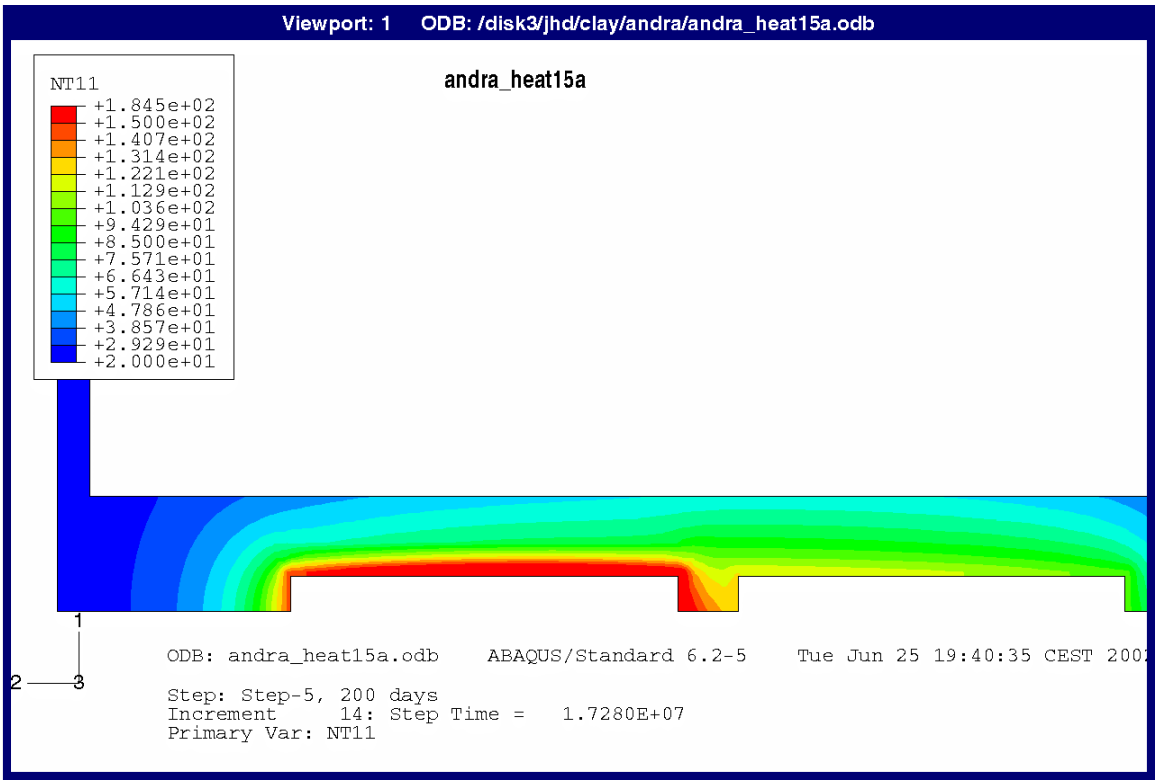

Figure 10. *Temperature after 400 days*

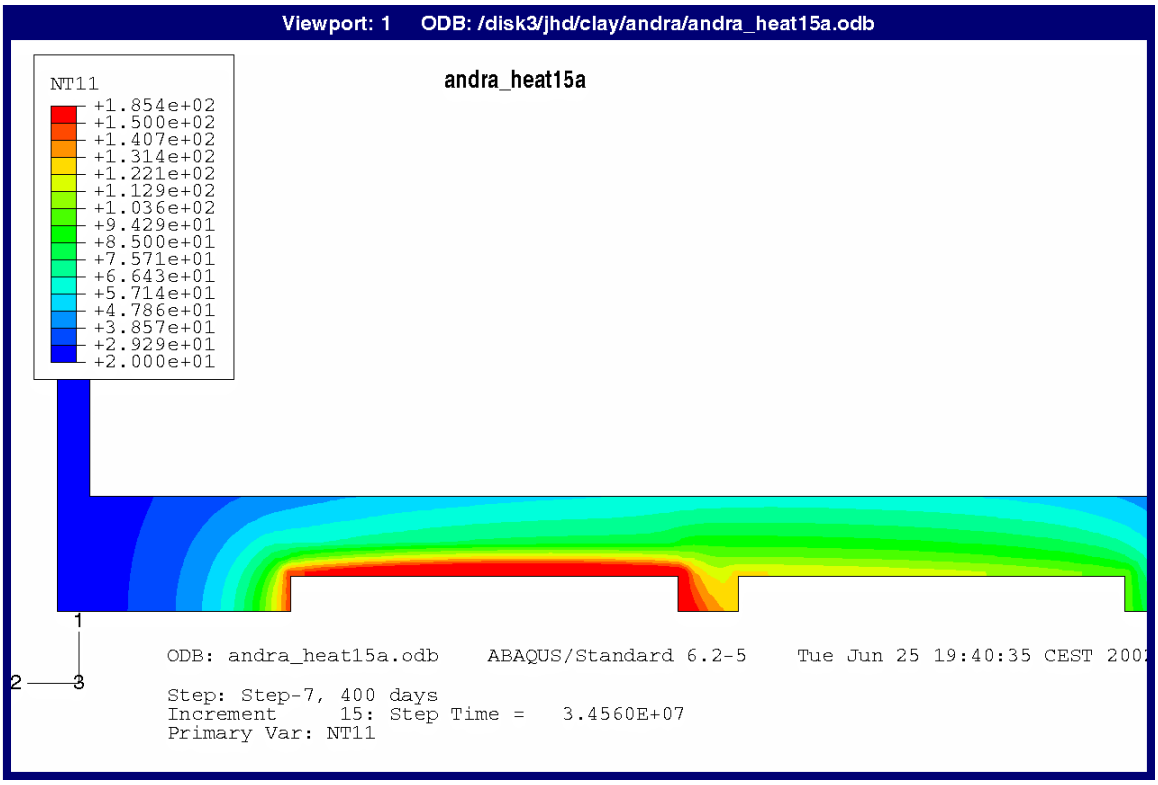

Figure 11. *Temperature after 1200 days*

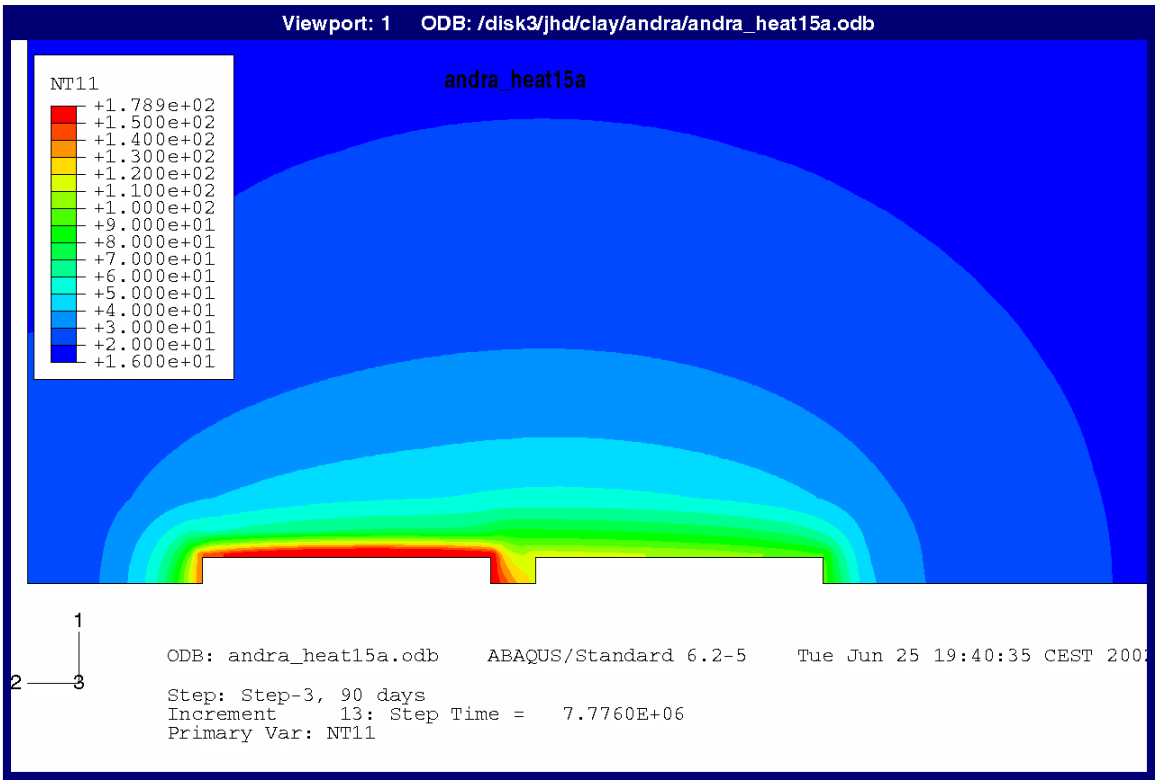

Figure 12. *Temperature after 100 days*

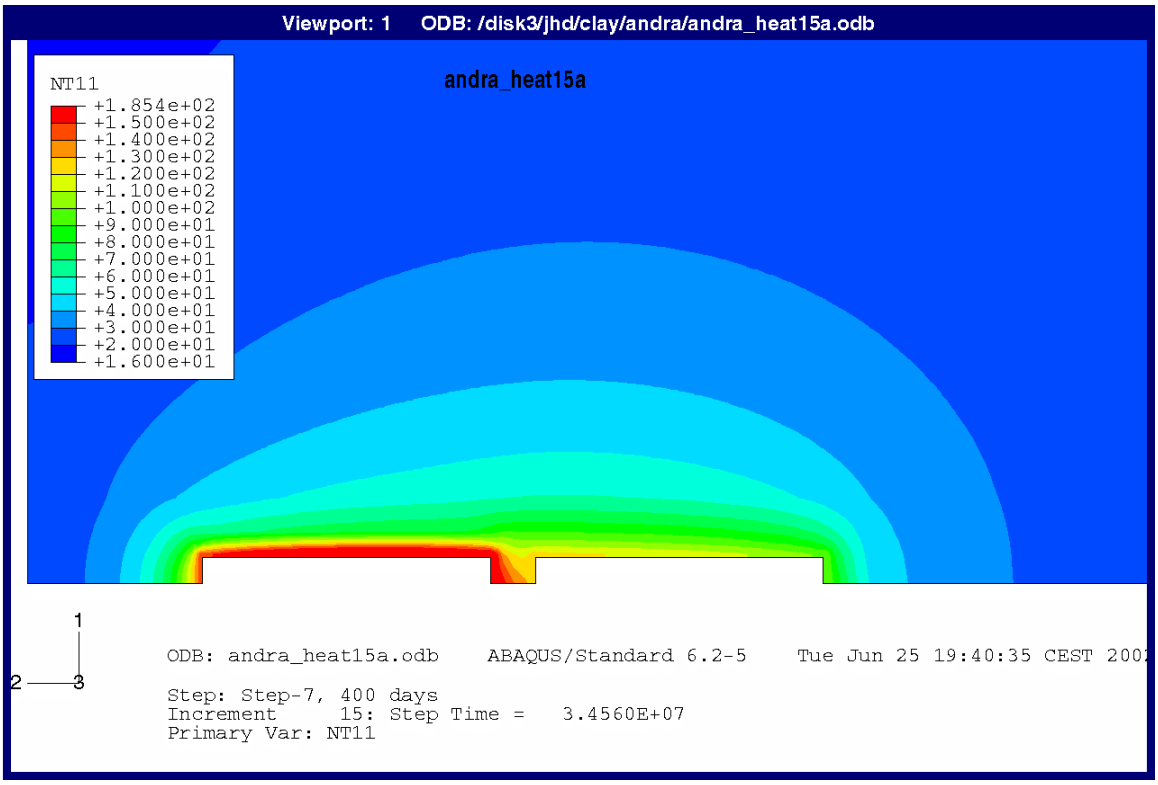

Figure 13. *Temperature after 1200 days*

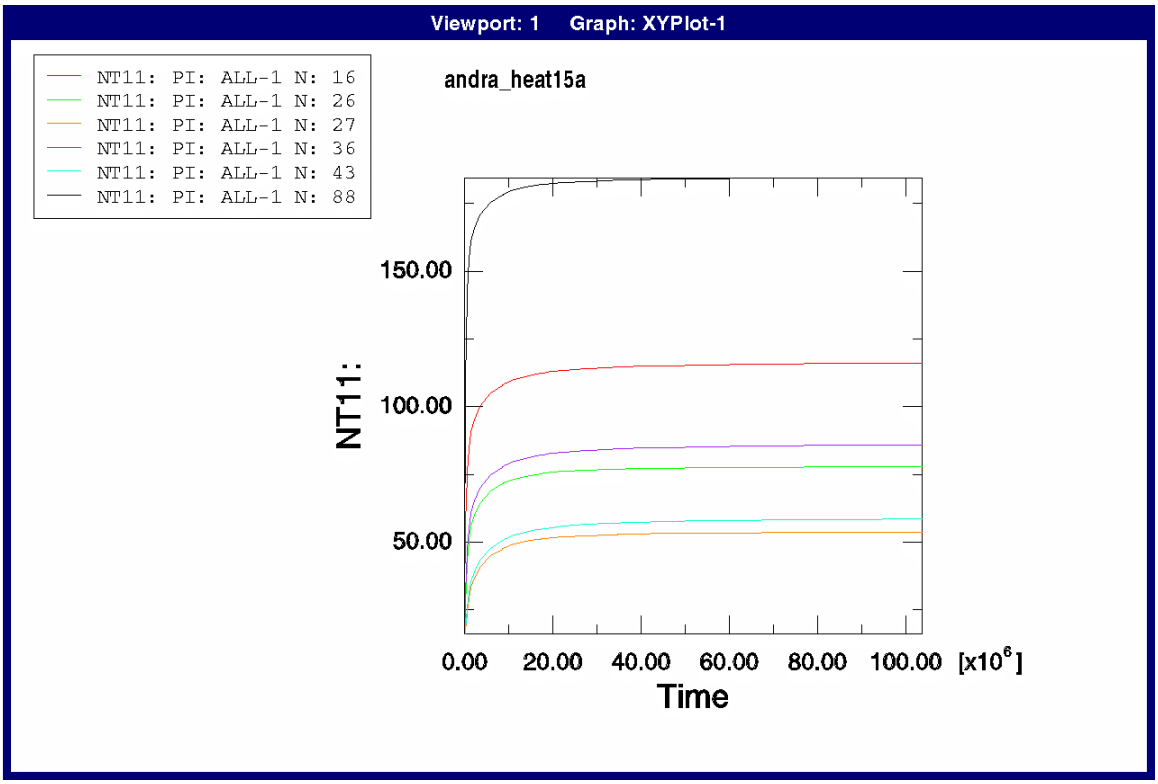

Figure 14. *Temperature in points a1 (88), b1 (16), a2 (36), b2 (26), a3 (43) and b3 (27)*

APPENDIX III

TEST OF VITRIFIED WASTES

STUDY 3 - HYDRATION

One-dimensional radial moisture movement in cavity interior

Harald Hökmark

Clay Technology AB

January 2002

1 Contents

1 Introduction and background

ANDRA plans to conduct a full scale Vitrified Waste Test at Äspö HRL.

The present text shows the results of the third study of a series of studies, aimed at assessing the feasibility, costs and general prospects of the test. This particular study regards the basics of moisture and heat transfer across the annular gap of unsaturated porous buffer material between the waste package and the rock wall. Moisture can move at least in two ways: from the rock wall towards the heater as a result of pore pressure gradients and in the opposite direction as a result of vapor concentration gradients. These processes depend on the temperature in the system and on the temperature gradients associated with the radial heat flux and together they determine the time-scale for saturation of the buffer material.

The rationale for the present study is the need to obtain reasonable saturation time-scale estimates. This report describes an estimation approach based on the use of a FEM simulation tool, specifically developed for analyzing coupled THM processes in unsaturated, porous media.

2 Problem statement – geometry and material

2.1 Geometry

A long cylindrical heater of radius R1 = 0.3 m is depositioned vertically in a cylindrical cavity of radius R3 = 0.88 m. The medium surrounding the cavity is granite. The annular space between heater and granite is filled with bentonite (case 1) or bentonite and sand (case 2). In case 2, the sand/bentonite interface is at radius R2 = 0.5 m. The bentonite is of the same type and has the same density as the material used in the prototype and retrieval tests, both tests being conducted by SKB at the site. At the test start, the bentonite has a saturation of 80%, while (for case 2) the sand is dry. At the granite/bentonite interface, there is free access to water of zero pressure.

The heater is long enough that both heat flow and moisture movement can be approximated to be purely radial over a central length section, or "plateau" corresponding to a couple of meters of axial length. The processes in the plateau are assumed to be representative for test as a whole. The problem addressed here is to estimate the time-scale for water saturation of the bentonite in that plateau.

The length of the heater is 8.7 m, and it emits a constant power of 500 W per m of heater length. These are values derived from ANDRA's test description and from the previously conducted thermal study (study 1). The temperature development in the rock surrounding the cavity was determined in the previous study.

Figure 1 shows a horizontal slice at package mid-height. The problem domain is between R1 and R3.

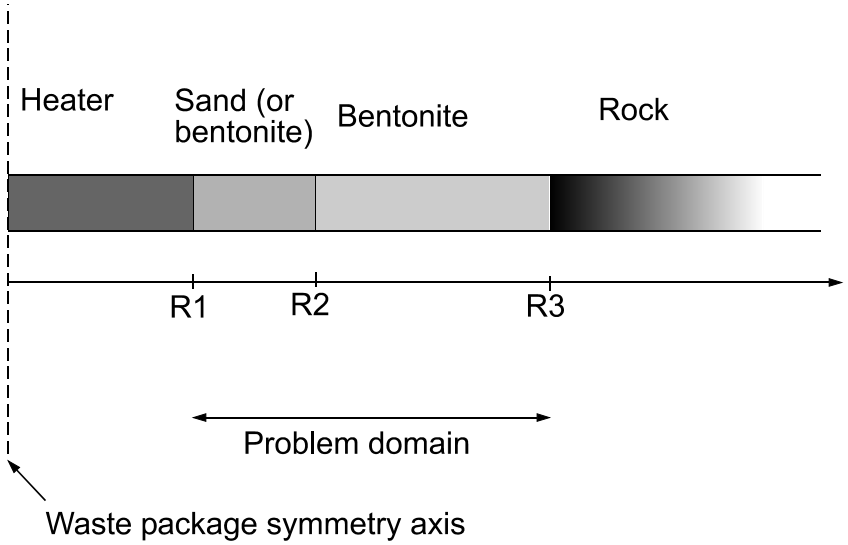

Figure 1. *Problem geometry.*

2.2 Bentonite material

The MX80 bentonite blocks produced for the prototype experiment at Äspö HRL have a dry density of about 1700 kg/m^3. The final density in the deposition hole will be smaller because of initial gaps and clearances. This applies also for the Vitrified Waste Test. Here, it is assumed that the reduction in dry density will be the same as the one assumed for the KBS-3 concept. This gives a dry density of 1570 kg/m^3, a void ratio of 0.77 and a porosity of 0.435 (Börgesson and Hernelind 1999).

3 Solution approach

3.1 General

The finite element code CODE_BRIGHT is used for the calculations (CIMNE, 2000).

Only the bentonite is explicitly modeled, see Fig. 1. The results obtained in the previous study 1 regarding rock wall temperature at heater mid-height, T3, are used to represent the thermal interaction with the granite. Because of its low retention properties, the dry sand (case 2) is assumed to interact thermally only, not hydraulically, with the bentonite.

3.2 Boundary and initial conditions

Figure 2 shows the geometrical model and the boundary conditions for case 1 and 2. On the right boundary, temperature and pore pressure are controlled. On the left boundary, a constant heat flux (corresponding to 500 W per meter of heater length) and zero mass flow are prescribed. The initial saturation is 80%, and the initial temperature is 15 °C.

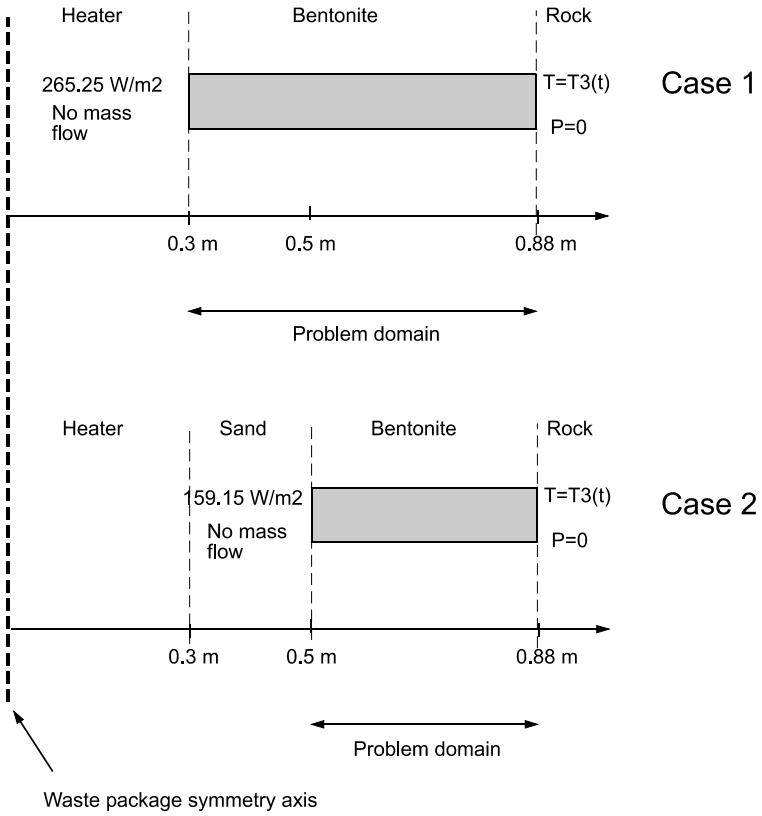

***Figure 2**. Model geometry and boundary conditions.*

Figure 3 shows the temperature boundary condition T3(t) applied at the right boundary. These conditions were determined in the previous study (study 1) and reflect the thermal response of the rock mass to the heat supplied from the 8.7 m long heater, assuming the rock mass conductivity to be 2.6 W/(m·K). At present, it is not possible in CODE_BRIGHT to prescribe continuously varying thermal boundary conditions. Therefore a stepwise scheme was adopted.

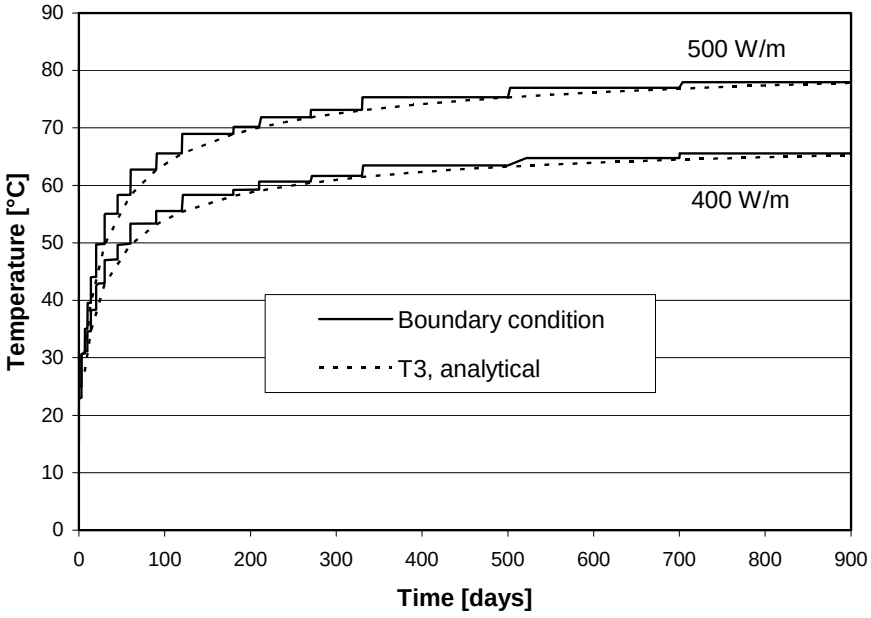

Figure 3. *Temperature boundary condition in buffer/granite interface. The analytical curves are from study 1.*

3.3 Outline of material model

3.3.1 General

Here, a brief description of the features that are of particular importance to the present study is given. A complete account of all details is not within the scope of this study.

3.3.2 Saturation-pressure relation

Figure 4 shows retention curves for MX80. Both experimental values and van Genuchten fits used in the CODE_BRIGHT models are shown.

The vanGenuchten relation is given by:

$$S_r = \left\{ 1 + \left(\frac{P_g - P}{P_0 \cdot \left(\frac{\sigma}{\sigma_0} \right)} \right)^{\frac{1}{1-\lambda}} \right\}^{-\lambda} , \qquad (1)$$

where P is the pore pressure and P_g is the gas pressure. P_0 = is a reference pressure and λ a shape parameter. P_0 and λ are set by fitting Eqn. 1 to experimental values. (σ/σ_0) is a built-in temperature dependent surface tension ratio. The quantity P_g - P is mostly referred to as suction.

For the reference material used here, (0.77 void ratio), P_0 is 19 MPa and λ is 0.45. For the low density material also shown in Fig 4 (0.80 void ratio), P_0 is 9 MPa, and λ is 0.40. The initial saturation assumed here, 80%, corresponds to a suction of 14.9 MPa for the base case (void ratio 0.77) and 7.6 MPa the low density case (void ratio 0.80)

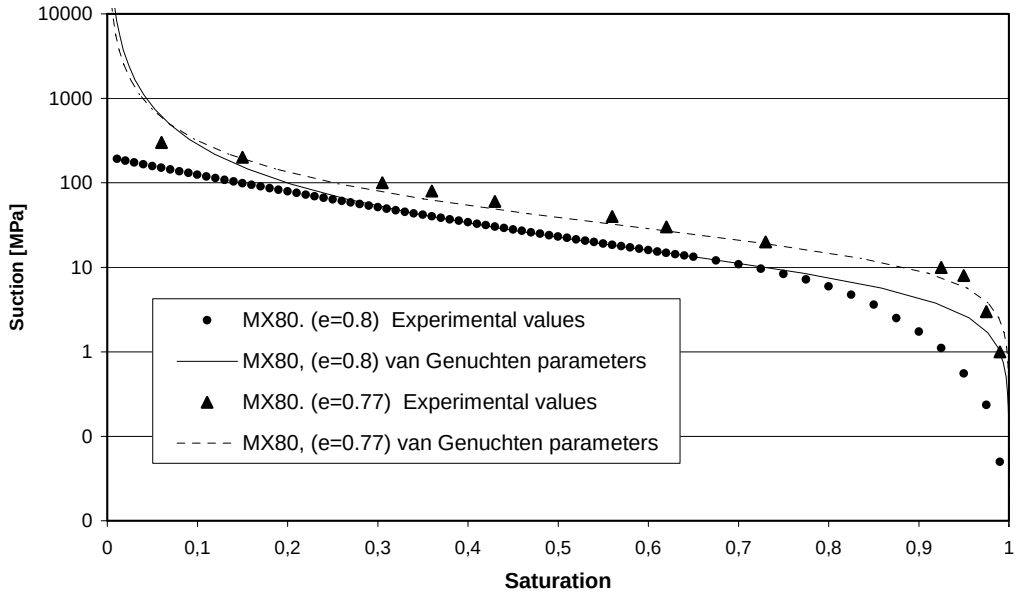

***Figure 4**. Retention curves for the MX80 reference material (void ratio = 0.77) and for MX80 bentonite compacted to a lower density (void ratio = 0.80).*

3.3.3 Moisture transport

There are two main transport modes to consider.

1. Moisture moves from the rock wall towards the heater driven by pore pressure gradients, obeying the Darcy law.

2. Moisture moves in the opposite direction in vapor form, driven by vapor concentration gradients, obeying laws of molecular diffusion.

If there is advective gas transport, there will also be advective flux of vapor. In this preliminary study, advective vapor flux is not considered. A constant atmospheric total gas pressure is assumed.

Darcy flow

The flux **q** is given by

$\mathbf{q} = -\frac{\mathbf{k}k_r}{\mu}\nabla P$,	(2)

where **k** is the intrinsic permeability, k_r is the relative permeability, μ is viscosity and P is the pore pressure. The pore pressures (and pore pressure gradients ∇P) are calculated from the retention relations (Eqn. 1; Fig. 4)

For the reference material, **k** is set to $0.5 \cdot 10^{-20}$ m^2. This corresponds to a hydraulic conductivity of $0.5 \cdot 10^{-13}$ m/s at room temperature and full saturation.

The relative permeability k_r is assumed to depend on the water saturation S_r according to the generalized power law:

$$k_r = A \cdot S_r^{\lambda} \qquad (3)$$

Here A is set at 1 and λ at 3. The generalized power law and the parameter values are in accordance with the material model suggested and used for MX80 bentonite in the THM calculations used as reference in the recently issued safety analysis SR 97. (Börgesson and Hernelind, 1999; SKB, 1999)

The viscosity of water depends on the temperature. CODE_BRIGHT uses a built-in standard expression for this (Fig. 5, left part). This means that flux is also temperature dependent. The right part of Fig. 5 shows the flow coefficient in Eqn. 2 recalculated as saturated hydraulic conductivity.

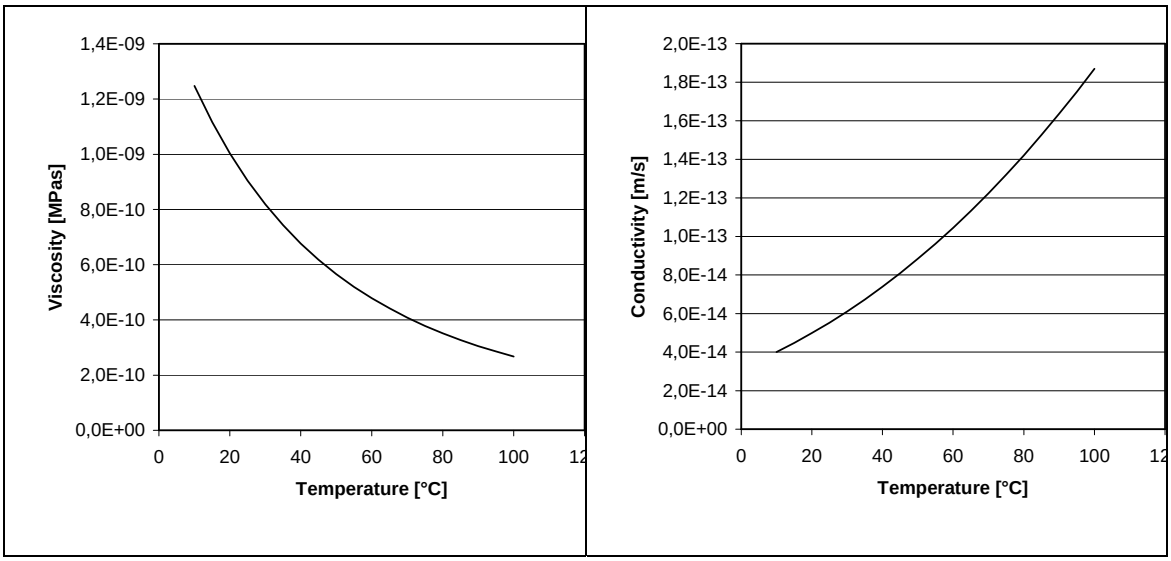

Figure 5. *Temperature influence on viscosity of water (left) and hydraulic conductivity of saturated reference material (right).*

Molecular diffusion

Non-advective flux of vapor is driven by vapor mass fraction gradients according to Eqn 4:

$$\mathbf{i} = -(\phi \cdot (1 - S_r) \cdot \rho \cdot D_v) \cdot \nabla \omega, \qquad (4)$$

where ϕ is the porosity, ρ is the gas phase density and ω is the mass fraction of vapor in the gas phase. The diffusion coefficient D_v is given by:

$$D_v = \tau \cdot D \cdot \left(\frac{(273.15 + T)^n}{P_g} \right) \quad (5)$$

where τ is the tortuosity and P_g is the gas pressure. Eqns. 4 and 5 are based on general theories of vapor transport in porous media, and do not relate specifically to the properties of highly compacted bentonite. Here, default values were used for all parameters: $D = 5.9 \cdot 10^{-6}$ $m^2 s^{-1} K^{-n} Pa$, $n = 2.3$, $\tau = 1$ (CIMNE, 2000).

3.3.4 Heat transfer

The CODE_BRIGHT model considers both conductive heat flux and advective heat flux associated with mass motions (solid, liquid and vapor). It can easily be shown that the advective fluxes are very minor in comparison with the conductive flux. For the thermal conductivity λ, CODE_BRIGHT uses the following relation:

$$\lambda = S_r \cdot \lambda_{sat} + (S_r - 1) \cdot \lambda_{dry}, \quad (6)$$

where λ_{sat} is the conductivity at full saturation and λ_{dry} is the conductivity in the dry state. Figure 6 shows this relation for λ_{dry} = 0.3 W/(mK) and λ_{sat} = 1.3 W/(mK) together with experimental data.

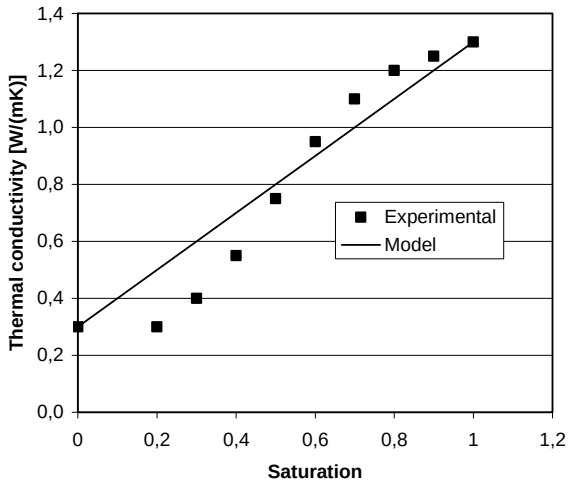

Figure 6. *Thermal conductivity as function of saturation.*

The expression underpredicts the conductivity at high saturation, and overpredicts it at low saturation. Note that the initial saturation assumed here, 80 %, will give a conductivity of 1.1 W/(mK).

4 Base Case results

4.1 General

A selection of results, relevant to the Base Case, is shown in this chapter. All properties are those described in previous sections.

4.2 Uncoupled, isothermal hydration

Figure 7 shows hydration assuming only Darcy flow, i.e. water moves only from right to left without any effects of thermally driven diffusion. At position R2 (see Fig. 1) the difference between case 1 (bentonite only) and case 2 (bentonite and sand) is significant. In case 1 some of the water moves into the region between R1 and R2. In case 2 water is trapped between R2 and R3, which gives a faster saturation in this region. As an average, the saturation in the region between R2 and R3 has increased from 80% to about 96% after 900 days in case 2. In case 1, this figure is about 94%.

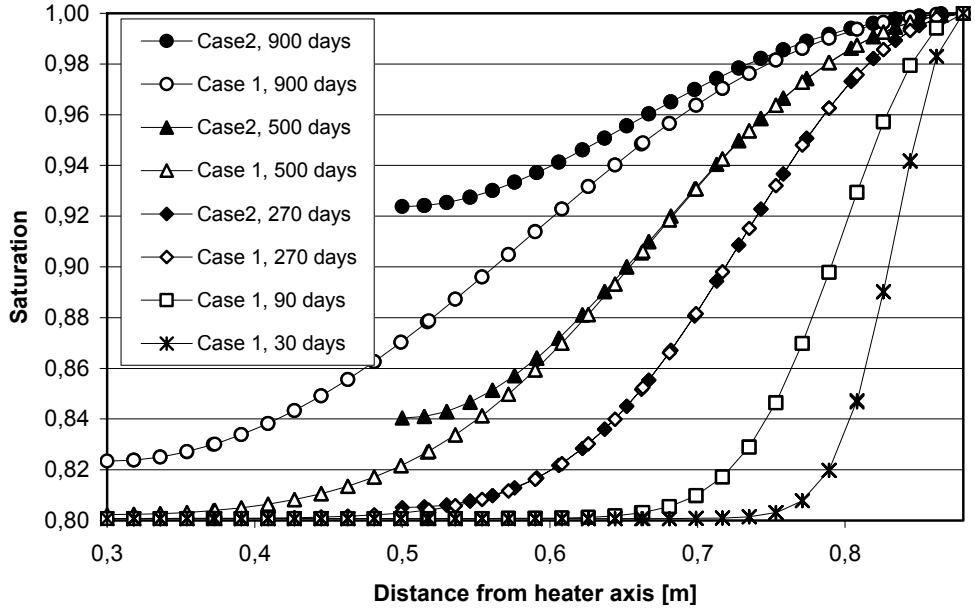

Figure 7. *Case 1 and case 2 saturation assuming isothermal conditions.*

4.3 Coupled analysis

4.3.1 Saturation

Figures 8 and 9 show the saturation at different times for case 1 and case 2, respectively. The thermal boundary conditions correspond to a constant power of 500 W/m, as described in section 3.2. Compared to the isothermal case (Fig. 7) the hydration proceeds much faster in the regions close to the rock. In case 1, there is almost complete saturation between r = 0.53 m and r = 0.88 m (rock wall) after 90 days. I case 2, the saturated region is between 0.63 m and 0.88 m.

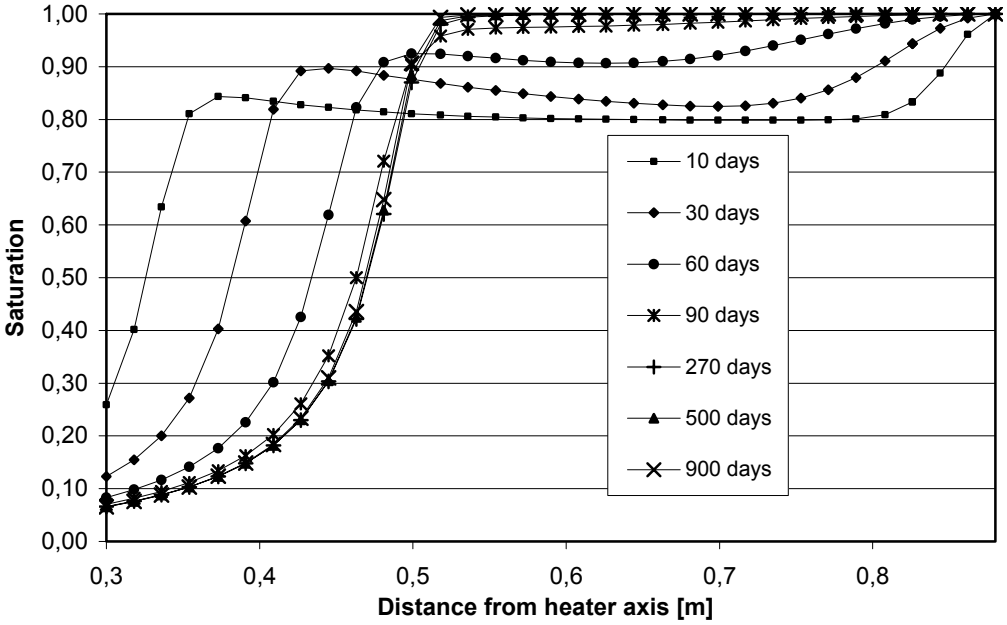

Figure 8. *Case 1 saturation*

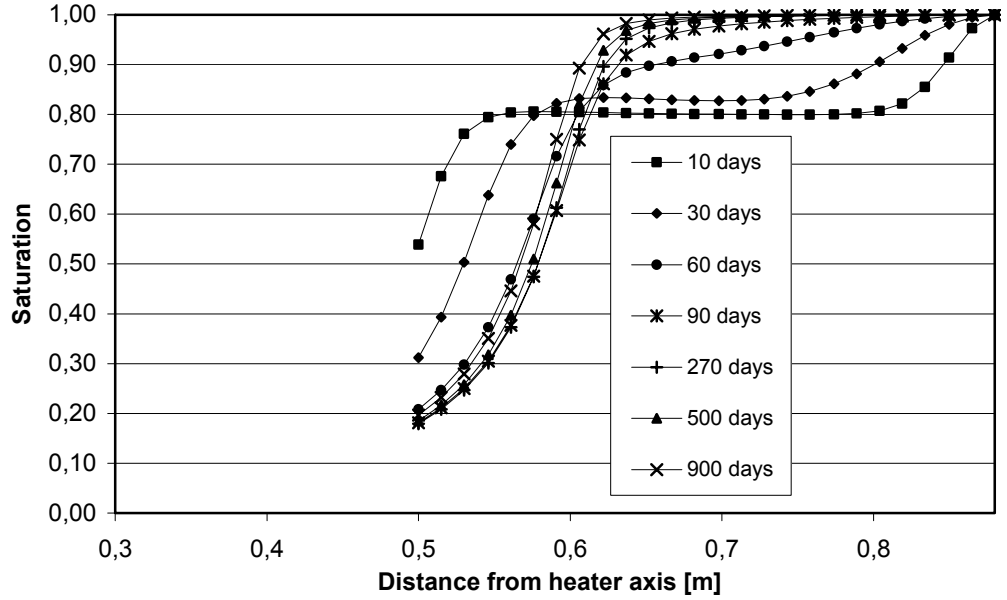

Figure 9*. Case 2 saturation*

There are two reasons for the faster saturation in the outermost part compared with isothermal case:

1. The Darcy flow from right to left is faster because of the lower viscosity associated with the elevated temperature (c.f. Fig. 5).

2. There is a thermally driven molecular diffusion from left to right.

To a large extent, the fast saturation of the parts close to the rock wall occurs at the expense of massive desaturation of the regions close to the heater. This is illustrated in a lucid way in Fig. 10, in which a direct comparison is made between case 1 and case 2. In case 1, there is reservoir of water in the region between R1 and R2 which contributes to the saturation of the region between R2 and R3, while the dry sand in case 2 does not contain any water. Therefore the saturation of the region between R2 and R3 is much more efficient in case 1.

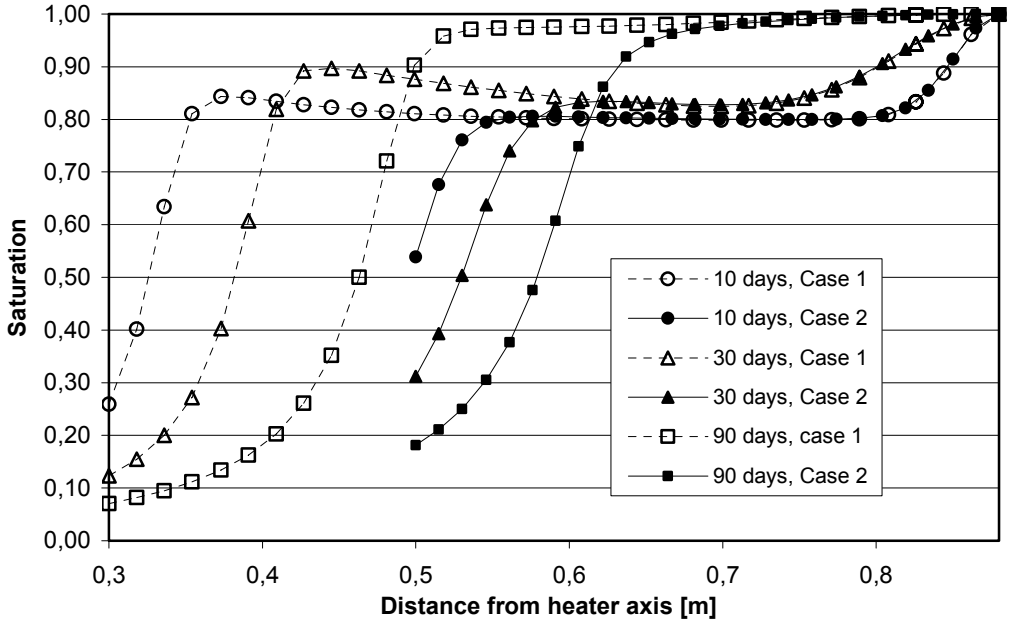

***Figure 10**. Comparison between case 1 and case 2.*

4.3.2 Temperatures

Figure 11 shows temperatures in the annular space between heater and rock wall. For comparison, curves showing the temperature that would result without any changes in saturation, (i.e. constant 1.1 W/(mK) conductivity) are included. There is also a curve showing the slope corresponding to dry conditions ((0.3 W/(mK)).

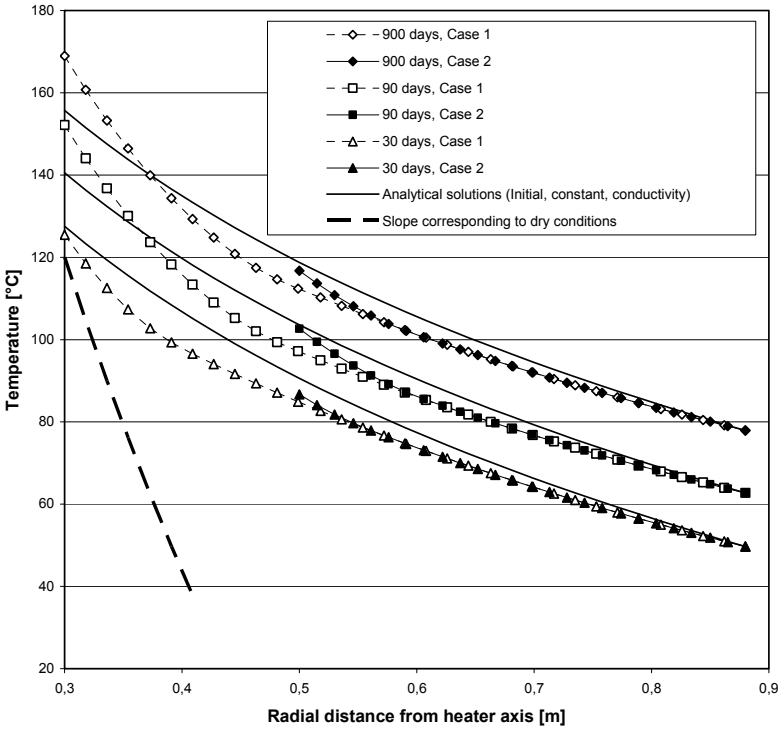

Figure 11. *Temperatures in the bentonite.*

The graphs in Fig.11 confirm the findings of the saturation plots and illustrate the effects of the Thermo-Hydraulic coupling. At the hot end, the temperature gradients are high, i.e. the slopes are steep, because of the low conductivity in the desaturated parts.

Fig 12 shows temperatures in the sand. These temperatures were calculated analytically, using Eqn. 7:

$$T(r) = T(0.5) + \frac{500}{2 \cdot \pi \cdot \lambda_s} \ln\left(\frac{r}{0.5}\right), \qquad (7)$$

assuming the thermal conductivity of the dry sand, λ_s, to be constant = 0.3 W/(mK).

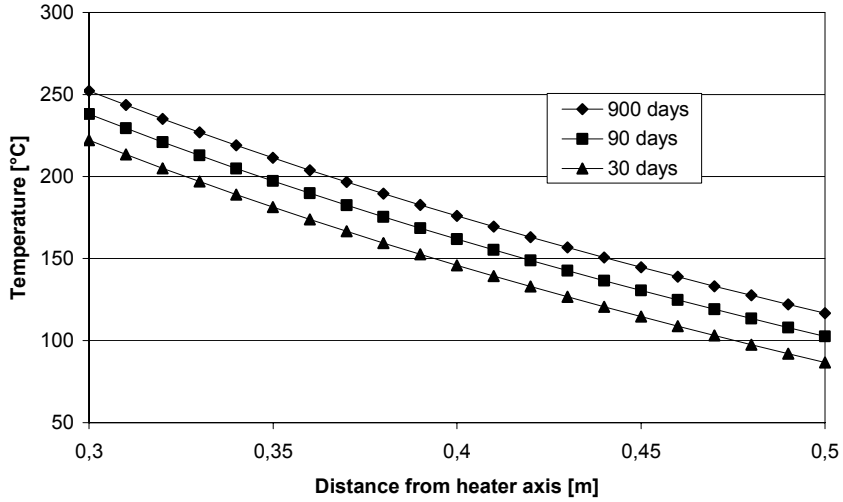

Figure 12*. Case 2. Temperatures in the sand*

5 Additional results

5.1 Reduced power

In the previous thermal study (study 1) it was concluded that a constant power of 500 W/m would give temperatures well in excess of the target temperature at R2 (100°). This has been verified in this study. In this chapter results from an analysis with a power of 400 W/m are presented and compared with corresponding base case (500 W/m) results. Only case 2 (sand shield) results are shown.

5.1.1 Saturation

Figures 13 and 14 show the saturation between R2 and R3 for both power cases. The desaturation is less severe in the 400 W/m case. After 900 days, the saturation front has moved about 3 cm further towards the sand/buffer interface than in the 500 W/m case.

The resaturation of the hottest parts proceeds at a higher rate in the 400 W/m case (bottommost curves in Fig.14).

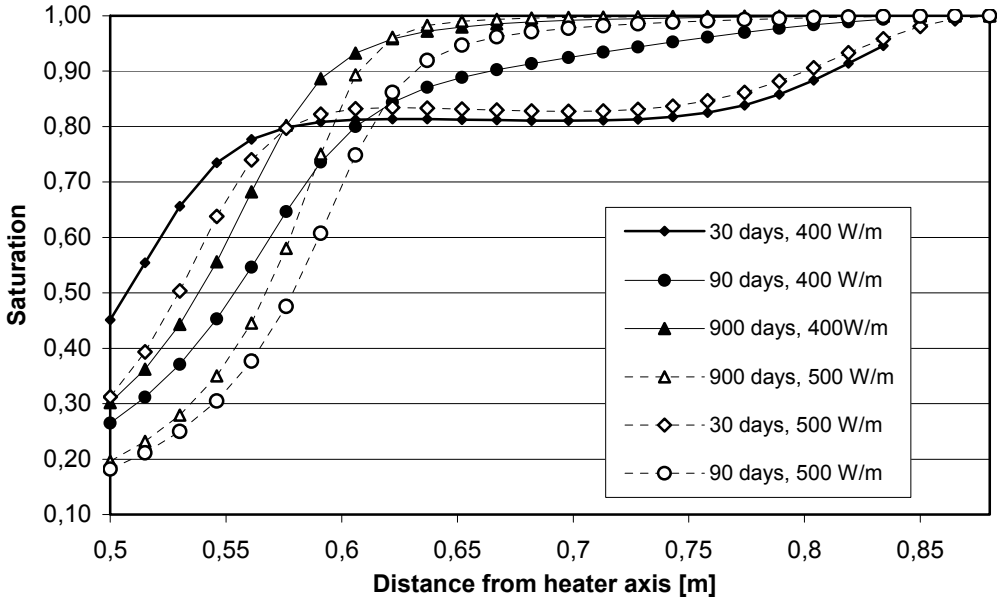

***Figure 13**. Bentonite saturation vs. distance at three different times.*

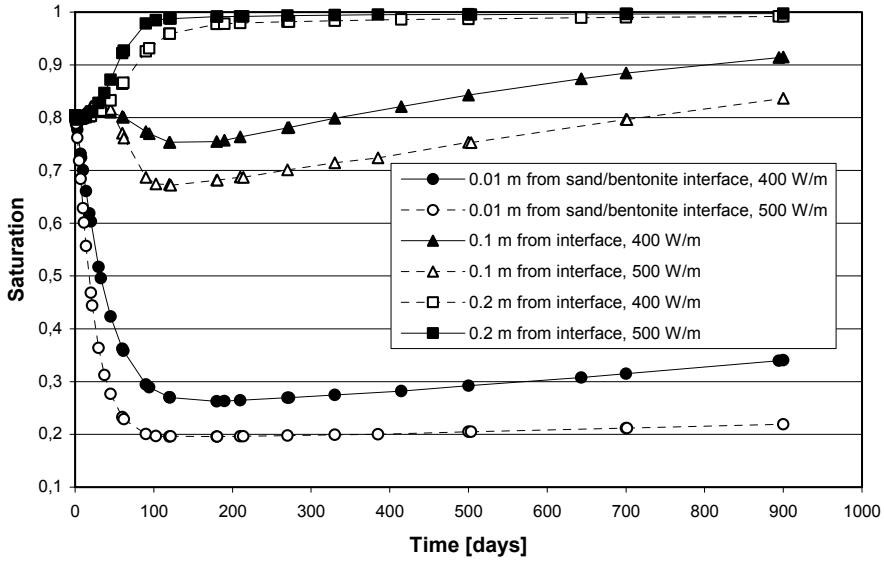

Figure 14. *Saturation vs. time for three points between R2 and R3.*

5.1.2 Temperatures

Figures 15 and 16 show temperatures in the bentonite and in the sand, respectively.

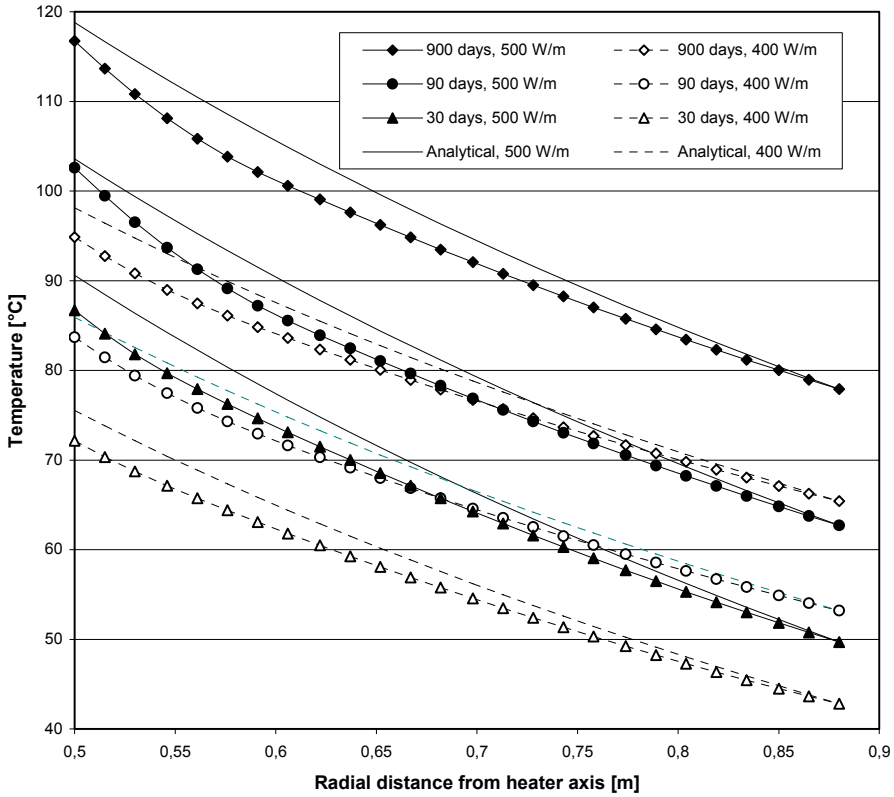

Figure 15*. Bentonite temperatures. For comparison, curves for both power assumptions are shown. Lines without markers: constant (1.1 W/(mK)) conductivity.*

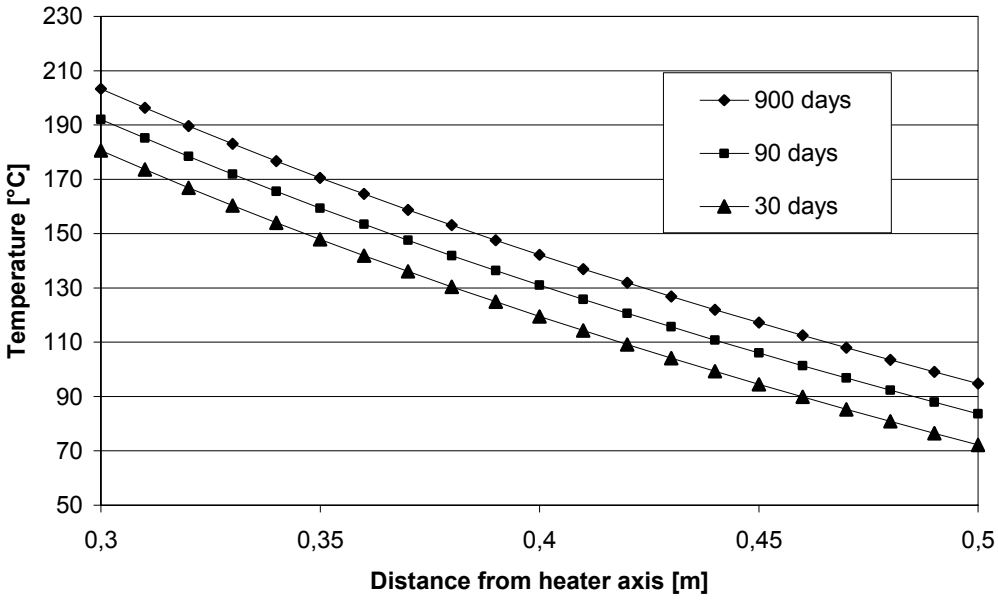

***Figure 16**. Sand temperatures. Case 2, 400 W/m.*

5.2 Lower density

All results presented previously regarded the reference density with associated void ratio and retention relation. Fig. 17 shows isothermal saturation for a material of void ratio = 0.80 and intrinsic permeability of $0.65 \cdot 10^{-20}$ m^2. The significantly slower saturation points to the importance of the water retention relation (c.f. Fig. 4).

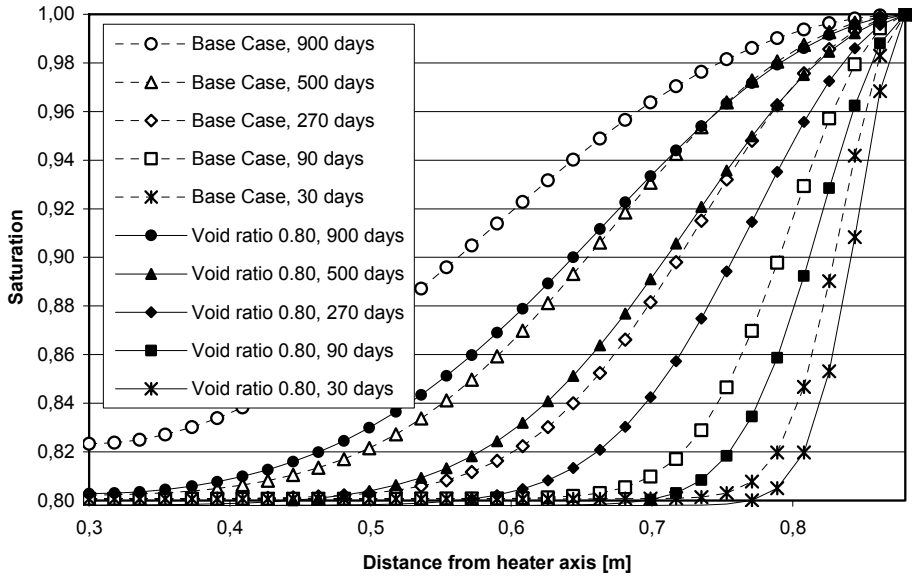

***Figure 17.** Isothermal saturation for reference material and material of lower density.*

6 Conclusions and discussion

6.1 Conclusion and comments

The saturation process of the bentonite part of the buffer surrounding the heater in a planned Vitrified Waste Test has been analyzed for two experimental options:

1. The bentonite fills out the entire annular space between heater and surrounding rock
2. There is 0.2 m sand shield between the heater and the bentonite.

There are two reasons for considering a sand shield:

1. Facilitate retrieval of the heater after completion of the experiment.
2. Protect the bentonite from the high heat fluxes that will prevail close to the heater.

A previous study (study 1) has shown that the power should be between 400 W/m and 500 W/m to arrive at a temperature of about 100 °C at position R2 corresponding to the sand/bentonite interface. Therefore, calculations were performed for two power assumptions: 400 W/m and 500 W/m.

The following preliminary conclusions can be drawn for the 500 W/m power case:

1. Very high temperatures will prevail in the bentonite. In case 1 (entire annular space filled with bentonite) the max temperature is about 170 °C at the heater/buffer interface. In case 2 (sand shield), the max temperature at the sand/buffer interface amounts to about 120 °C.
2. The bentonite between R2 and the rock wall seems to reach saturation within the 900 days simulated here. This applies for case1. For case 2, this does not happen.
3. The reason for the difference between case 1 and case 2 as regards saturation between R2 and the rock wall is that, for case 1, there is a water reservoir between heater and R2.
4. The 0.2 m annular space of bentonite between heater and R2 (case 1) does not seem to reach saturation within any reasonable time, and certainly not within the duration of the experiment. After little more than 100 days, a saturation front seems to form that moves very slowly or not at all (Figure 8).
5. A similar front seems to form in case 2. This front is however still moving slowly after 900 days (Figure 9). It is reasonable to believe that it will move much slower or stop moving when it has reached a bit closer to the heater.

The following preliminary conclusions can be drawn for the 400 W/m power case. Note that only case 2 (sand shield) was analyzed.

1. As opposed to the 500 W/m case, the temperature stayed below 100 °C in position R2 at 0.5 m radial distance (Figure 15).
2. As in the 500 W/m case, the bentonite does not seem to reach full saturation within the 900 days that were simulated. However, the saturation is significantly higher than in the 500 W/m case. And, more important, the saturation proceeds at a faster rate even at the end of the simulation (Figure 14).

The following conclusion can be drawn for the low density case. Note that only case 2 (sand shield) was analyzed.

1. The rate of saturation is very sensitive to variations in retention properties.

6.2 Discussion

Simultaneous transport of heat and moisture in unsaturated bentonite is a complicated problem of coupled processes. A large number of material laws and parameter values are required to perform relevant analyses, and there are many uncertainties. The CODE_BRIGHT material model used here has not yet been fully validated. The reason for using CODE_BRIGHT rather than the tool that otherwise has been used by SKB, i.e. ABAQUS, is that it has a better potential for a physically correct description of the fundamental processes. Therefore, for this type of analyses, CODE_BRIGHT is presently considered as an alternative by SKB. It is nevertheless recommended that, for comparison and for improving confidence, additional analyses are conducted with ABAQUS.

One uncertainty regards the coefficient of tortuosity. Here, this coefficient was set to 1, while a smaller value which would choke the vapor flux, might have been more realistic. So with respect to tortuosity, the results presented here are probably conservative.

Another uncertainty regards the hydraulic interaction between sand and bentonite. If there is a lower gas pressure in the sand than in the bentonite, vapor may, theoretically, escape into the sand because of advection. To capture this process, the gas phase (including dry air) must be explicitly modeled, and relevant gas phase boundary conditions derived. The approach here (assumption of a low constant total gas pressure) is, however, probably valid and sufficient for temperatures up to at least 100 °C (Olivella and Gens, 2000; Rutqvist et al, 2001).

In general, there is a risk that very high temperatures mean that models and concepts are being applied outside their range of validity, e.g. to steam-dominated systems. More work is needed to ensure proper use of the model when analyzing high-temperature systems.

There are also some uncertainties regarding the last conclusion above. It is true that the saturation rate depends strongly on the retention properties; the uncertainty lies in the input data, i.e. the retention curves shown in Fig 4. Suction in highly compacted bentonite is difficult to measure, and is not a simple function of the degree of saturation. Work is presently being done to analyze how suction is influenced by, for instance, confinement and swelling.

A final and general comment on the results presented here is that they should be interpreted with caution. The question of how well the bentonite will be saturated after completion of the experiment is a matter of delicate balance, where small variations in input assumptions can mean a lot, and where there is still a lack of understanding, in particular when it comes to high temperatures. A guess is that, at least for the 400 W/m case, the results are on the conservative side.

References

Börgesson L., Hernelind J., 1999. Coupled thermo-mechanical calculations of the water saturation phase of a KBS-3 deposition hole. SKB, Stockholm

Börgesson L., Fredriksson A., Johannesson L-E., 1994. Heat conductivity of buffer materials. SKB Technical Report TR-94-29. SKB, Stockholm.

CIMNE, 2000. CODE_BRIGHT. A 3-D program for thermo-hydro-mechanical analysis in geological media. Departamento de Ingeneria del Terreno; Cartgrafica y Geofisica, UPC, Barcelona, Spain.

Olivella S., Gens A., 2000. Vapor transport in low permeability unsaturated soil with capillary effects. Transp Porous Media, 2000;40:219-41

Rutqvist J., Börgesson L., Chijimatsu M., Kobayashi A., Jing L., Nguyen T.S., Noorishad J., Tsang C.-F., 2001. Thermohydromechanics of partially saturated geological media: governing equations and formulation of four finite element models. International Journey of Rock Mechanics and Mining Sciences, DECOVALEX II special issue.

SKB, 1999. SR 97 – Post closure safety, Main report Vol 1.SKB, Stockholm